Frequency domain modelling of wind turbine structures

Sørensen, Poul Ejnar

Publication date:
1994

Document Version
Publisher's PDF, also known as Version of record

Frequency Domain Modelling of Wind Turbine Structures

Risø-R-749(EN)

Poul Sørensen

Risø National Laboratory, Roskilde, Denmark
April 1994

Abstract

The report offers a detailed description of the development of a frequency domain model of the structure of an operating horizontal axis wind turbine. The frequency domain model is implemented along with an analogous time domain model in the Risø PC code Design Basis 2.

The structure of an operating wind turbine displays essential non-linearities between structural variables on blades and tower respectively. These non-linearities are due to the rotation of the blades causing the transformations between the blade coordinate systems and the tower coordinate system to depend on the instantaneous azimuth positions of the blades.

Conventional frequency domain methods do not allow non-linearities. It is shown, however, that decomposing the structural variables into sums of harmonics in the (constant) angular frequency of the rotor, the non-linear relations are transformed into linear relations between the amplitudes of the harmonics. These linear relations between the amplitudes of the harmonics of the structural variables are readily transformed into the frequency domain and solved there.

Thus, the derivation of the amplitudes of harmonics of the loads is based on conventional frequency domain methods applied to the relations between the amplitudes of harmonics. Finally, the loads themselves are determined uniquely by their respective amplitudes of harmonics.

Design Basis 2 is used to verify the frequency domain model comparing loads on the structure calculated with the frequency domain model both to loads calculated with the time domain model and to measured loads. Examples show that frequency and time domain calculations of typical PSD's of loads are in good agreement. Design Basis 2 has also shown that the frequency domain model results in an extremely fast and easy-to-use calculation method.

The report has passed an internal review at The Test Station for Wind Turbines at Risø performed by :

Gunner C. Larsen *Carl Jørgen Christensen*

The work has been funded by the EFP programme under the *Danish Ministry of Energy, contract no.* ENS-1364/92-0005.

ISBN 87-550-1978-1
ISSN 0106-2840

Grafisk Service · Risø · 1994

Contents

Summary

The report offers a detailed description of the development of a frequency domain model of the structure of an operating horizontal axis wind turbine. The frequency domain model is implemented along with an analogous time domain model in the Risø PC code Design Basis 2.

The structure of an operating wind turbine displays essential non-linearities between structural variables on blades and tower respectively. These non-linearities are due to the rotation of the blades causing the transformations between the blade coordinate systems and the tower coordinate system to depend on the instantaneous value of the periodic azimuth positions of the blades.

The non-linear terms in the dynamic equations for a complex wind turbine structure are normally thought to preclude the use of frequency domain methods. Frequency domain analysis are, on the other hand, always much faster and in some respects it gives more insight into the dynamics of the structure.

Therefore, a method is developed which uses the frequency domain analysis even in this case. The structural variables are decomposed into sums of harmonics in the (constant) angular frequency of the rotor. The amplitudes of these harmonics are in turn easily transformed into the frequency domain. The relations between the amplitudes of harmonics are then solved in the frequency domain.

The inputs to the wind turbine system are external loads on the structure, i.e. wind loads, gravity loads, and centrifugal loads. These loads are separated into deterministic loads and stochastic loads. The deterministic loads are caused by the gravity and the deterministic wind speed. The deterministic wind speed takes wind shear, tower shadow, yaw error etc into account. The stochastic loads are caused only by the turbulence.

The outputs from the wind turbine system are internal moments and forces in sections of either blades or tower. As a consequence of the separation of the inputs into deterministic and stochastic loads, also the outputs are separated into deterministic and stochastic parts.

In the frequency domain model, the stochastic part of a variable is calculated as a PSD (Power Spectral Density). The deterministic part is calculated as a series of Fourier coefficients of the periodic signal in the first place. Using an inverse Fourier transform these series of Fourier coefficients are easily transformed back into the time domain as one period of the signal.

By solving the relations between the amplitudes of harmonics in the frequency domain, transfer function matrices from the input amplitudes of harmonics to the output amplitudes of harmonics are obtained. These transfer function matrices are used to determine the stochastic parts and the deterministic parts of the output variables separately according to conventional frequency domain methods.

The output from the transfer function matrices are the amplitudes of the harmonics of the loads. Each amplitude has a PSD which represents the stochastic part of the amplitude and a constant complex number which represents the deterministic part of the amplitude.

The final task is to transform the amplitudes of harmonics of a load to the load itself. This is also done separately for the stochastic part and the deterministic part of the load.

The complex numbers representing the deterministic parts of the amplitudes of the series of all the harmonics of the load are simply the series of Fourier coefficients of the deterministic part of the load. These can inturn be transformed into one period of a periodic signal as explained above.

Likewise, the PSD's representing the stochastic parts of the amplitudes of the harmonics of the load shape the PSD of the stochastic part of the load itself. It is shown that the PSD of the load itself is determined, superimposing the narrow PSD's of the amplitudes of harmonics on the frequency axis according to their orders.

Test runs with Design Basis 2 have shown that the frequency domain code calculates up to 200 times faster than the time domain code. The rapid execution makes the frequency domain code eminently suited for parameter studies aiming at investigating the effect of changes in structural and aerodynamic parameters.

As previously mentioned, an important objective of the modelling of the wind turbine structure is to improve the understanding of the physics of the structure. The frequency domain models produce PSD's of the loads on the structure whereas time domain models produce time series. These PSD's provide more physical information than the time series because the PSD's clearly reveal the interaction between the harmonics in the rotor speed and the eigenfrequencies in the structure.

To get a PSD output from time domain models it must be generated from a time series. In principle, this is an easy task but it does require an extra effort on top of the time consuming calculation of time series. The improved understanding of the physics through the PSD's is obtained directly by the frequency domain models.

Another objective of the modelling of the wind turbine structure is to predict the fatigue lifetime and the extreme loads.

The conventional methods for predicting fatigue is to make rainflow counting on time series. However, Bishop and Zhihua [14] have developed fatigue methods based on PSD's. As expounded later, the knowledge from the present frequency domain model could be used in a refined frequency domain approach. A future development of such a method could be interesting.

For the calculations of extreme values, the time domain approach is to run through the time series looking for maximum and minimum. In the frequency domain, Davenport's method [1] of derivation of extremes from PSD's is a very simple and solid approach which has been adapted to wind turbines by Madsen [2] combining the influence of the deterministic and stochastic parts. Thus, it is a simple task to extend the frequency domain model with extreme value determinations.

The frequency domain model is implemented along with an analogous time domain model in the Risø PC code Design Basis 2. Therefore, Design Basis 2 is used to verify the frequency domain model comparing loads on the structure calculated with the frequency domain model both to loads calculated with the time domain model and to measured loads. Examples show that frequency and time domain calculations of typical PSD's of the stochastic parts of the loads are in good

agreement. For the deterministic parts of the loads, the agreement is excellent, which is a weighty verification of the transfer functions that are used by the stochastic as well as the deterministic calculations.

1 Introduction

The report offers a detailed description of the development of a frequency domain model of the structure of an operating horizontal axis wind turbine.

The inputs to the wind turbine system are external loads on the structure, i.e. wind loads, gravity loads, and centrifugal loads. In section 2, the external wind speeds experienced by the blades are decomposed into sums of harmonics in the (constant) angular speed of the rotor.

It is assumed that the structural variables of the wind turbine are sums of harmonics in general. In appendix A a set of the relevant linear and non-linear relations between blade and tower variables are then transformed into linear relations between the amplitudes of the harmonics of the variables. These linear relations are readily transformed into the frequency domain. The result is presented in section 2 as a *transformation table*. Using this table, the concrete transformations to Fourier transforms of amplitudes of harmonics are straight forward.

The generalized equations of motion related to blade and tower loads are established in a general matrix form in section 3. The non-linear azimuth dependence due to transformations between blade and tower coordinate systems are included in the formulation of the equations.

The generalized external loads on the right sides of the blade equations of motion are readily transformed into the Fourier transforms of amplitudes of the harmonics.

The generalized external loads on the right sides of the tower equations of motion are expressed as sums of contributions from external blade root loads. Using the transformation table, this relation is transformed into the frequency domain as a constant complex transfer function matrix from amplitudes of harmonics of external blade root loads to amplitudes of harmonics of generalized external tower loads.

Using the transformation table, the left side of the generalized equations of motion are transformed and solved in the frequency domain. Thus, the Fourier transforms of the amplitudes of harmonics of the *modal amplitudes* are determined by a transfer function matrix. The immediate inputs to the transfer function matrix are Fourier transforms of amplitudes of harmonics of generalized external loads.

Combining this transfer function matrix with the generalized tower load transfer function matrix mentioned above, a new transfer function matrix is then determined with Fourier transforms of amplitudes of harmonics of *external single blade loads* as the only inputs and amplitudes of harmonics of the modal amplitudes as outputs.

In order to determine the internal elastic loads in sections of blades and tower, the equations of equilibrium are established in section 4. The equations determine the internal loads as sums of external blade loads, inertia loads, etc. integrated from the blade tips to the considered sections.

Using the transformation table to transform these equations to relations between Fourier transforms of amplitudes of harmonics the final transfer function matri-

ces concerning amplitudes of harmonics from only external single blade loads to internal elastic loads are determined.

In section 5 it is shown how to determine the deterministic parts of the internal elastic loads. The deterministic variables are Fourier series which represent sums of harmonics with constant complex amplitudes of the harmonics. The transfer function matrices are used at the amplitude frequency $\Delta\omega = 0$ to determine the relations between the constant amplitudes of harmonics. Thus determining the Fourier coefficients of the internal elastic loads, the periodic response is determined versus time or versus azimuth angle.

In section 6 it is shown how to determine the stochastic parts of the internal elastic loads. First, the cross power spectrum matrices between the amplitudes of harmonics of external single blade turbulence loads are determined using numeric integration as described in appendix D. Using these cross power spectrum matrices as input to the transfer function matrices with external single blade loads as the only stochastic inputs, the power spectra of the amplitudes of harmonics of the internal elastic loads are determined. The power spectra of the internal elastic loads themselves are determined, placing the narrow power spectra of the amplitudes of harmonics on the frequency axis according to their orders. This simple power spectrum relation between variables and their amplitudes of harmonics is derived in appendix B.

In section 7, Design Basis 2 is used to make a limited verification of the frequency domain model comparing internal elastic loads calculated with the frequency domain model to loads calculated with the time domain model and to measured loads. Showing good agreement with measurements and excelent agreement with time simulation the present frequency domain method is trustworthy.

2 Transformations to Fourier transforms of amplitudes of harmonics

The rotating blade coordinate systems (x_r, y_r, z_r) are defined in figure 2.1, rotating the hub coordinate system (x_h, y_h, z_h) fixed to the tip of the nacelle with the azimuth angle θ about the y_h axis.

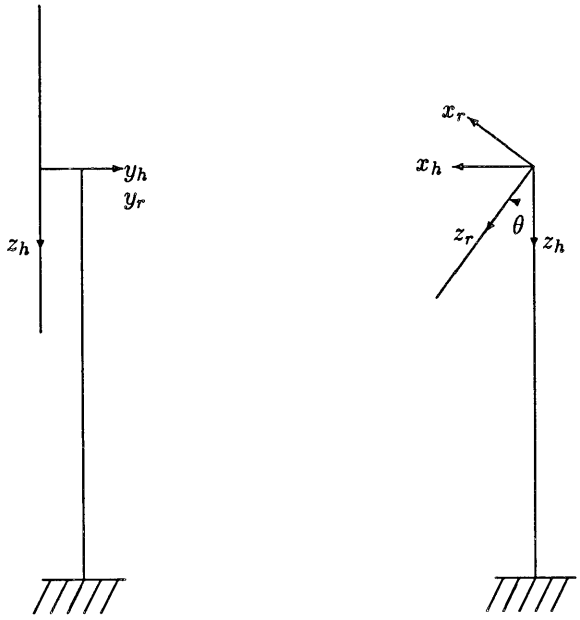

Figure 2.1. The transformations from the hub coordinate system (x_h, y_h, z_h) to the rotating blade coordinate systems (x_r, y_r, z_r) are determined by the instantaneous azimuth positions θ of the blades.

According to figure 2.1, the transformation is

$$\begin{pmatrix} x_r \\ y_r \\ z_r \end{pmatrix} = \begin{pmatrix} \cos\theta & 0 & -\sin\theta \\ 0 & 1 & 0 \\ \sin\theta & 0 & \cos\theta \end{pmatrix} \begin{pmatrix} x_h \\ y_h \\ z_h \end{pmatrix} \tag{2.1}$$

Assuming that the blades rotate with the constant angular speed ω_0, the azimuth angles of the blades are determined by

$$\theta(t, b) = \omega_0 t + \theta_0(b) \tag{2.2}$$

in which b is an integer blade index in the interval

$$0 \leq b < B \tag{2.3}$$

and $\theta_0(b)$ is the initial azimuth position of blade b. B in (2.3) is the number of blades. Assuming identical azimuth angles between neighbouring blades,

$$\theta_0(b) = \frac{2\pi b}{B} + \theta_{00} \tag{2.4}$$

in which θ_{00} is the initial azimuth position of blade $b = 0$.

Considering only the y_h component of the turbulence wind speed, and using the polar coordinates (z_r, θ), the turbulence wind speed is defined as a field $\underline{v}(t, z_r, \theta)$ in the rotor disk. Expanding $\underline{v}(t, z_r, \theta)$ in the azimuth angle θ yields

$$\underline{v}(t, z_r, \theta) = \sum_{n=-\infty}^{\infty} \tilde{v}_{\{n\}}(t, z_r)\, e^{jn\theta} \tag{2.5}$$

with the azimuth expansion coefficients

$$\tilde{v}_{\{n\}}(t, z_r) = \frac{1}{2\pi} \int_0^{2\pi} \underline{v}(t, z_r, \theta)\, e^{-jn\theta}\, d\theta \tag{2.6}$$

Inserting the time dependence of the azimuth angle (2.2) in the expansion (2.5) yields the turbulence wind speed at the rotating blade coordinate position $(0, 0, z_r)$ on blade b

$$v(t, b, z_r) = \sum_{n=-\infty}^{\infty} \hat{v}_{\{n\}}(t, b, z_r)\, e^{jn\omega_0 t} \tag{2.7}$$

Thus, $v(t, b, z_r)$ is a sum of *harmonics* $\hat{v}_{\{n\}}(t, b, z_r)e^{jn\omega_0 t}$ in the angular speed ω_0, and the *amplitude* of the n'th harmonic of $v(t, b, z_r)$

$$\hat{v}_{\{n\}}(t, b, z_r) = e^{jn\theta_0(b)}\, \tilde{v}_{\{n\}}(t, z_r) \tag{2.8}$$

determines the size as well as the phase of the n'th harmonic.

In general, for a wind turbine with symmetric rotor, any blade variable $f(t, b)$ is a sum of harmonics in the angular speed ω_0 of the blade rotation, i.e.

$$f(t, b) = \sum_{n=-\infty}^{\infty} \hat{f}_{\{n\}}(t, b)\, e^{jn\omega_0 t} \tag{2.9}$$

and the amplitudes $\hat{f}_{\{n\}}(t, b)$ of the harmonics on blade b are determined by

$$\hat{f}_{\{n\}}(t, b) = e^{jn\theta_0(b)}\, \tilde{f}_{\{n\}}(t) \tag{2.10}$$

In general, $\tilde{f}_{\{n\}}(t)$ is not the result of an azimuth expansion. According to (2.10), the size of the amplitude of the n'th harmonic is independent of the particular blade and given by

$$| \hat{f}_{\{n\}}(t,b) | = | \tilde{f}_{\{n\}}(t) | \tag{2.11}$$

whereas the angle depends on the particular blade and is given by

$$\angle \hat{f}_{\{n\}}(t,b) = \angle \tilde{f}_{\{n\}}(t) + n\theta_0(b) \tag{2.12}$$

Thus having the same size as the amplitude of harmonic of any blade according to (2.11), and moreover holding the phase offset according to (2.12), $\tilde{f}_{\{n\}}(t)$ is denoted the *generic amplitude of the n'th harmonic* of the blade variable $f(t,b)$.

A tower variable $f(t)$ is also a sum of harmonics in the angular speed ω_0 of the blade rotation. However, assuming symmetry tower variables include only those orders of harmonics that are multipla of the number of blades B, i.e.

$$f(t) = \sum_{k=-\infty}^{\infty} \hat{f}_{\{kB\}}(t)\, e^{jkB\omega_0 t} \tag{2.13}$$

and the amplitudes $\hat{f}_{\{kB\}}(t)$ of the harmonics are determined by the generic amplitudes of harmonics $\tilde{f}_{\{kB\}}(t)$ and the initial azimuth angle $\theta_0(b)$ of any blade b according to

$$\hat{f}_{\{kB\}}(t) = e^{jkB\theta_0(b)}\, \tilde{f}_{\{kB\}}(t) \tag{2.14}$$

Note that $e^{jkB\theta_0(b)}$ is actually independent of the blade index b, which is seen using the initial azimuth angles (2.4) to show

$$e^{jkB\theta_0(b)} = e^{jkB\theta_{00}} \tag{2.15}$$

In appendix A, (2.9) is Fourier transformed and it is shown that if $f(t,b)$ and $\hat{f}_{\{n\}}(t,b)$ have the Fourier transformed $F(\omega,b)$ and $\hat{F}_{\{n\}}(\Delta\omega,b)$ respectively, then (2.9) is replaced by

$$F(\omega,b) = \sum_{n=-\infty}^{\infty} \hat{F}_{\{n\}}(\omega - n\omega_0, b) \tag{2.16}$$

and if $\tilde{f}_{\{n\}}(t)$ has the Fourier transformed $\tilde{F}_{\{n\}}(\Delta\omega)$ then the relation (2.10) is replaced by

$$\hat{F}_{\{n\}}(\Delta\omega,b) = e^{jn\theta_0(b)}\, \tilde{F}_{\{n\}}(\Delta\omega) \tag{2.17}$$

Here $\Delta\omega$ substitutes for the frequency of the amplitude of the n'th harmonic in (2.16), i.e.

$$\Delta\omega \;=\; \omega - n\omega_0 \tag{2.18}$$

Likewise, (2.13) is replaced by

$$F(\omega) \;=\; \sum_{k=-\infty}^{\infty} \hat{F}_{\{kB\}}(\omega - kB\omega_0) \tag{2.19}$$

and (2.14) is replaced by

$$\hat{F}_{\{kB\}}(\Delta\omega) = e^{jn\theta_0(b)}\; \tilde{F}_{\{kB\}}(\Delta\omega) \tag{2.20}$$

substituting $\Delta\omega$ for the frequency of the amplitude of the kB'th harmonic in (2.19), i.e.

$$\Delta\omega = \omega - kB\omega_0 \tag{2.21}$$

Concerning the turbulence wind speeds experienced by the blades, $\tilde{V}_{\{n\}}(\Delta\omega, z_r)$ is determined as the Fourier transform of the n'th azimuth expansion coefficient of the turbulence wind speed field $\underline{v}(t, z_r, \theta)$. Therefore, the relevant frequency range of $\tilde{V}_{\{n\}}(\Delta\omega, z_r)$ is limited to the relevant frequency range of the turbulence wind speed field. These frequencies are destinctively smaller than the angular speed of wind turbine rotor. Thus, the relevant frequency range of the amplitudes

$$|\,\Delta\omega\,| < \frac{\omega_0}{2} \tag{2.22}$$

Therefore, the aliasing between the neighbouring harmonics in (2.16) is not considered any further.

In appendix A, linear as well as azimuth dependent non-linear relations between instantaneous values of blade variables as $f(t, b)$ and tower variables as $f(t)$ are studied. Relations are transformed to relations between Fourier transforms of amplitudes of harmonics. The results of these transformations are listed in table 2.1. Note that the blade variables are charactarized by the blade index b-parameter.

No	Instantaneous values	Fourier transforms of amplitudes of harmonics
1	$f(t,b) = a_1 f_1(t,b) + a_2 f_2(t,b)$	$\tilde{F}_{\{n\}}(\Delta\omega) = a_1 \tilde{F}_{1\{n\}}(\Delta\omega) + a_2 \tilde{F}_{2\{n\}}(\Delta\omega)$
2	$f(t,b) = \int_{z_{b1}}^{z_{b2}} g(t,b,z_b)\, dz_b$	$\tilde{F}_{\{n\}}(\Delta\omega) = \int_{z_{b1}}^{z_{b2}} \tilde{G}_{\{n\}}(\Delta\omega, z_b)\, dz_b$
3	$f(t) = a_1 f_1(t) + a_2 f_2(t)$	$\tilde{F}_{\{kB\}}(\Delta\omega) = a_1 \tilde{F}_{1\{kB\}}(\Delta\omega) + a_2 \tilde{F}_{2\{kB\}}(\Delta\omega)$
4	$f(t) = \sum_{b=0}^{B-1} g(t,b)$	$\tilde{F}_{\{kB\}}(\Delta\omega) = B\, \tilde{G}_{\{kB\}}(\Delta\omega)$
5	$f(t) = \sum_{b=0}^{B-1} \cos\theta(t,b)\, g(t,b)$	$\tilde{F}_{\{kB\}}(\Delta\omega) = \frac{B}{2} \tilde{G}_{\{kB-1\}}(\Delta\omega) + \frac{B}{2} \tilde{G}_{\{kB+1\}}(\Delta\omega)$
6	$f(t) = \sum_{b=0}^{B-1} \sin\theta(t,b)\, g(t,b)$	$\tilde{F}_{\{kB\}}(\Delta\omega) = -\frac{jB}{2} \tilde{G}_{\{kB-1\}}(\Delta\omega) + \frac{jB}{2} \tilde{G}_{\{kB+1\}}(\Delta\omega)$
7	$f(t,b) = g(t)$	$\tilde{F}_{\{kB\}}(\Delta\omega) = \tilde{G}_{\{kB\}}(\Delta\omega)$
8	$f(t,b) = \cos\theta(t,b)\, g(t)$	$\tilde{F}_{\{kB-1\}}(\Delta\omega) = \frac{1}{2} \tilde{G}_{\{kB\}}(\Delta\omega)$ $\tilde{F}_{\{kB+1\}}(\Delta\omega) = \frac{1}{2} \tilde{G}_{\{kB\}}(\Delta\omega)$
9	$f(t,b) = \sin\theta(t,b)\, g(t)$	$\tilde{F}_{\{kB-1\}}(\Delta\omega) = \frac{j}{2} \tilde{G}_{\{kB\}}(\Delta\omega)$ $\tilde{F}_{\{kB+1\}}(\Delta\omega) = -\frac{j}{2} \tilde{G}_{\{kB\}}(\Delta\omega)$
10	$f(t,b) = \dot{g}(t,b)$	$\tilde{F}_{\{n\}}(\Delta\omega) = j(n\omega_0 + \Delta\omega)\, \tilde{G}_{\{n\}}(\Delta\omega)$
11	$f(t) = \dot{g}(t)$	$\tilde{F}_{\{kB\}}(\Delta\omega) = j(kB\omega_0 + \Delta\omega)\, \tilde{G}_{\{kB\}}(\Delta\omega)$

Table 2.1. The transformations of instantaneous relations between blade and tower variables into relations between Fourier transforms of amplitudes of harmonics.

3 Generalized equations of motion

The structure of the wind turbine is separated into a rotating part represented by a number B of blade beams and a non-rotating part represented by a tower beam.

A blade beam is defined by the structural data of an actual blade and an appropriate part of the hub, whereas the tower beam is defined by the structural data of the nacelle, the actual tower, and the tower foundation. The flexibility of the structure is decomposed into modes that are flexible only on a single beam, i.e. blade modes and tower modes. Still, the flexibilities of shaft torsion and induction generator slip are included in the model. This is possible because these modes couple to other modes like the tower modes.

The mass distribution of the rotor is assumed to be symmetric, i.e. the tilt and yaw moments of inertia are independent of the instantaneous azimuth positions of the blades. Considering wind turbines with a number of blades $B \geq 3$ this is the case if the angle between neighbouring blades is $\frac{2\pi}{B}$ and the mass distribution is identical on each blade. Likewise, the aerodynamic properties of the blades are assumed to be identical.

The generalized equations of motion are equations of generalized load equilibria related to the selected modes. Each equilibrium is established in the coordinate system where the respective mode is defined.

Each blade mode is defined in a rotating blade coordinate system. A blade coordinate system is determined by a sequence of transformations from the rotating blade coordinate system (x_r, y_r, z_r) defined in figure 2.1. That way, coning of the rotor and constant pitching of the directions of the blade modes is included in the structural model in Design Basis 2. In the present frequency domain modelling the only restriction on the transformations is that eventual time dependence can be expressed by the modal amplitudes of the blade modes.

The modal amplitudes concerning each blade b are expressed as a vector $q_b(t, b)$. Including the first flapwise and the first edgewise mode in Design Basis 2 as described by Larsen [12] each blade b has a $q_b(t, b)$ vector with two elements.

Likewise, each tower mode is defined in a tower coordinate system. A tower coordinate system is determined by a sequence of transformations from the hub coordinate system (x_h, y_h, z_h) defined in figure 2.1. That way, tilt angle and yaw error are included in the structural model in Design Basis 2. In the present frequency domain modelling the only restriction on the transformations is that eventual time dependences can be expressed by the modal amplitudes of the tower modes.

The modal amplitudes of the tower modes are expressed as a vector $q_t(t)$. Including two backwards tower bending modes, one sidewards tower bending mode, one tower torsion mode, one shaft torsion mode, and one generator mode in Design Basis 2 as described by Larsen [12] the $q_t(t)$ vector gets six elements.

The generalized equations of motion concerning the loads on each blade b can be written in the general matrix form

$$
\begin{aligned}
& m_{bb}\ \ddot{q}_b(t,b) + c_{bb}\ \dot{q}_b(t,b) + k_{bb}\ q_b(t,b) + \\
& \left(m_{bt} + m_{bt}^{\cos}\cos\theta(t,b) + m_{bt}^{\sin}\sin\theta(t,b)\right)\ \ddot{q}_t(t) + \\
& \left(c_{bt} + c_{bt}^{\cos}\cos\theta(t,b) + c_{bt}^{\sin}\sin\theta(t,b)\right)\ \dot{q}_t(t) + \\
& \left(k_{bt} + k_{bt}^{\cos}\cos\theta(t,b) + k_{bt}^{\sin}\sin\theta(t,b)\right)\ q_t(t) = \\
& \int_0^L \Psi_b(z_b)\ v(t,b,z_b)\ dz_b
\end{aligned}
\tag{3.1}
$$

The right side of (3.2) is the generalized external turbulence loads. Thus, $\Psi_b(z_b)$ is a vector with an element for each blade mode. It involves aero load influence coefficients to determine the slope from wind speed to aero load and it involves the mode shapes of the selected blade modes. Using aero load influence coefficients that are independent of time and consequently independent of the azimuth angle assures that the $\Psi_b(z_b)$ vector is independent of time.

The left side is the sum of generalized internal and aerodynamic feedback loads related to the modal amplitudes $q_b(t,b)$ and $q_t(t)$ and their derivatives. Assuming small deflections in $q_b(t,b)$ and $q_t(t)$ only first order dependences are included in (3.2).

Note that the blades are coupled only through the tower. This coupling is expressed by blade loads related to tower displacement, velocity, and acceleration. The transformation from the hub coordinate system to the rotor coordinate system causes the azimuth dependence of these contributions.

The generalized equations of motion concerning the loads on the tower can be written in the general matrix form

$$
\begin{aligned}
& \sum_{b=0}^{B-1} \left(m_{tb} + m_{tb}^{\cos}\cos\theta(t,b) + m_{tb}^{\sin}\sin\theta(t,b)\right)\ \ddot{q}_b(t,b) + \\
& \sum_{b=0}^{B-1} \left(c_{tb} + c_{tb}^{\cos}\cos\theta(t,b) + c_{tb}^{\sin}\sin\theta(t,b)\right)\ \dot{q}_b(t,b) + \\
& \sum_{b=0}^{B-1} \left(k_{tb} + k_{tb}^{\cos}\cos\theta(t,b) + k_{tb}^{\sin}\sin\theta(t,b)\right)\ q_b(t,b) + \\
& m_{tt}\ \ddot{q}_t(t) + c_{tt}\ \dot{q}_t(t) + k_{tt}\ q_t(t) = \\
& A_t \sum_{b=0}^{B-1} \left(A_{\Sigma br} + A_{\Sigma br}^{\cos}\cos\theta(t,b) + A_{\Sigma br}^{\sin}\sin\theta(t,b)\right) \\
& \int_0^L \Psi_{br}(z_b)\ v(t,b,z_b)\ dz_b
\end{aligned}
\tag{3.2}
$$

The right side of (3.2) is the generalized external tower turbulence loads. Assuming that the external turbulence loads arise only on the blades, they are sums of

contributions from each blade. Thus, $\Psi_{br}(z_b)$ is a vector with values that ensures that the integral determines the blade root moments and blade root forces. These blade root loads are transformed from the rotor coordinate systems to the hub coordinate system by $A_{\Sigma br}(z_b)$, $A^{\cos}_{\Sigma br}(z_b)$, and $A^{\sin}_{\Sigma br}(z_b)$. In the hub coordinate system the contributions from all the blades are summed and finally A_t determines the transformation of the summed loads to generalized tower loads.

The left side is the sum of generalized internal and aerodynamic feedback loads caused by the modal amplitudes $q_b(t,b)$ and $q_t(t)$. Assuming small deflections in $q_b(t,b)$ and $q_t(t)$ only first order dependences are included in (3.2).

Note the azimuth dependence of the $q_b(t,b)$ dependent contributions to the generalized tower loads. The transformation from the rotor coordinate systems to the hub coordinate system causes this azimuth dependence.

Now the equations are established in the time domain in a general matrix form in (3.2) and (3.2). The remainding task of this section is to solve these equations in the frequency domain.

3.1 Generalized external blade loads

The generalized external turbulence loads in the blade equations of motion (3.2) are determined by the integral

$$g_b(t,b) = \int_0^L \Psi_b(z_b)\; v(t,b,z_b)\; dz_b \tag{3.1.1}$$

where the weight function $\Psi_b(z_b)$ is a vector with elements involving blade aero load influence coefficients and blade mode shapes.

Now (3.1.1) is replaced by relations between the Fourier transforms of the generic amplitudes of harmonics of $v(t,b,z_b)$ and $g_b(t,b)$ respectively. The replacement is done using transformation 1 in table 2.1 on the integrand, and subsequently transformation 2 on the integral. The transformed relations then become

$$\tilde{G}_{b\{n\}}(\Delta\omega) = \int_0^L \Psi_b(z_b)\; \tilde{V}_{\{n\}}(\Delta\omega, z_b)\; dz_b \tag{3.1.2}$$

3.2 Summed external blade root loads

The summed external blade root turbulence loads in the tower equations of motion (3.2) are determined as the sum of the external blade root turbulence loads transfered to non-rotating coordinates

$$p^{ext}_{\Sigma br}(t) = \sum_{b=0}^{B-1} \left(A_{\Sigma br} + A^{\cos}_{\Sigma br} \cos\theta(t,b) + A^{\sin}_{\Sigma br} \sin\theta(t,b)\right) p^{ext}_{br}(t,b) \tag{3.2.1}$$

where the external turbulence blade root moments and forces can be expressed as

$$p^{ext}_{br}(t,b) = \int_0^L \Psi_{br}(z_b)\, v(t,b,z_b)\, dz_b \tag{3.2.2}$$

Using transformation 2 in table 2.1, (3.2.2) is replaced by the corresponding relations between the Fourier transforms of the generic amplitudes of the harmonics

$$\tilde{P}^{ext}_{br\{n\}}(\Delta\omega) = \int_0^L \Psi_{br}(z_b)\, \tilde{V}_{\{n\}}(\Delta\omega, z_b)\, dz_b \tag{3.2.3}$$

Summing each term individually and applying the transformations 3, 4, 5, and 6 from table 2.1, (3.2.2) is replaced by

$$\begin{aligned}\tilde{P}^{ext}_{\Sigma br\{kB\}}(\Delta\omega) &= \left(\frac{B}{2} A^{\cos}_{\Sigma br} - \frac{jB}{2} A^{\sin}_{\Sigma br}\right) \tilde{P}^{ext}_{br\{kB-1\}}(\Delta\omega) \\ &+ B\, A_{\Sigma br}\, \tilde{P}^{ext}_{br\{kB\}}(\Delta\omega) \\ &+ \left(\frac{B}{2} A^{\cos}_{\Sigma br} + \frac{jB}{2} A^{\sin}_{\Sigma br}\right) \tilde{P}^{ext}_{br\{kB+1\}}(\Delta\omega)\end{aligned} \tag{3.2.4}$$

which is conviniently written

$$\tilde{P}^{ext}_{\Sigma br\{kB\}}(\Delta\omega) = C_{\Sigma br} \begin{pmatrix} \tilde{P}^{ext}_{br\{kB-1\}}(\Delta\omega) \\ \tilde{P}^{ext}_{br\{kB\}}(\Delta\omega) \\ \tilde{P}^{ext}_{br\{kB+1\}}(\Delta\omega) \end{pmatrix} \tag{3.2.5}$$

where the constant complex matrix is defined as

$$C_{\Sigma br} = \left(\tfrac{B}{2} A^{\cos}_{\Sigma br} - \tfrac{jB}{2} A^{\sin}_{\Sigma br} \;\middle|\; B\, A_{\Sigma br} \;\middle|\; \tfrac{B}{2} A^{\cos}_{\Sigma br} + \tfrac{jB}{2} A^{\sin}_{\Sigma br} \right) \tag{3.2.6}$$

3.3 Generalized external tower loads

The generalized external turbulence loads in the tower equations of motion (3.2) are now determined by the simple transformation

$$g_i(t) \;=\; A_t \; p^{ext}_{\Sigma br}(t) \tag{3.3.1}$$

where the summed external turbulence blade root moments and forces $p^{ext}_{\Sigma br}(t)$ were evaluated in subsection 3.2.

According to transformation 3 in table 2.1, (3.3.1) is transformed to

$$\tilde{G}_{t\{kB\}}(\Delta\omega) \;=\; A_t \; \tilde{P}^{ext}_{\Sigma br\{kB\}}(\Delta\omega) \tag{3.3.2}$$

3.4 Generalized mechanical impedances

Defining the generalized feedback loads

$$f_{bb}(t,b) = m_{bb}\,\ddot{q}_b(t,b) + c_{bb}\,\dot{q}_b(t,b) + k_{bb}\,q_b(t,b) \tag{3.4.1}$$

$$\begin{aligned} f_{bt}(t,b) &= \left(m_{bt} + m_{bt}^{\cos}\cos\theta(t,b) + m_{bt}^{\sin}\sin\theta(t,b) \right) \ddot{q}_t(t) \\ &+ \left(c_{bt} + c_{bt}^{\cos}\cos\theta(t,b) + c_{bt}^{\sin}\sin\theta(t,b) \right) \dot{q}_t(t) \\ &+ \left(k_{bt} + k_{bt}^{\cos}\cos\theta(t,b) + k_{bt}^{\sin}\sin\theta(t,b) \right) q_t(t) \end{aligned} \tag{3.4.2}$$

$$\begin{aligned} f_{tb}(t) &= \sum_{b=0}^{B-1} \left(m_{tb} + m_{tb}^{\cos}\cos\theta(t,b) + m_{tb}^{\sin}\sin\theta(t,b) \right) \ddot{q}_b(t,b) \\ &+ \sum_{b=0}^{B-1} \left(c_{tb} + c_{tb}^{\cos}\cos\theta(t,b) + c_{tb}^{\sin}\sin\theta(t,b) \right) \dot{q}_b(t,b) \\ &+ \sum_{b=0}^{B-1} \left(k_{tb} + k_{tb}^{\cos}\cos\theta(t,b) + k_{tb}^{\sin}\sin\theta(t,b) \right) q_b(t,b) \end{aligned} \tag{3.4.3}$$

$$f_{tt}(t) = m_{tt}\,\ddot{q}_t(t) + c_{tt}\,\dot{q}_t(t) + k_{tt}\,q_t(t) \tag{3.4.4}$$

the equations of motion (3.2) and (3.2) are reduced to

$$f_{bb}(t,b) + f_{bt}(t,b) = g_b(t,b) \tag{3.4.5}$$

$$f_{tb}(t) + f_{tt}(t) = g_t(t) \tag{3.4.6}$$

where $g_b(t,b)$ is defined according to (3.1.1) and $g_t(t)$ is defined according to (3.3.1) and (3.2.2). Combining transformation 10 and 1 from table 2.1, (3.4.1) is now transformed to

$$\tilde{F}_{bb\{n\}}(\Delta\omega) = Z_{bb}(n\omega_0 + \Delta\omega)\,\tilde{Q}_{b\{n\}}(\Delta\omega) \tag{3.4.7}$$

where the mechanical impedance

$$Z_{bb}(\omega) = (j\omega)^2\,m_{bb} + j\omega\,c_{bb} + k_{bb} \tag{3.4.8}$$

Shortening the mechanical impedances concerning amplitudes of harmonics according to

$$Z_{\{p\}}(\Delta\omega) = Z(p\omega_0 + \Delta\omega) \tag{3.4.9}$$

(3.4.7) can be written

$$\tilde{F}_{bb\{n\}}(\Delta\omega) = Z_{bb\{n\}}(\Delta\omega)\,\tilde{Q}_{b\{n\}}(\Delta\omega) \tag{3.4.10}$$

Combining transformation 11, 7, 8, 9, and 1 from table 2.1, (3.4.2) is transformed to

$$\tilde{F}_{bt\{kB-1\}}(\Delta\omega) = Z^{-}_{bt\{kB\}}(\Delta\omega)\,\tilde{Q}_{t\{kB\}}(\Delta\omega) \tag{3.4.11}$$

$$\tilde{F}_{bt\{kB\}}(\Delta\omega) = Z^{0}_{bt\{kB\}}(\Delta\omega)\,\tilde{Q}_{t\{kB\}}(\Delta\omega) \tag{3.4.12}$$

$$\tilde{F}_{bt\{kB+1\}}(\Delta\omega) = Z^{+}_{bt\{kB\}}(\Delta\omega)\,\tilde{Q}_{t\{kB\}}(\Delta\omega) \tag{3.4.13}$$

where the mechanical impedances

$$\begin{aligned} Z^{-}_{bt}(\omega) &= \frac{1}{2}\left((j\omega)^2\, m^{\cos}_{bt} + j\omega\, c^{\cos}_{bt} + k^{\cos}_{bt}\right) \\ &+ \frac{j}{2}\left((j\omega)^2\, m^{\sin}_{bt} + j\omega\, c^{\sin}_{bt} + k^{\sin}_{bt}\right) \end{aligned} \tag{3.4.14}$$

$$Z^{0}_{bt}(\omega) = (j\omega)^2\, m_{bt} + j\omega\, c_{bt} + k_{bt} \tag{3.4.15}$$

$$\begin{aligned} Z^{+}_{bt}(\omega) &= \frac{1}{2}\left((j\omega)^2\, m^{\cos}_{bt} + j\omega\, c^{\cos}_{bt} + k^{\cos}_{bt}\right) \\ &- \frac{j}{2}\left((j\omega)^2\, m^{\sin}_{bt} + j\omega\, c^{\sin}_{bt} + k^{\sin}_{bt}\right) \end{aligned} \tag{3.4.16}$$

are shortened according to (3.4.9) in (3.4.11), (3.4.12), and (3.4.13).

Transforming the blade equations of motion (3.4.5) according to transformation 1 in table 2.1, inserting (3.4.10) and (3.4.11), (3.4.12), and (3.4.13) respectively yields

$$\begin{aligned} &Z_{bb\{kB-1\}}(\Delta\omega)\,\tilde{Q}_{b\{kB-1\}}(\Delta\omega) + \\ &\quad Z^{-}_{bt\{kB\}}(\Delta\omega)\,\tilde{Q}_{t\{kB\}}(\Delta\omega) = \tilde{G}_{b\{kB-1\}}(\Delta\omega) \end{aligned} \tag{3.4.17}$$

if $n = kB - 1$,

$$\begin{aligned} &Z_{bb\{kB\}}(\Delta\omega)\,\tilde{Q}_{b\{kB\}}(\Delta\omega) + \\ &Z^{0}_{bt\{kB\}}(\Delta\omega)\,\tilde{Q}_{t\{kB\}}(\Delta\omega) = \tilde{G}_{b\{kB\}}(\Delta\omega) \end{aligned} \tag{3.4.18}$$

if $n = kB$, and

$$\begin{aligned} &Z_{bb\{kB+1\}}(\Delta\omega)\,\tilde{Q}_{b\{kB+1\}}(\Delta\omega) + \\ &\quad Z^{+}_{bt\{kB\}}(\Delta\omega)\,\tilde{Q}_{t\{kB\}}(\Delta\omega) = \tilde{G}_{b\{kB+1\}}(\Delta\omega) \end{aligned} \tag{3.4.19}$$

if $n = kB + 1$.

Concerning 3 bladed wind turbines, an arbitraryly selected n can always be expressed as $kB - 1$, kB, or $kB + 1$. For the sake of completeness, concerning wind turbines with more than 3 blades, some of the orders of blade harmonics are not coupled to any kB'th order of tower harmonics, and consequently the blade equations of motion concerning amplitudes of such orders are simply

$$Z_{bb\{n\}}(\Delta\omega)\ \tilde{Q}_{b\{n\}}(\Delta\omega) \;=\; \tilde{G}_{b\{n\}}(\Delta\omega) \tag{3.4.20}$$

Combining transformation 10, 4, 5, 6, and 3, (3.4.3) is transformed to

$$\begin{aligned}\tilde{F}_{tb\{kB\}}(\Delta\omega) \;&=\; Z^{-}_{tb\{kB-1\}}(\Delta\omega)\ \tilde{Q}_{b\{kB-1\}}(\Delta\omega)\\ &+\; Z^{0}_{tb\{kB\}}(\Delta\omega)\ \tilde{Q}_{b\{kB\}}(\Delta\omega)\\ &+\; Z^{+}_{tb\{kB+1\}}(\Delta\omega)\ \tilde{Q}_{b\{kB+1\}}(\Delta\omega)\end{aligned} \tag{3.4.21}$$

where the mechanical impedances

$$\begin{aligned}Z^{-}_{tb}(\omega) \;&=\; \frac{B}{2}\left((j\omega)^2\, m^{\cos}_{tb} \;+\; j\omega\, c^{\cos}_{tb} \;+\; k^{\cos}_{tb}\right)\\ &-\; \frac{jB}{2}\left((j\omega)^2\, m^{\sin}_{tb} \;+\; j\omega\, c^{\sin}_{tb} \;+\; k^{\sin}_{tb}\right)\end{aligned} \tag{3.4.22}$$

$$Z^{0}_{tb}(\omega) \;=\; B\left((j\omega)^2\, m_{tb} \;+\; j\omega\, c_{tb} \;+\; k_{tb}\right) \tag{3.4.23}$$

$$\begin{aligned}Z^{+}_{tb}(\omega) \;&=\; \frac{B}{2}\left((j\omega)^2\, m^{\cos}_{tb} \;+\; j\omega\, c^{\cos}_{tb} \;+\; k^{\cos}_{tb}\right)\\ &+\; \frac{jB}{2}\left((j\omega)^2\, m^{\sin}_{tb} \;+\; j\omega\, c^{\sin}_{tb} \;+\; k^{\sin}_{tb}\right)\end{aligned} \tag{3.4.24}$$

Combining transformation 11 and 3, (3.4.4) is transformed to

$$\tilde{F}_{tt\{kB\}}(\Delta\omega) \;=\; Z_{tt\{kB\}}(\Delta\omega)\ \tilde{Q}_{t\{kB\}}(\Delta\omega) \tag{3.4.25}$$

where the mechanical impedance

$$Z_{tt}(\omega) \;=\; (j\omega)^2\, m_{tt} \;+\; j\omega\, c_{tt} \;+\; k_{tt} \tag{3.4.26}$$

Transforming the generalized tower equations of motion (3.4.6) according to transformation 3 and inserting (3.4.21) and (3.4.25) yields

$$Z^{-}_{tb\{kB-1\}}(\Delta\omega)\ \tilde{Q}_{b\{kB-1\}}(\Delta\omega) \;+$$

$$
\begin{aligned}
Z^{0}_{tb\{kB\}}(\Delta\omega)\ \tilde{Q}_{b\{kB\}}(\Delta\omega) \quad &+ \\
Z^{+}_{tb\{kB+1\}}(\Delta\omega)\ \tilde{Q}_{b\{kB+1\}}(\Delta\omega) \quad &+ \\
Z_{tt\{kB\}}(\Delta\omega)\ \tilde{Q}_{t\{kB\}}(\Delta\omega) \quad &= \quad \tilde{G}_{t\{kB\}}(\Delta\omega) \qquad (3.4.27)
\end{aligned}
$$

3.5 Modal amplitudes

The equations (3.4.17), (3.4.18), (3.4.19), and (3.4.27) define a linear system concerning amplitudes of $(kB-1)$'th, kB'th, and $(kB+1)$'th blade harmonics coupled with amplitudes of kB'th tower harmonics

$$Z_{\{kB\}}(\Delta\omega) \begin{pmatrix} \tilde{Q}_{b\{kB-1\}}(\Delta\omega) \\ \hline \tilde{Q}_{b\{kB\}}(\Delta\omega) \\ \hline \tilde{Q}_{b\{kB+1\}}(\Delta\omega) \\ \hline \tilde{Q}_{t\{kB\}}(\Delta\omega) \end{pmatrix} = \begin{pmatrix} \tilde{G}_{b\{kB-1\}}(\Delta\omega) \\ \hline \tilde{G}_{b\{kB\}}(\Delta\omega) \\ \hline \tilde{G}_{b\{kB+1\}}(\Delta\omega) \\ \hline \tilde{G}_{t\{kB\}}(\Delta\omega) \end{pmatrix} \tag{3.5.1}$$

where the matrix concerning the generalized mechanical impedances is

$$Z_{\{kB\}}(\Delta\omega) = \tag{3.5.2}$$

$$\left(\begin{array}{c|c|c|c} Z_{bb\{kB-1\}}(\Delta\omega) & 0 & 0 & Z^{-}_{bt\{kB\}}(\Delta\omega) \\ \hline 0 & Z_{bb\{kB\}}(\Delta\omega) & 0 & Z^{0}_{bt\{kB\}}(\Delta\omega) \\ \hline 0 & 0 & Z_{bb\{kB+1\}}(\Delta\omega) & Z^{+}_{bt\{kB\}}(\Delta\omega) \\ \hline Z^{-}_{tb\{kB-1\}}(\Delta\omega) & Z^{0}_{tb\{kB\}}(\Delta\omega) & Z^{+}_{tb\{kB+1\}}(\Delta\omega) & Z_{tt\{kB\}}(\Delta\omega) \end{array}\right)$$

Solving (3.5.1) yields

$$\begin{pmatrix} \tilde{Q}_{b\{kB-1\}}(\Delta\omega) \\ \hline \tilde{Q}_{b\{kB\}}(\Delta\omega) \\ \hline \tilde{Q}_{b\{kB+1\}}(\Delta\omega) \\ \hline \tilde{Q}_{t\{kB\}}(\Delta\omega) \end{pmatrix} = H_{\{kB\}}(\Delta\omega) \begin{pmatrix} \tilde{G}_{b\{kB-1\}}(\Delta\omega) \\ \hline \tilde{G}_{b\{kB\}}(\Delta\omega) \\ \hline \tilde{G}_{b\{kB+1\}}(\Delta\omega) \\ \hline \tilde{G}_{t\{kB\}}(\Delta\omega) \end{pmatrix} \tag{3.5.3}$$

where the transfer function matrix is determined as the inverted generalized mechanical impedance matrix defined in (3.5.3), i.e.

$$H_{\{kB\}}(\Delta\omega) = Z^{-1}_{\{kB\}}(\Delta\omega) \tag{3.5.4}$$

For the sake of completeness, concerning wind turbines with more than 3 blades, (3.4.20) concerning blade harmonics that are not coupled with any tower harmonics yields

$$\tilde{Q}_{\{n\}}(\Delta\omega) = H_{\{n\}}(\Delta\omega)\, \tilde{G}_{\{n\}}(\Delta\omega) \tag{3.5.5}$$

where the transfer function matrix is simply

$$H_{\{n\}}(\Delta\omega) = Z^{-1}_{bb\{n\}}(\Delta\omega) \tag{3.5.6}$$

The transfer functions derived so far in this section concerning orders of harmonics coupling blades and tower are the transfer function matrix summing blade root loads (3.2.5), the transfer function matrix from summed blade root loads to generalized tower loads (3.3.2), and the central transfer function matrix from generalized loads to modal amplitudes (3.5.3).

Those transfer functions are combined in the block diagram figure 3.5.1, thus illustrating the total transfer function matrix from pure external single blade loads to modal amplitudes of blade modes as well as tower modes.

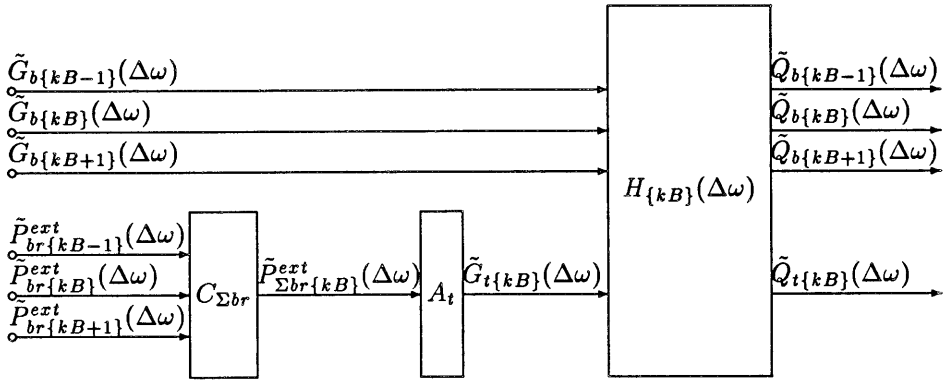

Figure 3.5.1. Block diagram of the transfer function matrix $H^{ext}_{\{kB\}}(\Delta\omega)$ from external blade loads to modal amplitudes.

The only inputs to the transfer function matrix are amplitudes of harmonics of external single blade loads. That ensures that the transfer function matrix can be used along with the cross power spectrum matrix between these inputs to determine the power spectra of the outputs. The transfer function matrix $H^{ext}_{\{kB\}}(\Delta\omega)$ is defined according to figure 3.5.1 by

$$\begin{pmatrix} \tilde{Q}_{b\{kB-1\}}(\Delta\omega) \\ \hline \tilde{Q}_{b\{kB\}}(\Delta\omega) \\ \hline \tilde{Q}_{b\{kB+1\}}(\Delta\omega) \\ \hline \tilde{Q}_{t\{kB\}}(\Delta\omega) \end{pmatrix} = H^{ext}_{\{kB\}}(\Delta\omega) \begin{pmatrix} \tilde{G}_{b\{kB-1\}}(\Delta\omega) \\ \hline \tilde{G}_{b\{kB\}}(\Delta\omega) \\ \hline \tilde{G}_{b\{kB+1\}}(\Delta\omega) \\ \hline \tilde{P}^{ext}_{br\{kB-1\}}(\Delta\omega) \\ \hline \tilde{P}^{ext}_{br\{kB\}}(\Delta\omega) \\ \hline \tilde{P}^{ext}_{br\{kB+1\}}(\Delta\omega) \end{pmatrix} \tag{3.5.7}$$

Now each row of $H^{ext}_{\{kB\}}(\Delta\omega)$ determines an amplitude of a harmonic of a modal amplitude related to either blade or tower. The inputs are integrals of amplitudes of harmonics of wind speed in the similar forms (3.1.2) and (3.2.3).

Thus, the remaining problem is simply to determine $H^{ext}_{\{kB\}}(\Delta\omega)$ using only the transfer functions defined in figure 3.5.1. Inspecting figure 3.5.1 the transfer function matrix $H_{\{kB\}}(\Delta\omega)$ must be separated into a generalized blade loads input part and a generalized tower loads input part, i.e.

$$H_{\{kB\}}(\Delta\omega) = \left(\; H_{\{kB\}}[\tilde{G}_b](\Delta\omega) \;\middle|\; H_{\{kB\}}[\tilde{G}_t](\Delta\omega) \; \right) \tag{3.5.8}$$

in which the sub matrices $H_{\{kB\}}[\tilde{G}_b](\Delta\omega)$ and $H_{\{kB\}}[\tilde{G}_t](\Delta\omega)$ are defined according to

$$\left(\begin{array}{c} \tilde{Q}_{b\{kB-1\}}(\Delta\omega) \\ \hline \tilde{Q}_{b\{kB\}}(\Delta\omega) \\ \hline \tilde{Q}_{b\{kB+1\}}(\Delta\omega) \\ \hline \tilde{Q}_{t\{kB\}}(\Delta\omega) \end{array} \right) = H_{\{kB\}}[\tilde{G}_b](\Delta\omega) \left(\begin{array}{c} \tilde{G}_{b\{kB-1\}}(\Delta\omega) \\ \hline \tilde{G}_{b\{kB\}}(\Delta\omega) \\ \hline \tilde{G}_{b\{kB+1\}}(\Delta\omega) \end{array} \right) + H_{\{kB\}}[\tilde{G}_t](\Delta\omega)\, \tilde{G}_{t\{kB\}}(\Delta\omega) \tag{3.5.9}$$

Inserting (3.3.2) and subsequently (3.2.5) in (3.5.9) yields

$$\left(\begin{array}{c} \tilde{Q}_{b\{kB-1\}}(\Delta\omega) \\ \hline \tilde{Q}_{b\{kB\}}(\Delta\omega) \\ \hline \tilde{Q}_{b\{kB+1\}}(\Delta\omega) \\ \hline \tilde{Q}_{t\{kB\}}(\Delta\omega) \end{array} \right) = \tag{3.5.10}$$

$$H_{\{kB\}}[\tilde{G}_b](\Delta\omega) \left(\begin{array}{c} \tilde{G}_{b\{kB-1\}}(\Delta\omega) \\ \hline \tilde{G}_{b\{kB\}}(\Delta\omega) \\ \hline \tilde{G}_{b\{kB+1\}}(\Delta\omega) \end{array} \right) +$$

$$H_{\{kB\}}[\tilde{G}_t](\Delta\omega)\, A_t\, C_{\Sigma br} \left(\begin{array}{c} \tilde{P}^{ext}_{br\{kB-1\}}(\Delta\omega) \\ \hline \tilde{P}^{ext}_{br\{kB\}}(\Delta\omega) \\ \hline \tilde{P}^{ext}_{br\{kB+1\}}(\Delta\omega) \end{array} \right)$$

which is equvivalent to the definition (3.5.7) substituting

$$H^{ext}_{\{kB\}}(\Delta\omega) = \left(\; H_{\{kB\}}[\tilde{G}_b](\Delta\omega) \;\middle|\; H_{\{kB\}}[\tilde{G}_t](\Delta\omega)\, A_t\, C_{\Sigma br} \; \right) \tag{3.5.11}$$

4 Internal elastic loads

The internal elastic loads in sections of blades and tower are determined in this section, using the modal amplitudes determined in section 3. Computing internal loads in a structure, various methods are discussed by Hurty and Rubinstein [8].

The method refered to as Method 2 in [8] is used here because it gives proper results even with very few modes. This method make use of the load equilibria in any section of the sturcture. The internal elastic loads pr. unit length in the section is determined as the sum of other loads, i.e. external loads, inertial loads, damping loads, and eventual geometric stiffness according to

$$f_z(t,z) = f_z^{ext}(t,z) - \sum_{i=1}^{n} m_i(z)\,\ddot{q}_i(t) - \sum_{i=1}^{n} c_i(z)\,\dot{q}_i(t) - \sum_{i=1}^{n} k_i(z)\,q_i(t) \quad (4.1)$$

Now, consider a cantilever beam with the length L fastened at $z = 0$ and with a load pr. unit length according to (4.1). The internal elastic moments and forces in section z_0 of the beam are then determined according to

$$m(t,z_0) = \int_{z_0}^{L} (z - z_0)\, f_z(t,z)\, dz \quad (4.2)$$

$$f(t,z_0) = \int_{z_0}^{L} f_z(t,z)\, dz \quad (4.3)$$

4.1 Internal elastic blade loads

Establishing the load equilibria as (4.1) in the sections of the rotating blade beams and using load integrals similar with (4.2) and (4.3), the internal elastic moments and forces in the blade section z_{bs} can be written in the general form

$$
\begin{aligned}
& p_{bs}(t,b,z_{bs}) \; = \qquad (4.1.1)\\
& \int_{z_{bs}}^{L} \Psi_{bs}(z_{bs},z_b)\; v(t,b,z_b)\; dz_b \\
& - m_{bsb}(z_{bs})\; \ddot{q}_b(t,b) \; - \; c_{bsb}(z_{bs})\; \dot{q}_b(t,b) \; - \; k_{bsb}(z_{bs})\; q_b(t,b) \\
& - \left(m_{bst}(z_{bs}) \; + \; m_{bst}^{\cos}(z_{bs})\; \cos\theta(t,b) \; + \; m_{bst}^{\sin}(z_{bs})\; \sin\theta(t,b)\right)\; \ddot{q}_t(t) \\
& - \left(c_{bst}(z_{bs}) \; + \; c_{bst}^{\cos}(z_{bs})\; \cos\theta(t,b) \; + \; c_{bst}^{\sin}(z_{bs})\; \sin\theta(t,b)\right)\; \dot{q}_t(t) \\
& - \left(k_{bst}(z_{bs}) \; + \; k_{bst}^{\cos}(z_{bs})\; \cos\theta(t,b) \; + \; k_{bst}^{\sin}(z_{bs})\; \sin\theta(t,b)\right)\; q_t(t)
\end{aligned}
$$

Denoting the external term of the loads

$$
p_{bs}^{ext}(t,b,z_{bs}) \; = \; \int_{z_{bs}}^{L} \Psi_{bs}(z_{bs},z_b)\; v(t,b,z_b)\; dz_b \qquad (4.1.2)
$$

and using the transformations in table 2.1, (4.1.2) is replaced by

$$
\begin{aligned}
\tilde{P}_{bs\{kB-1\}}(\Delta\omega,z_{bs}) \; &= \; \tilde{P}_{bs\{kB-1\}}^{ext}(\Delta\omega,z_{bs}) \\
&- \; Z_{bsb\{kB-1\}}(\Delta\omega,z_{bs})\; \tilde{Q}_{b\{kB-1\}}(\Delta\omega) \\
&- \; Z_{bst\{kB\}}^{-}(\Delta\omega,z_{bs})\; \tilde{Q}_{t\{kB\}}(\Delta\omega) \qquad (4.1.3)
\end{aligned}
$$

if $n = kB - 1$,

$$
\begin{aligned}
\tilde{P}_{bs\{kB\}}(\Delta\omega,z_{bs}) \; &= \; \tilde{P}_{bs\{kB\}}^{ext}(\Delta\omega,z_{bs}) \\
&- \; Z_{bsb\{kB\}}(\Delta\omega,z_{bs})\; \tilde{Q}_{b\{kB\}}(\Delta\omega) \\
&- \; Z_{bst\{kB\}}^{0}(\Delta\omega,z_{bs})\; \tilde{Q}_{t\{kB\}}(\Delta\omega) \qquad (4.1.4)
\end{aligned}
$$

if $n = kB$,

$$
\begin{aligned}
\tilde{P}_{bs\{kB+1\}}(\Delta\omega,z_{bs}) \; &= \; \tilde{P}_{bs\{kB+1\}}^{ext}(\Delta\omega,z_{bs}) \\
&- \; Z_{bsb\{kB+1\}}(\Delta\omega,z_{bs})\; \tilde{Q}_{b\{kB+1\}}(\Delta\omega) \\
&- \; Z_{bst\{kB\}}^{+}(\Delta\omega,z_{bs})\; \tilde{Q}_{t\{kB\}}(\Delta\omega) \qquad (4.1.5)
\end{aligned}
$$

if $n = kB + 1$, and

$$\begin{aligned} \tilde{P}_{bs\{n\}}(\Delta\omega, z_{bs}) &= \tilde{P}^{ext}_{bs\{n\}}(\Delta\omega, z_{bs}) \\ &- Z_{bsb\{n\}}(\Delta\omega, z_{bs})\ \tilde{Q}_{b\{n\}}(\Delta\omega) \end{aligned} \tag{4.1.6}$$

otherwise.

The Fourier transforms of the amplitudes of harmonics of the external loads (4.1.2) used in (4.1.3), (4.1.4), (4.1.5), and (4.1.6) are determined by

$$\tilde{P}^{ext}_{bs\{n\}}(\Delta\omega, z_{bs}) = \int_{z_{bs}}^{L} \Psi_{bs}(z_{bs}, z_b)\ \tilde{V}_{\{n\}}(t, z_b)\ dz_b \tag{4.1.7}$$

and the mechanical impedances are

$$Z_{bsb}(\omega, z_{bs}) = (j\omega)^2\ m_{bsb}(z_{bs}) + j\omega\ c_{bsb}(z_{bs}) + k_{bsb}(z_{bs}) \tag{4.1.8}$$

$$\begin{aligned} Z^{-}_{bst}(\omega, z_{bs}) &= \frac{1}{2}\ \left((j\omega)^2\ m^{\cos}_{bst}(z_{bs}) + j\omega\ c^{\cos}_{bst}(z_{bs}) + k^{\cos}_{bst}(z_{bs})\right) \\ &+ \frac{j}{2}\ \left((j\omega)^2\ m^{\sin}_{bst}(z_{bs}) + j\omega\ c^{\sin}_{bst}(z_{bs}) + k^{\sin}_{bst}(z_{bs})\right) \end{aligned} \tag{4.1.9}$$

$$Z^{0}_{bst}(\omega, z_{bs}) = (j\omega)^2\ m_{bst}(z_{bs}) + j\omega\ c_{bst}(z_{bs}) + k_{bst}(z_{bs}) \tag{4.1.10}$$

$$\begin{aligned} Z^{+}_{bst}(\omega, z_{bs}) &= \frac{1}{2}\ \left((j\omega)^2\ m^{\cos}_{bst}(z_{bs}) + j\omega\ c^{\cos}_{bst}(z_{bs}) + k^{\cos}_{bst}(z_{bs})\right) \\ &- \frac{j}{2}\ \left((j\omega)^2\ m^{\sin}_{bst}(z_{bs}) + j\omega\ c^{\sin}_{bst}(z_{bs}) + k^{\sin}_{bst}(z_{bs})\right) \end{aligned} \tag{4.1.11}$$

shortened according to (3.4.9).

Using the diagonal unit matrix E to define the transfer functions

$$H_{bs\{kB-1\}}(\Delta\omega, z_{bs}) = \tag{4.1.12}$$
$$\left(E \,\middle|\, -Z_{bsb\{kB-1\}}(\Delta\omega, z_{bs}) \,\middle|\, -Z^{-}_{bst\{kB\}}(\Delta\omega, z_{bs}) \right)$$

$$H_{bs\{kB\}}(\Delta\omega, z_{bs}) = \tag{4.1.13}$$
$$\left(E \,\middle|\, -Z_{bsb\{kB\}}(\Delta\omega, z_{bs}) \,\middle|\, -Z^{0}_{bst\{kB\}}(\Delta\omega, z_{bs}) \right)$$

$$H_{bs\{kB+1\}}(\Delta\omega, z_{bs}) = \tag{4.1.14}$$

$$\left(E \;\middle|\; -Z_{bsb\{kB+1\}}(\Delta\omega, z_{bs}) \;\middle|\; -Z^{+}_{bst\{kB\}}(\Delta\omega, z_{bs}) \right)$$

$$H_{bs\{n\}}(\Delta\omega, z_{bs}) = \left(E \;\middle|\; -Z_{bsb\{n\}}(\Delta\omega, z_{bs}) \right) \tag{4.1.15}$$

(4.1.3), (4.1.4), (4.1.5), and (4.1.6) respectively yields the output amplitudes concerning internal moments and forces expressed as

$$\tilde{P}_{bs\{kB-1\}}(\Delta\omega, z_{bs}) = H_{bs\{kB-1\}}(\Delta\omega, z_{bs}) \begin{pmatrix} \tilde{P}^{ext}_{bs\{kB-1\}}(\Delta\omega, z_{bs}) \\ \hline \tilde{Q}_{b\{kB-1\}}(\Delta\omega) \\ \hline \tilde{Q}_{t\{kB\}}(\Delta\omega) \end{pmatrix} \tag{4.1.16}$$

$$\tilde{P}_{bs\{kB\}}(\Delta\omega, z_{bs}) = H_{bs\{kB\}}(\Delta\omega, z_{bs}) \begin{pmatrix} \tilde{P}^{ext}_{bs\{kB\}}(\Delta\omega, z_{bs}) \\ \hline \tilde{Q}_{b\{kB\}}(\Delta\omega) \\ \hline \tilde{Q}_{t\{kB\}}(\Delta\omega) \end{pmatrix} \tag{4.1.17}$$

$$\tilde{P}_{bs\{kB+1\}}(\Delta\omega, z_{bs}) = H_{bs\{kB+1\}}(\Delta\omega, z_{bs}) \begin{pmatrix} \tilde{P}^{ext}_{bs\{kB+1\}}(\Delta\omega, z_{bs}) \\ \hline \tilde{Q}_{b\{kB+1\}}(\Delta\omega) \\ \hline \tilde{Q}_{t\{kB\}}(\Delta\omega) \end{pmatrix} \tag{4.1.18}$$

$$\tilde{P}_{bs\{n\}}(\Delta\omega, z_{bs}) = H_{bs\{n\}}(\Delta\omega, z_{bs}) \begin{pmatrix} \tilde{P}^{ext}_{bs\{n\}}(\Delta\omega, z_{bs}) \\ \hline \tilde{Q}_{b\{n\}}(\Delta\omega) \end{pmatrix} \tag{4.1.19}$$

Thus, using the transfer function matrix $H^{ext}_{\{kB\}}(\Delta\omega)$ the amplitudes of harmonics of the blade section loads $\tilde{P}_{bs\{kB-1\}}(\Delta\omega, z_{bs})$, $\tilde{P}_{bs\{kB\}}(\Delta\omega, z_{bs})$, and $\tilde{P}_{bs\{kB+1\}}(\Delta\omega, z_{bs})$ are determined as illustrated in the block diagram in figure 4.1.1.

Inspecting figure 4.1.1, the conclusive transfer function matrix $H^{ext}_{bs\{p\}}(\Delta\omega, z_{bs})$ determining the amplitudes of the p'th harmonics of the blade section loads from amplitudes of harmonics of only external blade loads is defined as

$$\tilde{P}_{bs\{p\}}(\Delta\omega, z_{bs}) = H^{ext}_{bs\{p\}}(\Delta\omega, z_{bs}) \begin{pmatrix} \tilde{P}^{ext}_{bs\{p\}}(\Delta\omega, z_{bs}) \\ \hline \tilde{G}_{b\{kB-1\}}(\Delta\omega) \\ \hline \tilde{G}_{b\{kB\}}(\Delta\omega) \\ \hline \tilde{G}_{b\{kB+1\}}(\Delta\omega) \\ \hline \tilde{P}^{ext}_{br\{kB-1\}}(\Delta\omega) \\ \hline \tilde{P}^{ext}_{br\{kB\}}(\Delta\omega) \\ \hline \tilde{P}^{ext}_{br\{kB+1\}}(\Delta\omega) \end{pmatrix} \tag{4.1.20}$$

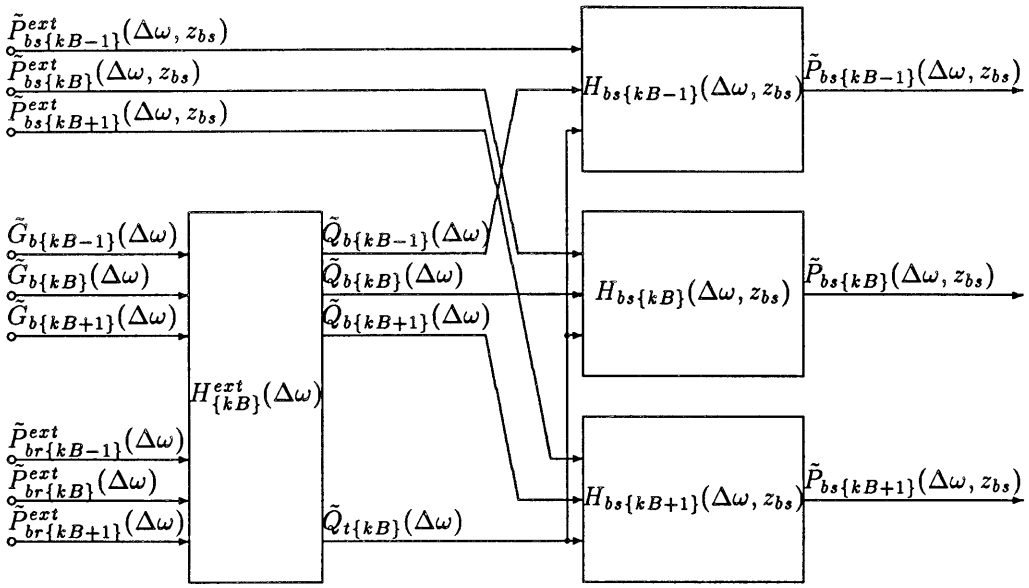

Figure 4.1.1. Block diagram determining the amplitudes of harmonics of the blade section loads $\tilde{P}_{bs\{p\}}(\Delta\omega, z_{bs})$ of orders $p = kB - 1$, kB, and $kB + 1$ from amplitudes of harmonics of only external blade loads.

where the harmonic order p can be

$$p = \begin{cases} kB - 1 \\ kB \\ kB + 1 \end{cases} \tag{4.1.21}$$

Deriving $H^{ext}_{bs\{p\}}(\Delta\omega, z_{bs})$, $H^{ext}_{\{kB\}}(\Delta\omega)$ is separated into

$$H^{ext}_{\{kB\}}(\Delta\omega) = \begin{pmatrix} \dfrac{H^{ext}_{\{kB\}}[\tilde{Q}_{b\{kB-1\}}](\Delta\omega)}{H^{ext}_{\{kB\}}[\tilde{Q}_{b\{kB\}}](\Delta\omega)} \\ \dfrac{H^{ext}_{\{kB\}}[\tilde{Q}_{b\{kB+1\}}](\Delta\omega)}{H^{ext}_{\{kB\}}[\tilde{Q}_{t\{kB\}}](\Delta\omega)} \end{pmatrix} \tag{4.1.22}$$

in which the sub transfer function $H^{ext}_{\{kB\}}[\tilde{Q}_{b\{p\}}](\Delta\omega)$ of any of the orders p in (4.1.21) determines $\tilde{Q}_{b\{p\}}(\Delta\omega)$ according to

$$\tilde{Q}_{b\{p\}}(\Delta\omega) \;=\; H^{ext}_{\{kB\}}[\tilde{Q}_{b\{p\}}](\Delta\omega) \left(\begin{array}{c} \tilde{G}_{b\{kB-1\}}(\Delta\omega) \\ \hline \tilde{G}_{b\{kB\}}(\Delta\omega) \\ \hline \tilde{G}_{b\{kB+1\}}(\Delta\omega) \\ \hline \tilde{P}^{ext}_{br\{kB-1\}}(\Delta\omega) \\ \hline \tilde{P}^{ext}_{br\{kB\}}(\Delta\omega) \\ \hline \tilde{P}^{ext}_{br\{kB+1\}}(\Delta\omega) \end{array} \right) \tag{4.1.23}$$

and likewise, $H^{ext}_{\{kB\}}[\tilde{Q}_{t\{kB\}}](\Delta\omega)$ determines $\tilde{Q}_{t\{kB\}}(\Delta\omega)$ according to

$$\tilde{Q}_{t\{kB\}}(\Delta\omega) \;=\; H^{ext}_{\{kB\}}[\tilde{Q}_{t\{kB\}}](\Delta\omega) \left(\begin{array}{c} \tilde{G}_{b\{kB-1\}}(\Delta\omega) \\ \hline \tilde{G}_{b\{kB\}}(\Delta\omega) \\ \hline \tilde{G}_{b\{kB+1\}}(\Delta\omega) \\ \hline \tilde{P}^{ext}_{br\{kB-1\}}(\Delta\omega) \\ \hline \tilde{P}^{ext}_{br\{kB\}}(\Delta\omega) \\ \hline \tilde{P}^{ext}_{br\{kB+1\}}(\Delta\omega) \end{array} \right) \tag{4.1.24}$$

According to the definition (4.1.20) of $H^{ext}_{bs\{p\}}(\Delta\omega, z_{bs})$, insertion of (4.1.23) and (4.1.24) in (4.1.3), (4.1.4), and (4.1.5) respectively yields the common formula

$$H^{ext}_{bs\{p\}}(\Delta\omega, z_{bs}) \;=\; \left(\; E \;\middle|\; H^{Q}_{bs\{p\}}(\Delta\omega, z_{bs}) \; \right) \tag{4.1.25}$$

with the specific influence due to modal amplitudes determined by

$$\begin{aligned} H^{Q}_{bs\{kB-1\}}(\Delta\omega, z_{bs}) \;=\; & - Z_{bsb\{kB-1\}}(\Delta\omega, z_{bs})\; H^{ext}_{\{kB\}}[\tilde{Q}_{b\{kB-1\}}](\Delta\omega) \\ & - Z^{-}_{bst\{kB\}}(\Delta\omega, z_{bs})\; H^{ext}_{\{kB\}}[\tilde{Q}_{t\{kB\}}](\Delta\omega) \end{aligned} \tag{4.1.26}$$

$$\begin{aligned} H^{Q}_{bs\{kB\}}(\Delta\omega, z_{bs}) \;=\; & - Z_{bsb\{kB\}}(\Delta\omega, z_{bs})\; H^{ext}_{\{kB\}}[\tilde{Q}_{b\{kB\}}](\Delta\omega) \\ & - Z^{0}_{bst\{kB\}}(\Delta\omega, z_{bs})\; H^{ext}_{\{kB\}}[\tilde{Q}_{t\{kB\}}](\Delta\omega) \end{aligned} \tag{4.1.27}$$

$$\begin{aligned} H^{Q}_{bs\{kB+1\}}(\Delta\omega, z_{bs}) \;=\; & - Z_{bsb\{kB+1\}}(\Delta\omega, z_{bs})\; H^{ext}_{\{kB\}}[\tilde{Q}_{b\{kB+1\}}](\Delta\omega) \\ & - Z^{+}_{bst\{kB\}}(\Delta\omega, z_{bs})\; H^{ext}_{\{kB\}}[\tilde{Q}_{t\{kB\}}](\Delta\omega) \end{aligned} \tag{4.1.28}$$

4.2 Internal elastic tower loads

Establishing the load equilibria as (4.1) in the sections of the tower beam and using load integrals similar with (4.2) and (4.3), the internal elastic moments and forces in the tower section z_{ts} can be written in the general form

$$
\begin{aligned}
& p_{ts}(t, z_{ts}) \; = \qquad\qquad (4.2.1)\\
& A_{ts}(z_{ts})\; p^{ext}_{\Sigma br}(t)\\
& - \sum_{b=0}^{B-1} \left(m_{tsb}(z_{ts}) \;+\; m^{\cos}_{tsb}(z_{ts})\; \cos\theta(t,b) \;+\; m^{\sin}_{tsb}(z_{ts})\; \sin\theta(t,b)\right)\; \ddot{q}_b(t,b)\\
& - \sum_{b=0}^{B-1} \left(c_{tsb}(z_{ts}) \;+\; c^{\cos}_{tsb}(z_{ts})\; \cos\theta(t,b) \;+\; c^{\sin}_{tsb}(z_{ts})\; \sin\theta(t,b)\right)\; \dot{q}_b(t,b)\\
& - \sum_{b=0}^{B-1} \left(k_{tsb}(z_{ts}) \;+\; k^{\cos}_{tsb}(z_{ts})\; \cos\theta(t,b) \;+\; k^{\sin}_{tsb}(z_{ts})\; \sin\theta(t,b)\right)\; q_b(t,b)\\
& - m_{tst}(z_{ts})\; \ddot{q}_t(t) \;+\; c_{tst}(z_{ts})\; \dot{q}_t(t) \;+\; k_{tst}(z_{ts})\; q_t(t)
\end{aligned}
$$

where $p^{ext}_{\Sigma br}(t)$ is defined in (3.2.2), and $A_{ts}(z_{ts})$ determines the transformation of the summed blade root moments and forces to moments and forces at the tower coordinate $(0, 0, z_{ts})$.

Using the transformations in table 2.1 (4.2.2) is replaced by

$$
\begin{aligned}
\tilde{P}_{ts\{kB\}}(\Delta\omega, z_{ts}) \;=\; & A_{ts}(z_{ts})\; \tilde{P}^{ext}_{\Sigma br\{kB\}}(\Delta\omega)\\
& - Z^{-}_{tsb\{kB-1\}}(\Delta\omega, z_{ts})\; \tilde{Q}_{b\{kB-1\}}(\Delta\omega)\\
& - Z^{0}_{tsb\{kB\}}(\Delta\omega, z_{ts})\; \tilde{Q}_{b\{kB\}}(\Delta\omega)\\
& - Z^{+}_{tsb\{kB+1\}}(\Delta\omega, z_{ts})\; \tilde{Q}_{b\{kB+1\}}(\Delta\omega)\\
& - Z_{tst\{kB\}}(\Delta\omega, z_{ts})\; \tilde{Q}_{t\{kB\}}(\Delta\omega) \qquad (4.2.2)
\end{aligned}
$$

where the mechanical impedances

$$
\begin{aligned}
Z^{-}_{tsb}(\omega, z_{ts}) \;=\; & \frac{B}{2}\; \left((j\omega)^2\; m^{\cos}_{tsb}(z_{ts}) \;+\; j\omega\; c^{\cos}_{tsb}(z_{ts}) \;+\; k^{\cos}_{tsb}(z_{ts})\right)\\
& - \frac{jB}{2}\; \left((j\omega)^2\; m^{\sin}_{tsb}(z_{ts}) \;+\; j\omega\; c^{\sin}_{tsb}(z_{ts}) \;+\; k^{\sin}_{tsb}(z_{ts})\right) \qquad (4.2.3)
\end{aligned}
$$

$$
Z^{0}_{tsb}(\omega, z_{ts}) \;=\; B\left((j\omega)^2\; m_{tsb}(z_{ts}) \;+\; j\omega\; c_{tsb}(z_{ts}) \;+\; k_{tsb}(z_{ts})\right) \qquad (4.2.4)
$$

$$Z^{+}_{tsb}(\omega, z_{ts}) = \frac{B}{2}\left((j\omega)^2\, m^{\cos}_{tsb}(z_{ts}) + j\omega\, c^{\cos}_{tsb}(z_{ts}) + k^{\cos}_{tsb}(z_{ts})\right) + \frac{jB}{2}\left((j\omega)^2\, m^{\sin}_{tsb}(z_{ts}) + j\omega\, c^{\sin}_{tsb}(z_{ts}) + k^{\sin}_{tsb}(z_{ts})\right) \quad (4.2.5)$$

$$Z_{tst}(\omega, z_{ts}) = (j\omega)^2\, m_{tst}(z_{ts}) + j\omega\, c_{tst}(z_{ts}) + k_{tst}(z_{ts}) \quad (4.2.6)$$

are shortened according to (3.4.9).

(4.2.2) can be written in the transfer form

$$\tilde{P}_{ts\{kB\}}(\Delta\omega, z_{ts}) = H_{ts\{kB\}}(\Delta\omega, z_{ts}) \begin{pmatrix} \tilde{P}^{ext}_{\Sigma br\{kB\}}(\Delta\omega) \\ \hline \tilde{Q}_{b\{kB-1\}}(\Delta\omega) \\ \hline \tilde{Q}_{b\{kB\}}(\Delta\omega) \\ \hline \tilde{Q}_{b\{kB+1\}}(\Delta\omega) \\ \hline \tilde{Q}_{t\{kB\}}(\Delta\omega) \end{pmatrix} \quad (4.2.7)$$

where the transfer function

$$H_{ts\{kB\}}(\Delta\omega, z_{ts}) = \left(A_{ts}(z_{ts}) \,\middle|\, -Z_{ts\{kB\}}(\Delta\omega, z_{ts}) \right) \quad (4.2.8)$$

substituting

$$Z_{ts\{kB\}}(\Delta\omega, z_{ts}) = \quad (4.2.9)$$
$$\left(Z^{-}_{tsb\{kB-1\}}(\Delta\omega, z_{ts}) \,\middle|\, Z^{0}_{tsb\{kB\}}(\Delta\omega, z_{ts}) \,\middle|\, Z^{+}_{tsb\{kB+1\}}(\Delta\omega, z_{ts}) \,\middle|\, Z_{tst\{kB\}}(\Delta\omega, z_{ts}) \right)$$

Thus, using the transfer function of the amplitudes of harmonics of the modal amplitudes $H^{ext}_{\{kB\}}(\Delta\omega)$ according to (3.5.7), and using the constant complex transfer of the amplitudes of harmonics of the summed blade root loads $C_{\Sigma br}$ according to (3.2.5), the amplitudes of harmonics of the tower section loads $\tilde{P}_{ts\{kB\}}(\Delta\omega, z_{ts})$ are determined as illustrated in the block diagram in figure 4.2.1.

Inspecting figure 4.2.1, the conclusive transfer functions $H^{ext}_{ts\{kB\}}(\Delta\omega, z_{ts})$ determining the amplitudes of the kB'th harmonics of the tower section loads from amplitudes of harmonics of only external blade loads are defined according to

$$\tilde{P}_{ts\{kB\}}(\Delta\omega, z_{ts}) = H^{ext}_{ts\{kB\}}(\Delta\omega, z_{ts}) \begin{pmatrix} \tilde{G}_{b\{kB-1\}}(\Delta\omega) \\ \hline \tilde{G}_{b\{kB\}}(\Delta\omega) \\ \hline \tilde{G}_{b\{kB+1\}}(\Delta\omega) \\ \hline \tilde{P}^{ext}_{br\{kB-1\}}(\Delta\omega) \\ \hline \tilde{P}^{ext}_{br\{kB\}}(\Delta\omega) \\ \hline \tilde{P}^{ext}_{br\{kB+1\}}(\Delta\omega) \end{pmatrix} \quad (4.2.10)$$

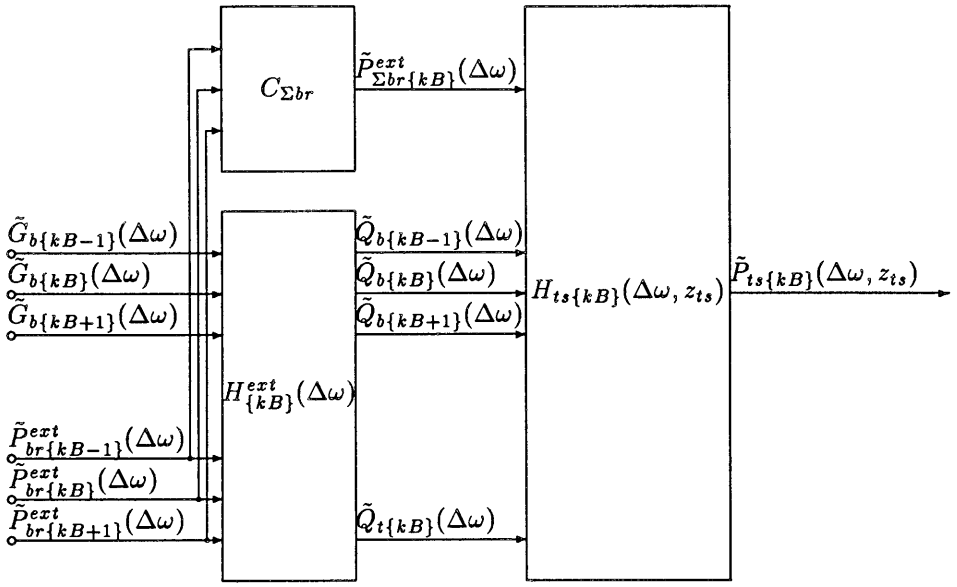

Figure 4.2.1. Block diagram determining the amplitudes of harmonics of the tower section loads $\tilde{P}_{ts\{kB\}}(\Delta\omega, z_{ts})$ from amplitudes of harmonics of only external blade loads.

In order to derive $H^{ext}_{ts\{kB\}}(\Delta\omega, z_{ts})$, (4.2.8) is inserted in (4.2.7) yielding

$$\begin{aligned}\tilde{P}_{ts\{kB\}}(\Delta\omega, z_{ts}) &= A_{ts}(z_{ts})\ \tilde{P}^{ext}_{\Sigma br\{kB\}}(\Delta\omega) \\ &\quad - Z_{ts\{kB\}}(\Delta\omega, z_{ts}) \begin{pmatrix} \tilde{Q}_{b\{kB-1\}}(\Delta\omega) \\ \tilde{Q}_{b\{kB\}}(\Delta\omega) \\ \tilde{Q}_{b\{kB+1\}}(\Delta\omega) \\ \tilde{Q}_{t\{kB\}}(\Delta\omega) \end{pmatrix}\end{aligned} \tag{4.2.11}$$

Inserting (3.2.5), (4.2.11) yields

$$\begin{aligned}\tilde{P}_{ts\{kB\}}(\Delta\omega, z_{ts}) &= A_{ts}(z_{ts})\ C_{\Sigma br} \begin{pmatrix} \tilde{P}^{ext}_{br\{kB-1\}}(\Delta\omega) \\ \tilde{P}^{ext}_{br\{kB\}}(\Delta\omega) \\ \tilde{P}^{ext}_{br\{kB+1\}}(\Delta\omega) \end{pmatrix} \\ &\quad - Z_{ts\{kB\}}(\Delta\omega, z_{ts}) \begin{pmatrix} \tilde{Q}_{b\{kB-1\}}(\Delta\omega) \\ \tilde{Q}_{b\{kB\}}(\Delta\omega) \\ \tilde{Q}_{b\{kB+1\}}(\Delta\omega) \\ \tilde{Q}_{t\{kB\}}(\Delta\omega) \end{pmatrix}\end{aligned} \tag{4.2.12}$$

Separating (3.5.7) into

$$\begin{pmatrix} \frac{\tilde{Q}_{b\{kB-1\}}(\Delta\omega)}{\tilde{Q}_{b\{kB\}}(\Delta\omega)} \\ \frac{\tilde{Q}_{b\{kB+1\}}(\Delta\omega)}{\tilde{Q}_{t\{kB\}}(\Delta\omega)} \end{pmatrix} = H^{ext}_{\{kB\}}[\tilde{G}_b](\Delta\omega) \begin{pmatrix} \frac{\tilde{G}_{b\{kB-1\}}(\Delta\omega)}{\tilde{G}_{b\{kB\}}(\Delta\omega)} \\ \frac{\tilde{G}_{b\{kB+1\}}(\Delta\omega)}{\tilde{G}_{b\{kB+1\}}(\Delta\omega)} \end{pmatrix}$$

$$+ H^{ext}_{\{kB\}}[\tilde{P}^{ext}_{br}](\Delta\omega) \begin{pmatrix} \frac{\tilde{P}^{ext}_{br\{kB-1\}}(\Delta\omega)}{\tilde{P}^{ext}_{br\{kB\}}(\Delta\omega)} \\ \frac{\tilde{P}^{ext}_{br\{kB+1\}}(\Delta\omega)}{\tilde{P}^{ext}_{br\{kB+1\}}(\Delta\omega)} \end{pmatrix} \quad (4.2.13)$$

and inserting this in (4.2.12), $H^{ext}_{ts\{kB\}}(\Delta\omega, z_{ts})$ match the definition (4.2.10) with

$$H^{ext}_{ts\{kB\}}(\Delta\omega, z_{ts}) = \left(H^{ext}_{ts\{kB\}}[\tilde{G}_b](\Delta\omega, z_{ts}) \,\middle|\, H^{ext}_{ts\{kB\}}[\tilde{P}^{ext}_{br}](\Delta\omega, z_{ts}) \right) \quad (4.2.14)$$

with the submatrices

$$H^{ext}_{ts\{kB\}}[\tilde{G}_b](\Delta\omega, z_{ts}) = - Z_{ts\{kB\}}(\Delta\omega, z_{ts})\, H^{ext}_{\{kB\}}[\tilde{G}_b](\Delta\omega) \quad (4.2.15)$$

and

$$H^{ext}_{ts\{kB\}}[\tilde{P}^{ext}_{br}](\Delta\omega, z_{ts}) = A_{ts}(z_{ts})\, C_{\Sigma br} - Z_{ts\{kB\}}(\Delta\omega, z_{ts})\, H^{ext}_{\{kB\}}[\tilde{P}^{ext}_{br}](\Delta\omega) \quad (4.2.16)$$

5 Deterministic response

In this section it is shown how to determine the deterministic parts of the internal elastic loads.

The time dependence of the deterministic inputs is determined only implicit through the time dependence of the azimuth position. Thus, the deterministic wind field $\underline{u}(z_r, \theta)$ has no explicit time parameter as the stochastic turbulence wind field $\underline{v}(t, z_r, \theta)$

Therefore, the deterministic blade variables are sums of harmonics

$$f(t,b) = \sum_{n=-\infty}^{\infty} \hat{f}_{\{n\}}(b)\, e^{jn\omega_0 t} \tag{5.1}$$

with *constant* amplitudes

$$\hat{f}_{\{n\}}(b) = e^{jn\theta_0(b)}\, \tilde{f}_{\{n\}} \tag{5.2}$$

The sum (5.1) is also a Fourier series with the Fourier coefficients $\hat{f}_{\{n\}}(b)$ determining the periodic time dependence corresponding to the period time of one rotation

$$T = 2\pi\, \omega_0 \tag{5.3}$$

According to Newland [7], the Fourier transform of the constant amplitude $\tilde{f}_{\{p\}}$ is

$$\tilde{F}_{\{p\}}(\Delta\omega) = \tilde{f}_{\{p\}}\, \delta(\Delta\omega) \tag{5.4}$$

where $\delta(\Delta\omega)$ is the delta function. Inserting (5.4) and the frequency

$$\Delta\omega = 0 \tag{5.5}$$

in the right column in table 2.1 and deviding by $\delta(0)$ yields relations between the deterministic Fourier coefficients that are similar with the relations between the stochastic Fourier transforms of amplitudes of harmonics with the simplification (5.5). Thus, the transfer functions derived in section 3 and section 4 can also be used to determine the deterministic amplitudes (i.e. Fourier coefficients) if (5.5) is inserted.

So far, only external *aero* loads have been included in the model. However, it is straight forward to extend the model with exitation from deterministic gravity loads and centrifugal loads as well. Thus, the amplitudes of harmonics of the determinsitic generalized blade loads are determined by

$$\tilde{g}_{b\{n\}} = \begin{cases} \int_0^L \Psi_b(z_b)\ \tilde{u}_{\{n\}}(z_b)\ dz_b\ +\ \tilde{g}_{b*\{n\}} & \text{if } -1 \leq n \leq 1 \\ \\ \int_0^L \Psi_b(z_b)\ \tilde{u}_{\{n\}}(z_b)\ dz_b & \text{otherwise} \end{cases} \tag{5.6}$$

where the integrals are obtained by (3.1.2) and the amplitudes $\tilde{g}_{b*\{n\}}$ are determined by the expansion of the generalized gravity and centrifugal blade load field experienced by the rotating blades

$$\underline{g}_{b*}(\theta) = \sum_{n=-1}^{1} \tilde{g}_{b*\{n\}}\ e^{jn\theta} \tag{5.7}$$

Using (3.3.2) and (3.2.5) the amplitudes of harmonics of the determinsitic generalized tower loads are determined as

$$\tilde{g}_{t\{kB\}} = \begin{cases} A_t\ C_{\Sigma br} \begin{pmatrix} \tilde{p}^{ext}_{br\{-1\}} \\ \hline \tilde{p}^{ext}_{br\{0\}} \\ \hline \tilde{p}^{ext}_{br\{1\}} \end{pmatrix} + \tilde{g}_{t*} & \text{if } k = 0 \\ \\ A_t\ C_{\Sigma br} \begin{pmatrix} \tilde{p}^{ext}_{br\{kB-1\}} \\ \hline \tilde{p}^{ext}_{br\{kB\}} \\ \hline \tilde{p}^{ext}_{br\{kB+1\}} \end{pmatrix} & \text{otherwise} \end{cases} \tag{5.8}$$

where $\tilde{g}_{t*}$ is the generalized tower gravity loads.

Now, (3.5.3) yields the Fourier coefficients of the deterministic modal amplitudes

$$\begin{pmatrix} \tilde{q}_{b\{kB-1\}} \\ \hline \tilde{q}_{b\{kB\}} \\ \hline \tilde{q}_{b\{kB+1\}} \\ \hline \tilde{q}_{t\{kB\}} \end{pmatrix} = H_{\{kB\}}(0) \begin{pmatrix} \tilde{g}_{b\{kB-1\}} \\ \hline \tilde{g}_{b\{kB\}} \\ \hline \tilde{g}_{b\{kB+1\}} \\ \hline \tilde{g}_{t\{kB\}} \end{pmatrix} \tag{5.9}$$

Likewise, the Fourier coefficients of the internal elastic loads are determined multiplying the tranfer functions in section 4 with appropriate Fourier coefficients corresponding to the aero, gravity and centrifugal loads.

Thus determining the Fourier coefficients of the internal elastic loads, the periodic sequence is determined versus time according to (5.1) and (5.2) or simply versus the azimuth angle according to

$$\underline{f}(\theta) = \sum_{n=-\infty}^{\infty} \tilde{f}_{\{n\}}\ e^{jn\theta} \tag{5.10}$$

which is expressed in reals according to Newland [7] as

$$\underline{f}(\theta) = \Re\left\{\tilde{f}_{\{0\}}\right\} + \sum_{n=1}^{\infty}\left(2\,\Re\left\{\tilde{f}_{\{n\}}\right\}\cos(n\theta) - 2\,\Im\left\{\tilde{f}_{\{n\}}\right\}\sin(n\theta)\right) \quad (5.11)$$

6 Stochastic response

This section aims at determining the power spectra of the modal amplitudes and the internal elastic loads. This task is separated into 3 steps.

The first step is to determine the cross power spectra between the generic amplitudes of harmonics of the *external single blade turbulence loads.* This step is based on the cross power spectra between the azimuth expansion coefficients of the *turbulence wind speed* which are determined in appendix C.

The next step is to determine the power spectrum of the amplitudes of harmonics of a response, utilizing the transfer functions between the generic amplitudes of harmonics of only external single blade loads and the response. Those transfer functions were determined in section 3 and section 4

The final step is to determine the power spectrum of the response from the power spectra of the generic amplitudes of the harmonics of the response. This step is based on the conclusion in appendix B concerning the power spectrum of a sum of harmonics.

The first step is performed in subsection 6.1 whereas the remainder two steps are performed in subsection 6.2.

6.1 Cross power spectra between amplitudes of harmonics of external blade turbulence loads

The external blade turbulence loads treated in this section are the generalized external blade loads (3.1.1), the external blade root loads (3.2.2), and the external blade section loads (4.1.2). Those loads are characterized by the common form

$$p(t,b) = \int_{z_0}^{L} \Psi(z_b)\, v(t,b,z_b)\, dz_b \tag{6.1.1}$$

This section aims at determining the cross power spectrum between two amplitudes of harmonics of such external blade turbulence loads, i.e. the cross spectrum between

$$\tilde{p}_{1\{m\}}(t) = \int_{z_{10}}^{L} \Psi_1(z_b)\, \tilde{v}_{\{m\}}(t,z_b)\, dz_b \tag{6.1.2}$$

and

$$\tilde{p}_{2\{n\}}(t) = \int_{z_{20}}^{L} \Psi_2(z_b)\, \tilde{v}_{\{n\}}(t,z_b)\, dz_b \tag{6.1.3}$$

According to the definition of cross covariance between complex variables (C.7) in appendix C, the cross covariance becomes

$$R_{\tilde{p}_{1\{m\}},\tilde{p}_{2\{n\}}}(\tau) = E\left\{\overline{\tilde{p}_{1\{m\}}(t)}\, \tilde{p}_{2\{n\}}(t+\tau)\right\} \tag{6.1.4}$$

where E denotes the mean value operator.

Inserting (6.1.2) and (6.1.3), merging the z_b integrals, concentrating the mean value operator on the only time dependent factors $\overline{\tilde{v}_{\{m\}}(t,z_1)}\, \tilde{v}_{\{n\}}(t+\tau,z_2)$, and finally using (C.7) to substitute for the mean value, (6.1.4) yields

$$R_{\tilde{p}_{1\{m\}},\tilde{p}_{2\{n\}}}(\tau) = \int_{z_{10}}^{L}\int_{z_{20}}^{L} \Psi_1(z_1)\, \Psi_2(z_2)\, R_{\tilde{v}_{\{m\}}(z_1),\tilde{v}_{\{n\}}(z_2)}(\tau)\, dz_1\, dz_2 \tag{6.1.5}$$

where $R_{\tilde{v}_{\{m\}}(z_1),\tilde{v}_{\{n\}}(z_2)}(\tau)$ is the cross covariance between the azimuth expansion coefficients of the turbulence. Fourier transforming (6.1.5) yields the corresponding cross power spectrum relation

$$S_{\tilde{p}_{1\{m\}},\tilde{p}_{2\{n\}}}(\Delta\omega) = \int_{z_{10}}^{L}\int_{z_{20}}^{L} \Psi_1(z_1)\, \Psi_2(z_2)\, S_{\tilde{v}_{\{m\}}(z_1),\tilde{v}_{\{n\}}(z_2)}(\Delta\omega)\, dz_1\, dz_2 \tag{6.1.6}$$

where $S_{\tilde{v}_{\{m\}}(z_1),\tilde{v}_{\{n\}}(z_2)}(\Delta\omega)$ is the cross power spectrum between the azimuth expansion coefficients of the turbulence. Inserting this according to (C.17), (6.1.6) is rewritten

$$S_{\tilde{p}_{1\{m\}},\tilde{p}_{2\{n\}}}(\Delta\omega) = F_{\tilde{p}_{1\{m\}},\tilde{p}_{2\{n\}}}(\Delta\omega) \int_{z_{10}}^{L} \Psi_1(z)dz \int_{z_{20}}^{L} \Psi_2(z)dz\, S_u(\Delta\omega) \tag{6.1.7}$$

where $S_u(\Delta\omega)$ is the fixed point power spectrum of the turbulence wind speed and the admittance function between the amplitudes of harmonics of the external blade turbulence loads is given by

$$F_{\tilde{p}_{1\{m\}},\tilde{p}_{2\{n\}}}(\Delta\omega) = \frac{\int_{z_{10}}^{L}\int_{z_{20}}^{L} \Psi_1(z_1)\,\Psi_2(z_2)\,F_{\tilde{v}_{\{m\}}(z_1),\tilde{v}_{\{n\}}(z_2)}(\Delta\omega)\,dz_1\,dz_2}{\int_{z_{10}}^{L}\Psi_1(z)dz\int_{z_{20}}^{L}\Psi_2(z)dz} \quad (6.1.8)$$

using the admittance function between azimuth expansion coefficients of turbulence $F_{\tilde{v}_{\{m\}}(z_1),\tilde{v}_{\{n\}}(z_2)}(\Delta\omega)$. Inserting this according to (C.18), (6.1.8) yields

$$F_{\tilde{p}_{1\{m\}},\tilde{p}_{2\{n\}}}(\Delta\omega) = \quad (6.1.9)$$

$$\begin{cases} \dfrac{\int_{z_{10}}^{L}\int_{z_{20}}^{L} \Psi_1(z_1)\,\Psi_2(z_2)\,\dfrac{1}{2\pi}\int_0^{2\pi}\chi\left(\Delta\omega,\sqrt{{z_1}^2+{z_2}^2-2z_1z_2\cos\theta}\right)\cos n\theta\,d\theta\,dz_1\,dz_2}{\int_{z_{10}}^{L}\Psi_1(z)dz\int_{z_{20}}^{L}\Psi_2(z)dz} & \\ \quad \text{if } m=n & \\ 0 \quad \text{otherwise} & \end{cases}$$

where $\chi^2(\omega, D)$ is the coherence function of wind turbulence in the rotor plane.

According to (6.1.7) and (6.1.9), the cross power spectrum between generic amplitudes of harmonics of external blade turbulence loads has a non zero value only if the orders of the harmonics are identical.

This property is inherited from the azimuth expansion coefficients of the turbulence. Thus, the azimuth expansion coefficients of turbulence in different radii are correlated only if the orders of the expansion coefficients are identical.

6.2 Power spectra of response

The next step is to determine the power spectrum of the amplitudes of harmonics of a response, combining the transfer functions determined in section 3 and section 4 with the input cross power spectra determined in subsection 6.1.

According to Newland [7], the power spectrum of an N inputs linear variable

$$Y(\omega) = \sum_{r=1}^{N} H_r(\omega)\, X_r(\omega) \tag{6.2.1}$$

is determined by the cross power spectra between the input variables $S_{x_r,x_s}(\omega)$ as

$$S_y(\omega) = \sum_{r=1}^{N} \sum_{s=1}^{N} \overline{H_r(\omega)}\, H_s(\omega)\, S_{x_r,x_s}(\omega) \tag{6.2.2}$$

According to (6.1.7) and (6.1.9), the considered input cross power spectra are real. Thus, the reverse cross power spectrum $S_{x_s,x_r}(\omega)$ is not only complex conjugated to $S_{x_r,x_s}(\omega)$ as usual, but

$$S_{x_s,x_r}(\omega) = S_{x_r,x_s}(\omega) \tag{6.2.3}$$

Thus utilizing (6.2.3) and utilizing that the imaginary parts of the terms in (6.2.2) add up to zero, (6.2.2) is implemented most effective as

$$S_y(\omega) = \sum_{r=1}^{N} (S_{x_r}(\omega) + 2 \sum_{s=r+1}^{N} (\Re\{H_r(\omega)\}\, \Re\{H_s(\omega)\} + \Im\{H_r(\omega)\}\, \Im\{H_s(\omega)\})\, S_{x_r,x_s}(\omega)) \tag{6.2.4}$$

According to (3.5.7), (4.1.20), and (4.2.10), the transfer functions $H^{ext}_{\{kB\}}(\Delta\omega)$ concerning modal amplitudes, $H^{ext}_{bs\{p\}}(\Delta\omega, z_{bs})$ concerning blade section loads, and $H^{ext}_{ts\{kB\}}(\Delta\omega, z_{ts})$ concerning tower section loads involve transfers from the 3 orders $kB-1$, kB, and $kB+1$ of external blade turbulence load to each order of response.

According to (6.1.7) and (6.1.9), the cross power spectra between inputs of different orders are zero. Thus writing any response amplitude in (3.5.7), (4.1.20), or (4.2.10) as the sum of 3 groups

$$\begin{aligned} \tilde{Y}_{\{p\}}(\Delta\omega) &= \sum_{r=1}^{N_-} H_{\{kB-1\}r}(\Delta\omega)\, \tilde{X}_{\{kB-1\}r}(\Delta\omega) \\ &+ \sum_{r=1}^{N_0} H_{\{kB\}r}(\Delta\omega)\, \tilde{X}_{\{kB\}r}(\Delta\omega) \\ &+ \sum_{r=1}^{N_+} H_{\{kB+1\}r}(\Delta\omega)\, \tilde{X}_{\{kB+1\}r}(\Delta\omega) \end{aligned} \tag{6.2.5}$$

the power spectrum of $\tilde{y}_{\{p\}}(t)$ is determined as the sum

$$S_{\tilde{y}_{\{p\}}}(\Delta\omega) = S_{\tilde{y}_{\{p\}}-}(\Delta\omega) + S_{\tilde{y}_{\{p\}}0}(\Delta\omega) + S_{\tilde{y}_{\{p\}}+}(\Delta\omega) \tag{6.2.6}$$

where the individual terms $S_{\tilde{y}_{\{p\}}-}$, $S_{\tilde{y}_{\{p\}}0}$, and $S_{\tilde{y}_{\{p\}}+}$ each are determined according to (6.2.4) considering the relevant cross power spectra according to the separation in (6.2.5). This approach saves calculations rather than using (6.2.4) only once including all $N_- + N_0 + N_+$ transfers. Thus, (6.2.6) avoids waste of calculations due to a very large number of zero cross power contributions to $S_{\tilde{y}_{\{p\}}}$.

Finally, the power spectrum of the response $y(t)$ itself is determined by the power spectra of the amplitudes of harmonics according to (B.2)

$$S_y(\omega) = \sum_{p=-\infty}^{\infty} S_{\tilde{y}_{\{p\}}}(\omega - p\omega_0) \tag{6.2.7}$$

Note that (6.2.7) formally differs from (B.2) using the power spectra of the *generic* amplitudes of harmonics rather than the power spectra of the actual actual amplitudes of harmonics. However using the symmetry relations (2.10) and (2.14) along with the cross covariance definition (6.1.4) it is easily verified that those cross power spectra are identical.

7 Calculation examples versus measurements

The present frequency domain method has a general formulation. I has been applied to a specific structural model and implemented in the PC programme Design Basis 2 as a suplement to the time domain implementation of the similar model. The structural model of Design Basis 2 is briefly described by Larsen in [12].

Test runs with Design Basis 2 have shown that the frequency domain code calculates up to 200 times faster than the time domain code. The rapid execution makes the frequency domain code eminently suited for parameter studies aiming at investigating the effect of changes in structural and aerodynamic parameters.

The primary test example is the measurements on one of the 31 m 300 kW Nordtank NTK300F wind turbines sited in the wind turbine park in Nørrekær Enge. In this test example, the blade root bending moments are measured in the flapwise and edgewise directions. The tower base bending moment is also measured.

The figures 7.1 - 7.6 show comparisons between frequency domain calculations, time simulations, and measurements. Concerning the time simulations and the measurements the deterministic and stochastic parts of the loads are separated using azimuth binning. Thus, the deterministic part is determined as the azimuth mean. After that, the stochastic part is simply determined subtracting the deterministic part from the total load.

Especially concerning the deterministic calculations, the equality between frequency domain calculations and time simulations is evident. Actually, the frequency domain model has shown the ability of revealing too long time steps in the time simulations because of the splended agreement. Thus, too long time steps generates differencies in the deterministic results that are much larger than the differencies between frequency domain and time simulation with sufficiently small time steps.

Concerning the stochastic calculations, a general difference is the dips in the PSD's at the harmonic frequencies in the frequency domain calculations. Similar dips are not predicted in the rotating spectrum of Kristensen [9], and it is hardly seen in any measurements.

However, the dips were observed and explained by Dragt [16] and [17]. Moreover, Winkelaar [15] has studdied turbulence simulation methods and demonstrated that the dips also appear in rotationally sampled simulated turbulence. Winkelaar has shown this for turbulence simulated with the Sandia method used in Design Basis 2 as well as turbulence simulated with the SWIFT method. The dips do not appear in the present graphs in the Design Basis 2 time simulation as they are smoothed because of the relatively large frequency steps. This smoothing effect was also observed and explained by Dragt.

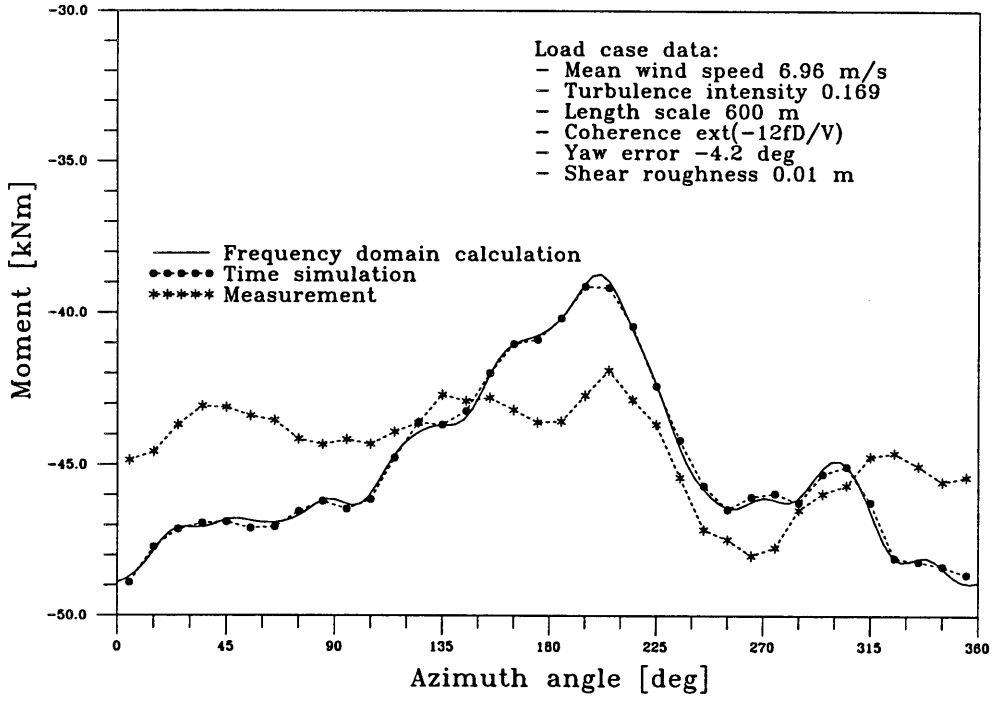

Figure 7.1. Deterministic frequency domain calculation compared to azimuth binned time simulation and measurements of Nordtank NTK300F flapwise root bending moment.

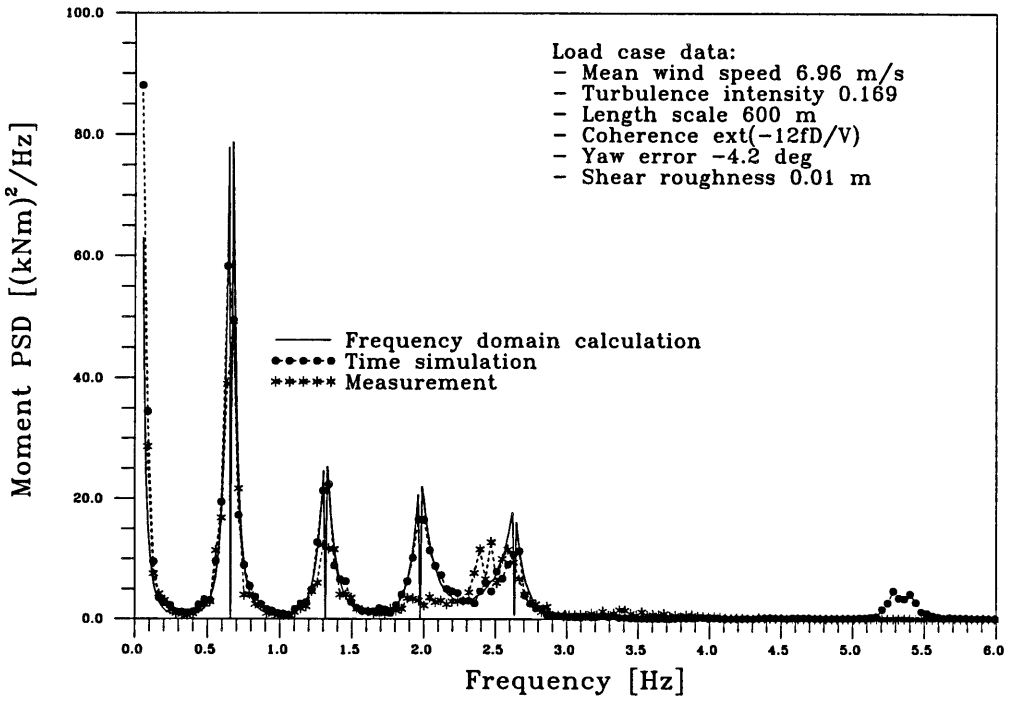

Figure 7.2. Frequency domain PSD calculation compared to PSD of stochastic part of time simulation and measurements of Nordtank NTK300F flapwise root bending moment.

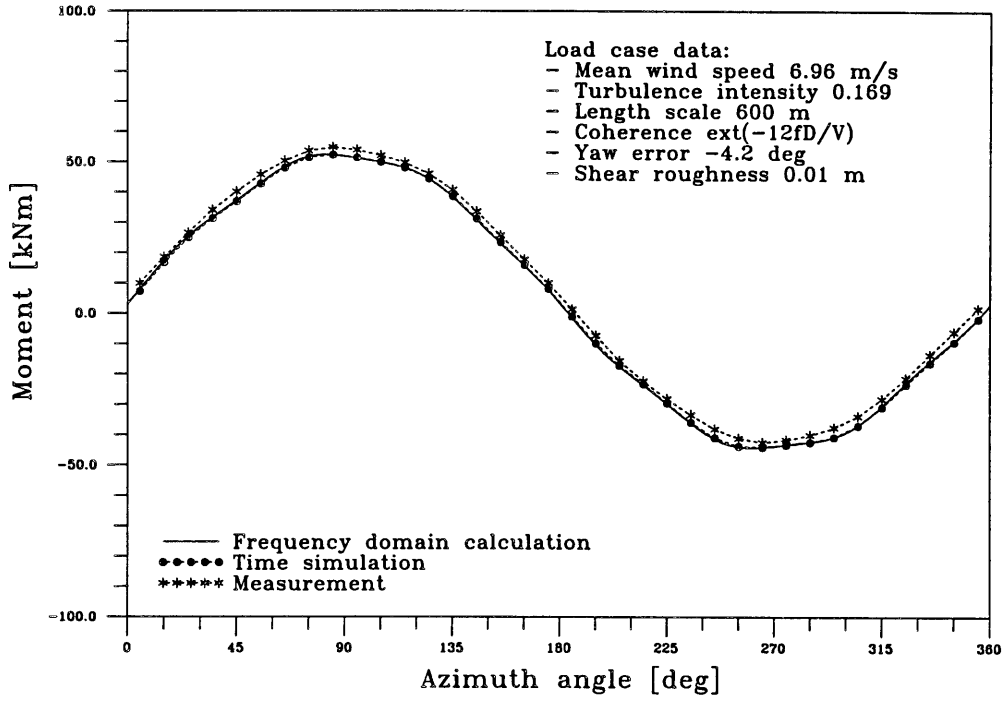

Figure 7.3. Deterministic frequency domain calculation compared to azimuth binned time simulation and measurements of Nordtank NTK300F edgewise root bending moment.

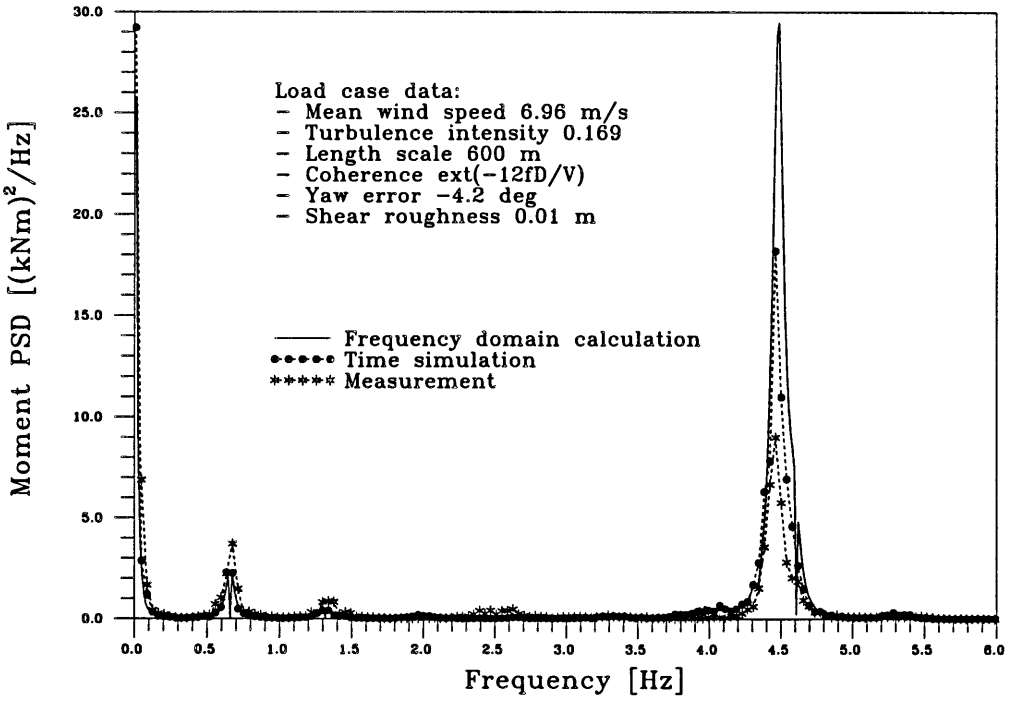

Figure 7.4. Frequency domain PSD calculation compared to PSD of stochastic part of time simulation and measurements of Nordtank NTK300F edgewise root bending moment.

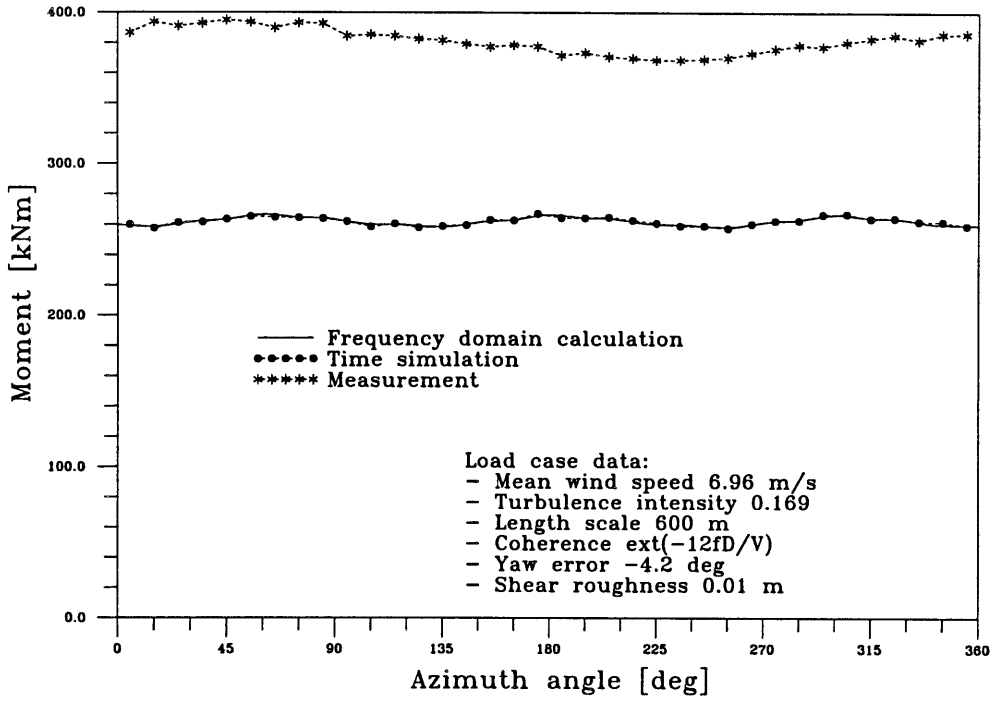

Figure 7.5. Deterministic frequency domain calculation compared to azimuth binned time simulation and measurement of Nordtank NTK300F east-west tower base bending moment.

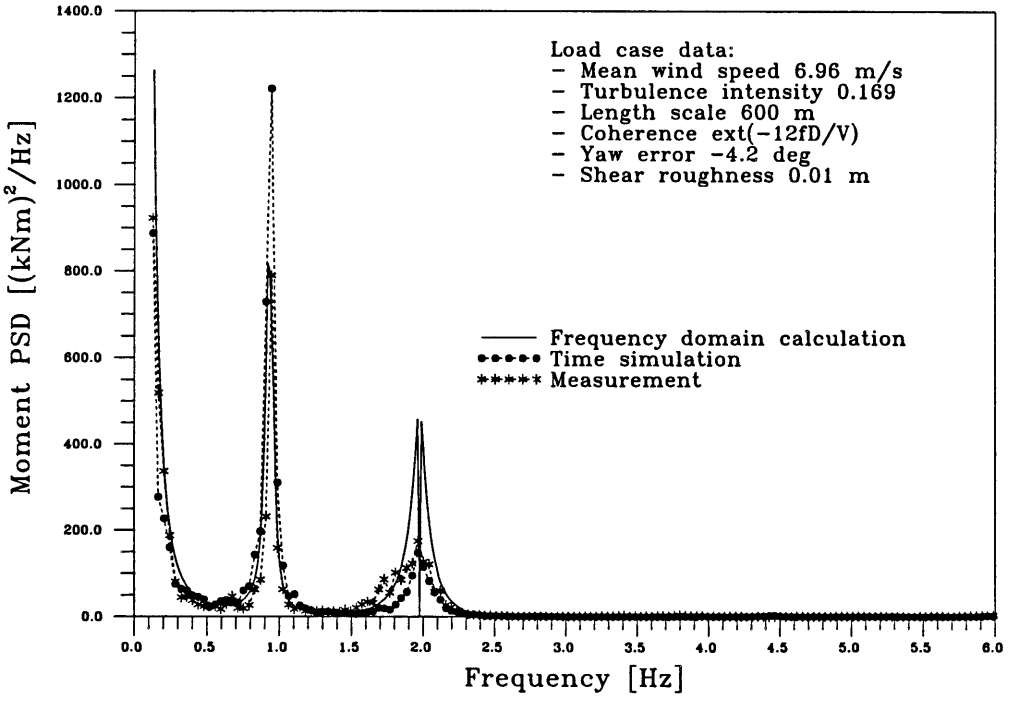

Figure 7.6. Frequency domain PSD calculation compared to PSD of stochastic part of time simulation and measurements of Nordtank NTK300F east-west tower base bending moment.

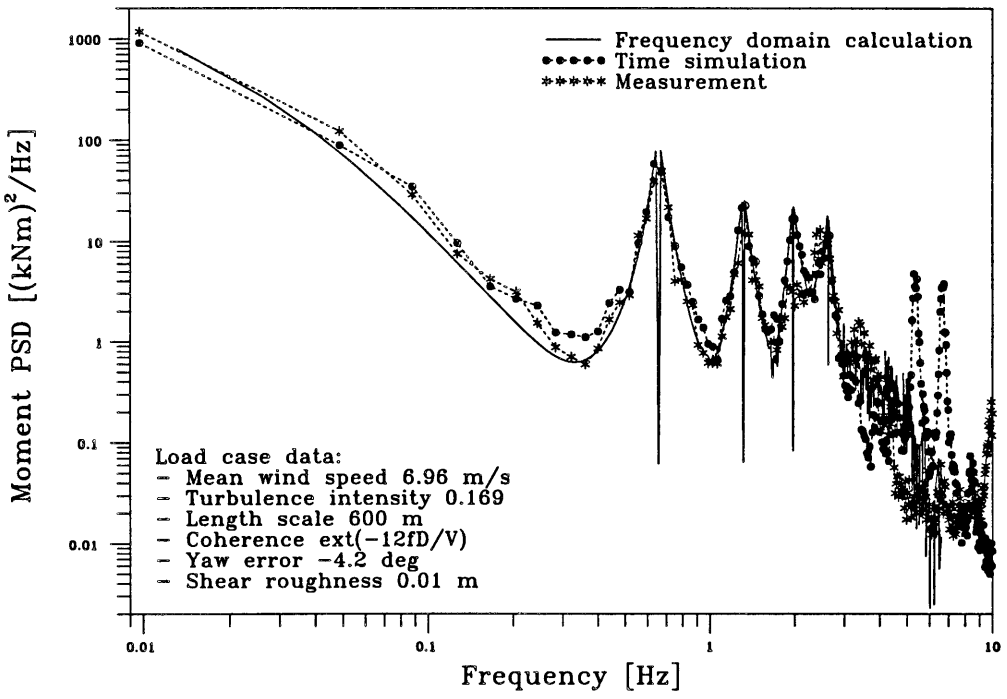

Figure 7.7. Frequency domain PSD calculation compared to PSD of stochastic part of time simulation and measurements of Nordtank NTK300F flapwise root bending moment.

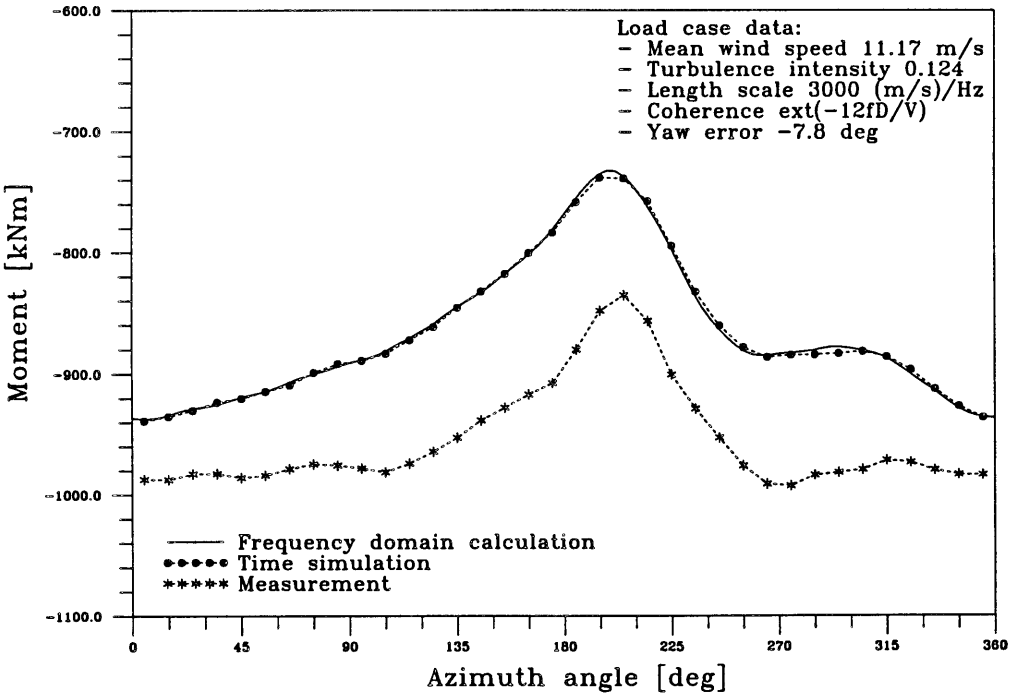

Figure 7.8. Deterministic frequency domain calculation compared to azimuth binned time simulation and measurements of Tjæreborg flapwise root bending moment.

The present frequency domain model shows that the dips are caused by the assumption that the longitudinal coherence is one at zero frequency i.e. $\chi(0, D) = 1$ in the admittance function (6.1.9). This is the case with the applied Davenport coherence [3] which is prescribed by the Danish code of practice for wind turbines [13].

A more realistic coherence function for the longitudinal coherence is suggested by Madsen in [4]. Madsens model is also implemented in Design Basis 2 and it does not produce dips because $\chi(0, D)$ is sufficiently less than 1. For instance, with a distance $D = 30$ m Madsens model yields $\chi(0, 30) = 0.64$ which agrees quite well with Manns Great Belt coherence studies [10].

Apart from the dips, the predicted PSD's of the frequency domain model generally agree quite well with the time simulation predictions. The rotor speed is 39.5 rpm, i.e. 0.66 Hz.

The PSD of the flapwise blade root bending moment figure 7.2 shows how higher orders of harmonics generally have less energy than lower orders of harmonics. This tendensy is modified by the flapwise bending eigenfrequency at 2.4 Hz which amplifies the 3'rd and especially the 4'th harmonics.

A similar pattern is observed on the PSD of the edgewise blade root bending moment figure 7.4. Only here the edgewise bending eigenfrequency at 4.5 Hz amplifies the 7'th harmonic.

The PSD of the tower base bending moment 7.6 shows that only the 0'th and 3'rd harmonics are predicted in frequency domain as well as time domain. Typically, a 1'st harmonic in the tower load measurements reveal asymetri in the rotors. The stochastic 1'st harmonic in the measurement is very weak on the present turbine. The frequency domain model agree with the time domain model and the measurement about the spike at 0.95 Hz which is caused by the tower bending eigenfrequency. The frequency domain model overestimates the 3'rd harmonic and the time domain model underestimates it. This difference could be caused by the rough spacial discretisation of the turbulence which is used in the time simulation.

The agreement between the models and the measurements is good also at the lower frequencies. This is seen in the log-log plot of the PSD of the flapwise blade bending moment in figure 7.7.

Comparing the calculations with the *measurements*, the most evident difference is in the deterministic tower bending moments figure 7.5. The difference is in static level as well as dynamics. The main dynamic difference is that the measured moment has a deterministic 1'st harmonic. How the measurement gets a deterministic but not a stochastic 1'st harmonic is an interesting question which however should not be discussed here.

Another evident difference between calculations and measurements is the dynamics of the deterministic blade flapwise bending moments in figure 7.1. This is a general weakness of the applied potential flow model for the tower shadow.

The model is described in [11]. The potential flow model is more convinsing for larger rotors. This is shown in figure 7.8 with measurement on the 61 m 2 MW ELSAM wind turbine in Tjæreborg where the dynamics of the deterministic flapwise blade bending moments is very good determined by frequency domain model

as well as time simulation.

8 Conclusions

This report offers a detailed description of the derivation of a frequency domain model from a time domain model of the structure of a steadily operating horizontal axis wind turbine. The frequency domain model is implemented along with the time domain model in the PC code Design Basis 2. Thus, Design Basis 2 is used to verify the frequency domain model comparing internal elastic loads on the structure calculated with the frequency domain model to loads calculated with the time domain model and to measured loads.

The structure of an operating wind turbine displays essential non-linearities between structural variables on blades and tower respectively. These non-linearities are due to the rotation of the blades causing the transformations between the blade coordinate systems and the tower coordinate system to depend on the instantaneous azimuth positions of the blades.

Conventional frequency domain methods do not allow non-linearities. However, assuming constant angular speed of the wind turbine rotor the structural variables are replaced by sums of harmonics in this angular speed. The relations between the amplitudes of those harmonics appear to be linear, replacing the non linearities of the variables with changes in orders of harmonics. The relations between the amplitudes of the harmonics of the variables are then transformed into the frequency domain and solved there.

Thus, the derivation of the amplitudes of harmonics of the internal elastic loads is based on conventional frequency domain methods applied to the relations between the amplitudes of harmonics. Finally, the internal elastic loads themselves are determined uniquely by their respective amplitudes of harmonics.

The frequency domain code calculates up to 200 times faster than the time domain code. The rapid calculations makes the frequency domain code exceptionally suited for parameter studies aiming at investigating the effect of changes in structural and aerodynamic parameters. Moreover, the frequency domain model provides methods and results that improves the understanding of the physics of the wind turbine structure.

The ultimate objective of the modelling of the wind turbine structure is to predict the fatigue lifetime and the extreme stresses.

The conventional way to predict fatigue is first to perform a time simulation of the stress time history, next make a rainflow range probability density function counting on the time series and finally predict the fatigue damage using the Palmgren-Miner sum relation. The present frequency domain model calculated PSD's and deterministic periodic parts of the loads rather than time series. Therefore, there is a missing link to the fatigue calculation. As the PSD's and the deterministic periodic parts could be comprised into PSD's with δ-functions, the missing link could be inserted by a method that calculates the rainflow range probability density function from a PSD.

Bishop and Zhihua [14] presents such methods which relate closely to the rainflow counting. The focus on the amplitudes of the harmonics in the present frequency domain model could suggest another approach transforming the statistics of the

amplitudes of the harmonics into the statistics in a range probability density function.

The present frequency domain model shows that the cross power spectra between the amplitudes of some orders of harmonics are not zero. The non zero cross power spectra reveal that the amplitudes of different orders are correlated. Popular speaking, this means that they appear at the same time. The correlation is not contained in the PSD's themselves. Therefore, the PSD's do not contain the complete information about the fatigue effect of the loads.

This is expected to be unimportant for the state of the art wind turbine, but it could be important for a future wind turbine with a more flexible structure. The cross power spectra between the amplitudes of harmonics could be included in a statistic method which would make it safer than Bishop's and Zhihua's method. Such a method may be developed in the future.

Concerning extreme values, Davenport's methods [1] of derivation of extremes from PSD's is a very solid approach which has been extended to include superposition with a deterministic periodic part by Madsen [2].

References

[1] Davenport: Note on the distribution of the largest value of a random function with application to gust loading. Proc. Inst. Civ. Eng., London 1964. pp. 187-196.

[2] Madsen, Frandsen, Holley and Hansen: Dynamics and fatigue damage of wind turbine rotors during steady operation. Risø-R-512. July 1984.

[3] Davenport. The spectrum of Horizontal Gustiness Near the Ground in High Winds. Quart. J. Royal Met. Soc., 87, pp 194-211, 1961.

[4] Madsen. On rotationally sampled wind turbulence. Solar Energy Research Institute, Golden Colorado, 1987. DRAFT.

[5] Madsen, Hock, and Hausfeld. Turbulence loads on Howden 26 m-Diameter Wind Turbine. Solar Energy Research Institute, Golden Colorado, November 1987.

[6] Madsen and Rasmussen. Rotor loading on a three-bladed wind turbine. European Wind Energy Conference, Glasgow EWEC'89.

[7] Newland. An introduction to random vibrations and spectral analysis. Longman Inc. New York, 1984.

[8] Hurty and Rubinstein. Dynamics of structures. Prentice Hall Inc. London 1964.

[9] Kristensen and Frandsen. Model for power spectra of the blade of a wind turbine. Measured from the moving frame of reference. Wind Eng. Ind. Aerodyn. 10, pp. 249-262, 1982.

[10] Mann, Kristensen, and Courtney. The Great Belt Coherence Experiment. A Study of Atmospheric Turbulence over Water. Risø-R-596. August 1991.

[11] Larsen, Frandsen, Sørensen, and Courtney. Design Basis for Horizontal-Axis wind Turbines - Teoretical Background. Risø-M-2836. 1989.

[12] Larsen and Sørensen. Verification of Design Basis Program 2 - a coupled aeroelastic wind turbine model. Risø-R-730(EN). 1994.

[13] Dansk Ingeniørforenings og ingeniør-sammenslutningens norm for last og sikkerhed for vindmøllekonstruktioner. Teknisk Forlag NP-409-N. 1. udgave maj 1992. Dansk Standard DS 472.

[14] Bishop and Zhihua. The fatigue analysis of wind turbine blades using frequency domain techniques. European Wind Energy Conference, Amsterdam, EWEC'91.

[15] Winkelaar. Fast three-dimensional wind simulation and the prediction of stochastic blade loads. 10'th ASME Wind Energy Symposium. Houston, January 1991.

[16] Dragt. The spectra of Wind speed fluctuations met by a rotating blade and resulting load fluctuations. European Wind Energy Conference, Hamburg, 1984.

[17] Dragt. Load fluctuations and response of rotor systems in turbulent wind fields. Netherland Energy Research Foundation ECN-172. The Netherlands, 1985.

Appendices

A Fourier transforms of amplitudes of harmonics

The scope of this appendix is to determine calculation rules for transformations of relations between time dependent wind turbine variables. The variables are either blade variables or tower variables, and they are either wind speeds seen from rotating blades, loads, or modal amplitudes. The relations are transformed from relations between instantaneous values into relations between Fourier transforms of amplitudes of harmonics.

Let $f(t,b)$ be a blade variable which is a sum of harmonics

$$f(t,b) = \sum_{n=-\infty}^{\infty} \hat{f}_{\{n\}}(t,b)\, e^{jn\omega_0 t} \tag{A.1}$$

with the amplitudes

$$\hat{f}_{\{n\}}(t,b) = e^{jn\theta_0(b)}\, \tilde{f}_{\{n\}}(t) \tag{A.2}$$

using the initial azimuth angle

$$\theta_0(b) = \frac{2\pi b}{B} + \theta_{00} \tag{A.3}$$

in which θ_{00} is the initial azimuth position of blade $b = 0$. Fourier transforming both sides of (A.1) yields

$$F(\omega,b) = \sum_{n=-\infty}^{\infty} \hat{F}_{\{n\}}(\omega,b) * \delta(\omega - n\omega_0) \tag{A.4}$$

where * is the convolution operator

$$G_1(\omega) * G_2(\omega) = \int_{-\infty}^{\infty} G_1(\omega - s)\, G_2(s)\, ds \tag{A.5}$$

according to Newland [7], and the δ function is defined according to

$$\begin{aligned} &\delta(\omega) = 0 \text{ if } \omega \neq 0 \\ &\int_{-\varepsilon}^{+\varepsilon} \delta(\omega)\, d\omega = 1 \end{aligned} \tag{A.6}$$

using an infinitely small positive ε. Performing the convolutions in (A.4) yields (A.7).

$$F(\omega,b) = \sum_{n=-\infty}^{\infty} \hat{F}_{\{n\}}(\omega - n\omega_0, b) \tag{A.7}$$

*

Likewise, if $f(t)$ is a tower variable which is a sum of harmonics

$$f(t) = \sum_{k=-\infty}^{\infty} \hat{f}_{\{kB\}}(t)\, e^{jkB\omega_0 t} \tag{A.8}$$

with the amplitudes

$$\hat{f}_{\{kB\}}(t) = e^{jkB\theta_0(b)}\, \tilde{f}_{\{kB\}}(t) \tag{A.9}$$

then the relations between the Fourier transforms are

$$F(\omega) = \sum_{k=-\infty}^{\infty} \hat{F}_{\{kB\}}(\omega - kB\omega_0) \tag{A.10}$$

*

Let the blade variables $f(t,b)$ be linear transformations of the blade variables $f_1(t,b)$ and $f_2(t,b)$ according to

$$f(t,b) = a_1 f_1(t,b) + a_2 f_2(t,b) \tag{A.11}$$

Expanding $f_1(t,b)$ and $f_2(t,b)$ in (A.11) according to (A.1) yields

$$f(t,b) = \sum_{n=-\infty}^{\infty} e^{jn\theta_0(b)} a_1\, \tilde{f}_{1\{n\}}(t) e^{jn\omega_0 t} + \sum_{n=-\infty}^{\infty} e^{jn\theta_0(b)} a_2\, \tilde{f}_{2\{n\}}(t) e^{jn\omega_0 t} \tag{A.12}$$

Uniting the sums in (A.12) yields

$$f(t,b) = \sum_{n=-\infty}^{\infty} e^{jn\theta_0(b)} \left(a_1\, \tilde{f}_{1\{n\}}(t) + a_2\, \tilde{f}_{2\{n\}}(t) \right) e^{jn\omega_0 t} \tag{A.13}$$

corresponding to an expansion of $f(t,b)$ according to (A.1) using the generic amplitudes of the harmonics

$$\tilde{f}_{\{n\}}(t) = a_1\, \tilde{f}_{1\{n\}}(t) + a_2\, \tilde{f}_{2\{n\}}(t) \tag{A.14}$$

Fourier transforming (A.14) on both sides yields

$$\tilde{F}_{\{n\}}(\Delta\omega) = a_1 \tilde{F}_{1\{n\}}(\Delta\omega) + a_2 \tilde{F}_{2\{n\}}(\Delta\omega) \tag{A.15}$$

*

If the instantaneous value of the blade variable $f(t,b)$ is an integral

$$f(t,b) = \int_{z_{b1}}^{z_{b2}} g(t,b,z_b)\, dz_b \tag{A.16}$$

of the instantaneous value of a blade line variable $g(t,b,z_b)$ then the relation between Fourier transforms of the corresponding generic amplitudes of harmonics are similar integrals, i.e.

$$\tilde{F}_{\{n\}}(\Delta\omega) = \int_{z_{b1}}^{z_{b2}} \tilde{G}_{\{n\}}(\Delta\omega, z_b)\, dz_b \tag{A.17}$$

(A.16) is actually only and extension of (A.11) using an infinite sum of infinitesimal terms. Therefore, the proof is omitted.

*

If the tower variable $f(t)$ is a linear transformation of the tower variables $f_1(t)$, and $f_2(t)$ according to

$$f(t) = a_1 f_1(t) + a_2 f_2(t) \tag{A.18}$$

then the Fourier transforms of the corresponding generic amplitudes of harmonics are also linear, i.e.

$$\tilde{F}_{\{kB\}}(\Delta\omega) = a_1 \tilde{F}_{1\{kB\}}(\Delta\omega) + a_2 \tilde{F}_{2\{kB\}} \qquad (\Delta\omega) \tag{A.19}$$

*

Let the instantaneous value of the tower variable $f(t)$ be a sum of blade contributions from the blade variables $g(t,b)$, i.e.

$$f(t) = \sum_{b=0}^{B-1} g(t,b) \tag{A.20}$$

Expanding the blade variables $g(t,b)$ according to (A.1) and the inserting the initial azimuth angles (A.3) yields

$$g(t,b) = \sum_{n=-\infty}^{\infty} e^{jn\theta_{00}}\, e^{jn\frac{2\pi b}{B}}\, \tilde{g}_{\{n\}}(t)\, e^{jn\omega_0 t} \tag{A.21}$$

Inserting (A.21) in (A.20), subsequently reversing the b and n sum orders, and finally using

$$\sum_{b=0}^{B-1} e^{jn\frac{2\pi b}{B}} = \begin{cases} B & \text{if } n = kB \\ 0 & \text{otherwise} \end{cases} \tag{A.22}$$

to determine the sums of blade contributions,

$$f(t) = \sum_{k=-\infty}^{\infty} e^{jkB\theta_{00}}\, B\, \tilde{g}_{\{kB\}}(t)\, e^{jkB\omega_0 t} \tag{A.23}$$

According to (A.8), (A.23) corresponds to an expansion of $f(t)$ using the generic amplitudes of harmonics

$$\tilde{f}_{\{kB\}}(t) = B\, \tilde{g}_{\{kB\}}(t) \tag{A.24}$$

Fourier transforming (A.24) yields

$$\tilde{F}_{\{kB\}}(\Delta\omega) \;=\; B\, \tilde{G}_{\{kB\}}(\Delta\omega) \tag{A.25}$$

*

Let the instantaneous value of the tower variable $f(t)$ be a sum of azimuth dependent blade contributions from the blade variables $g(t,b)$ according to

$$f(t) \;=\; \sum_{b=0}^{B-1} \cos\theta(t,b)\; g(t,b) \tag{A.26}$$

in which $\theta(t,b)$ is the instantaneous value of the azimuth angle of blade b.

Proving (A.32), and (A.8) in this cases, $\cos\theta(t,b)$ is replaced according to the Euler formula

$$\cos\theta(t,b) = \frac{e^{j\theta(t,b)} + e^{-j\theta(t,b)}}{2} \tag{A.27}$$

Inserting (A.27) using the azimuth angle

$$\theta(t,b) \;=\; \omega_0 t \;+\; \theta_0(b) \tag{A.28}$$

and (A.3) and inserting $g(t,b)$ according to (A.21), (A.26) yields

$$f(t) = \frac{1}{2}\sum_{b=0}^{B-1}\left(\sum_{n=-\infty}^{\infty} e^{j(n+1)\theta_{00}}\, e^{j(n+1)\frac{2\pi b}{B}}\, \tilde{g}_{\{n\}}(t)\, e^{j(n+1)\omega_0 t} + \sum_{n=-\infty}^{\infty} e^{j(n-1)\theta_{00}}\, e^{j(n-1)\frac{2\pi b}{B}}\, \tilde{g}_{\{n\}}(t)\, e^{j(n-1)\omega_0 t}\right) \tag{A.29}$$

Replacing the sums over n in (A.29) by sums over $p = n+1$ and $p = n-1$ respectively, subsequently reversing the b and p sum orders, and finally using (A.22) with $p = n$ to determine the sums of blade contributions,

$$f(t) = \sum_{k=-\infty}^{\infty} e^{jkB\theta_{00}} \frac{B}{2}\left(\tilde{g}_{\{kB-1\}}(t,b) + \tilde{g}_{\{kB+1\}}(t,b)\right) e^{jkB\omega_0 t} \tag{A.30}$$

According to (A.8), (A.30) corresponds to an expansion of $f(t)$ using the generic amplitudes of harmonics

$$\tilde{f}_{\{kB\}}(t) = \frac{B}{2}\left(\tilde{g}_{\{kB-1\}}(t) + \tilde{g}_{\{kB+1\}}(t)\right) \tag{A.31}$$

Fourier transforming (A.31) yields

$$\tilde{F}_{\{kB\}}(\Delta\omega) \;=\; \frac{B}{2}\,\tilde{G}_{\{kB-1\}}(\Delta\omega) \;+\; \frac{B}{2}\,\tilde{G}_{\{kB+1\}}(\Delta\omega) \tag{A.32}$$

*

Let the instantaneous value of the tower variable $f(t)$ be a sum of azimuth dependent blade contributions from the blade variables $g(t,b)$ according to

$$f(t) \;=\; \sum_{b=0}^{B-1} \sin\theta(t,b)\; g(t,b) \tag{A.33}$$

in which $\theta(t,b)$ is the instantaneous value of the azimuth angle of blade b, then the Fourier transformed of the generic amplitudes of the harmonics of $f(t)$ are determined according to

$$\tilde{F}_{\{kB\}}(\Delta\omega) \;=\; -\,\frac{jB}{2}\tilde{G}_{\{kB-1\}}(\Delta\omega) \;+\; \frac{jB}{2}\tilde{G}_{\{kB+1\}}(\Delta\omega) \tag{A.34}$$

Proving (A.34) using the Euler formula

$$\sin\theta(t,b) = \frac{e^{j\theta(t,b)} - e^{-j\theta(t,b)}}{2j} \tag{A.35}$$

is similar with proving (A.32) using (A.27). Therefore, the proof is omitted.

*

If the blade variable $f(t,b)$ is the time derived of the blade variable $g(t,b)$, i.e.

$$f(t,b) \;=\; \dot{g}(t,b) \tag{A.36}$$

then the relations between the Fourier transforms of the corresponding generic amplitudes of harmonics are

$$\tilde{F}_{\{n\}}(\Delta\omega) \;=\; j(n\omega_0 + \Delta\omega)\;\tilde{G}_{\{n\}}(\Delta\omega) \tag{A.37}$$

Likewise, concerning the tower variables

$$f(t) \;=\; \dot{g}(t) \tag{A.38}$$

the corresponding relations are

$$\tilde{F}_{\{kB\}}(\Delta\omega) \;=\; j(kB\omega_0 + \Delta\omega)\;\tilde{G}_{\{kB\}}(\Delta\omega) \tag{A.39}$$

(A.37) and (A.39) are simply an application of conventional frequency domain derivation

$$\dot{X}(\omega) \;=\; j\omega\; X(\omega) \tag{A.40}$$

remembering that the frequencies $\Delta\omega$ of the amplitudes of the n'th harmonics of the blade variables correspond to the frequencies

$$\omega \;=\; n\omega_0 + \Delta\omega \tag{A.41}$$

of the variables themselves according to (A.7). Likewise, the frequencies $\Delta\omega$ of the amplitudes of the kB'th harmonics of the tower variables correspond to the frequencies

$$\omega \;=\; kB\omega_0 + \Delta\omega \tag{A.42}$$

Since it is the variables themselves that are derived, (A.41) and (A.42) must be used to substitute for ω in (A.40), which is done in (A.37) and (A.39) respectively.

*

If the instantaneous value of the blade variables $f(t,b)$ is equal to the instantaneous value of the tower variable $g(t)$, i.e.

$$f(t,b) \;=\; g(t) \tag{A.43}$$

expanding the tower variable $g(t)$ is according to (A.8)

$$g(t) \;=\; \sum_{k=-\infty}^{\infty} e^{jkB\theta_0(b)}\;\tilde{g}_{\{kB\}}(t)\;e^{jkB\omega_0 t} \tag{A.44}$$

which corresponds to an expansion of $f(t,b)$ according to (A.1) using only the amplitudes of the kB'th harmonics

$$\tilde{f}_{\{kB\}}(t) = \tilde{g}_{\{kB\}}(t) \tag{A.45}$$

Fourier transforming (A.45) yields

$$\tilde{F}_{\{kB\}}(\Delta\omega) \;=\; \tilde{G}_{\{kB\}}(\Delta\omega) \tag{A.46}$$

*

Let the instantaneous value of the blade variable $f(t,b)$ depend on the tower variable $g(t)$ according to

$$f(t,b) = \cos\theta(t,b)\; g(t) \tag{A.47}$$

in which $\theta(t,b)$ is the instantaneous value of the azimuth angle of blade b. Inserting the Euler formula (A.27) using the azimuth angles (A.28) and inserting $g(t)$ according to (A.44), (A.47) yields

$$\begin{aligned} f(t,b) &= \frac{1}{2}\sum_{k=-\infty}^{\infty} e^{j(kB+1)\theta_0(b)}\, e^{j(kB+1)\frac{2\pi b}{B}}\, \tilde{g}_{\{kB\}}(t)\, e^{j(kB+1)\omega_0 t} \\ &+ \frac{1}{2}\sum_{k=-\infty}^{\infty} e^{j(kB-1)\theta_0(b)}\, e^{j(kB-1)\frac{2\pi b}{B}}\, \tilde{g}_{\{kB\}}(t)\, e^{j(kB-1)\omega_0 t} \end{aligned} \tag{A.48}$$

According to (A.1), (A.48) corresponds to an expansion of $f(t,b)$ using the generic amplitudes of harmonics

$$\tilde{f}_{\{kB-1\}}(t) = \frac{1}{2}\,\tilde{g}_{\{kB\}}(t) \tag{A.49}$$

$$\tilde{f}_{\{kB+1\}}(t) = \frac{1}{2}\,\tilde{g}_{\{kB\}}(t) \tag{A.50}$$

Fourier transforming (A.49) and (A.50) yields

$$\tilde{F}_{\{kB-1\}}(\Delta\omega) = \frac{1}{2}\,\tilde{G}_{\{kB\}}(\Delta\omega) \tag{A.51}$$

$$\tilde{F}_{\{kB+1\}}(\Delta\omega) = \frac{1}{2}\,\tilde{G}_{\{kB\}}(\Delta\omega) \tag{A.52}$$

*

If the instantaneous value of the blade variable $f(t,b)$ depends on the tower variables $g(t)$ according to

$$f(t,b) = \sin\theta(t,b)\; g(t) \tag{A.53}$$

in which $\theta(t,b)$ is the instantaneous value of the azimuth angle of blade b, then

$$\tilde{F}_{\{kB-1\}}(\Delta\omega) = \frac{j}{2}\,\tilde{G}_{\{kB\}}(\Delta\omega) \tag{A.54}$$

$$\tilde{F}_{\{kB+1\}}(\Delta\omega) = -\frac{j}{2}\,\tilde{G}_{\{kB\}}(\Delta\omega) \tag{A.55}$$

Proving (A.54) and (A.55) using the Euler formula (A.35) is similar with proving (A.51) and (A.52) using the Euler formula (A.27). Therefore, the proof is omitted.

*

B Power spectrum of a sum of harmonics

The variable $x(t)$ considered in this appendix is assumed to be a random variable decomposed into the sum of harmonics in the frequency ω_0, i.e.

$$x(t) = \sum_{n=-\infty}^{\infty} \hat{x}_{\{n\}}(t)\, e^{jn\omega_0 t} \tag{B.1}$$

where $\hat{x}_{\{n\}}(t)$ is the complex amplitude of the n'th harmonic of $x(t)$.

The purpose of the appendix is to derive the power spectrum of $x(t)$, $S_x(\omega)$, as the simple sum

$$S_x(\omega) = \sum_{n=-\infty}^{\infty} S_{\hat{x}_{\{n\}}}(\omega - n\omega_0) \tag{B.2}$$

where $S_{\hat{x}_{\{n\}}}(\Delta\omega)$ is the power spectrum of the amplitude $\hat{x}_{\{n\}}(t)$

The basic assumption leading to this result is that the relevant frequencies of the amplitudes, $\Delta\omega$, are low compared to ω_0.

The method used to proof (B.2) is first to assume that $x(t)$ is periodic with an arbitrarily long still finite period time T. The connection between the frequencies of $x(t)$ and its amplitudes of harmonics is then shown if $x(t)$ is periodic. Having assumed arbitrarily large period times, these frequency connections are still valid when the period time goes toward infinite. Thus, the relations are valid also for non periodic variables $x(t)$.

Assuming that $x(t)$ is periodic with the period time T the power spectra become sums of δ-functions rather than continious functions. The position of each δ-function on the frequency axis connects it to a frequency which is a multiplum of the periodic frequency $1/T$.

With infinite period time, the variables are no longer periodic, and the power spectra get continious. This limit is obtained as the frequency step between the δ-functions decreases towards zero. At the same time, the size of the δ-functions decrease because the energy is distributed on more δ-functions.

Denoting the mean value of a variable $f(t)$ $E\{f(t)\}$, the conventional definition of the auto covariance of the real variable $x(t)$ is

$$R_x(\tau) = E\{x(t)\, x(t+\tau)\} \tag{B.3}$$

and the corresponding definition of the power spectrum is

$$S_x(\omega) = \frac{1}{2\pi}\int_{-\infty}^{\infty} R_x(\tau)\, e^{-j\omega\tau}\, d\tau \tag{B.4}$$

Concerning the complex amplitudes of harmonics, the definition (B.3) is useless to evaluate the actual auto covariance of the amplitudes. Instead, denoting the complex conjugated of a complex variable c by $\bar{c}$, the definition

$$R_{\hat{x}_{\{n\}}}(\tau) = E\left\{\overline{\hat{x}_{\{n\}}(t)}\ \hat{x}_{\{n\}}(t+\tau)\right\} \tag{B.5}$$

is used as the auto covariance of the complex amplitude of the n'th harmonic $\hat{x}_{\{n\}}(t)$. Using this definition, and similarly with (B.4)

$$S_{\hat{x}_{\{n\}}}(\omega) = \frac{1}{2\pi}\int_{-\infty}^{\infty} R_{\hat{x}_{\{n\}}}(\tau)\, e^{-j\omega\tau}\, d\tau \tag{B.6}$$

the convenient result (B.2) is obtained.

Thus, $x(t)$ is assumed to be perodic with the period time

$$T = A\, T_0 \tag{B.7}$$

in which A is a large positive integer and T_0 is the period time corresponding to ω_0,

$$T_0 = \frac{2\pi}{\omega_0} \tag{B.8}$$

Assuming that the decomposition (B.1) is unique, also the amplitudes of the harmonics are periodic with the period time T. Then the amplitudes can be decomposed again according to

$$\hat{x}_{\{n\}}(t) = \sum_{p=-\infty}^{\infty} \hat{\hat{x}}_{\{n\}p}\, e^{jp\omega_T t} \tag{B.9}$$

in which ω_T is the frequency of the period in $x(t)$ and its amplitudes of harmonics, i.e.

$$\omega_T = \frac{2\pi}{T} \tag{B.10}$$

Using (B.8) along with (B.10) yields that the period time relation in (B.7) corresponds to the frequency relation

$$\omega_T = \frac{\omega_0}{A} \tag{B.11}$$

(B.9) demonstrates how $\hat{\hat{x}}_{\{n\}p}$ represents the frequency

$$\Delta\omega = p\,\omega_T = \frac{p}{A}\,\omega_0 \tag{B.12}$$

of $\hat{x}_{\{n\}}(t)$. Inserting (B.9) in (B.1) yields that $\hat{\hat{x}}_{\{n\}p}$ simultaniously represents the frequency

$$\omega = n\,\omega_0 + p\,\omega_T = \left(n + \frac{p}{A}\right)\omega_0 \tag{B.13}$$

of $x(t)$ itself. Consequently, the frequency $\Delta\omega$ of the n'th harmonic amplitude of $x(t)$ simply represents the frequency

$$\omega = n\,\omega_0 + \Delta\omega \tag{B.14}$$

of $x(t)$ itself.

Now it is used that the $-n$'th amplitude is equal to the complex conjugated to the n'th amplitude, i.e.

$$\hat{x}_{\{-n\}}(t) = \overline{\hat{x}_{\{n\}}(t)} \tag{B.15}$$

Basically, this assumption is simply a consequence of the variable $x(t)$ being real, which can be verified inserting (B.15) in (B.1) and using Eulers formulas to derive

$$x(t) = x_0(t) + \sum_{n=1}^{\infty} \left(2\,\Re\left\{\hat{x}_{\{n\}}(t)\right\}\,\cos(n\omega_0 t) \;-\; 2\,\Im\left\{\hat{x}_{\{n\}}(t)\right\}\,\sin(n\omega_0 t)\right) \tag{B.16}$$

in which $\Re\{c\}$ and $\Im\{c\}$ denote the real part and the imaginary part respectively of the complex variable c.

Reversing the sum order in (B.1) and using (B.15) yields

$$x(t) \;=\; \sum_{m=-\infty}^{\infty} \overline{\hat{x}_{\{m\}}(t)}\; \mathrm{e}^{-jm\omega_0 t} \tag{B.17}$$

Inserting (B.9) in (B.17) yields

$$x(t) = \sum_{m=-\infty}^{\infty} \sum_{p=-\infty}^{\infty} \overline{\hat{\hat{x}}_{\{m\}p}}\; \mathrm{e}^{-j(m\omega_0 + p\omega_T)t} \tag{B.18}$$

Likewise, yet not reversing the sum order in (B.1), but substituting $t+\tau$ for t, $x(t+\tau)$ can be decomposed into

$$x(t+\tau) = \sum_{n=-\infty}^{\infty} \sum_{q=-\infty}^{\infty} \hat{\hat{x}}_{\{n\}q}\; \mathrm{e}^{j(n\omega_0 + q\omega_T)\,(t+\tau)} \tag{B.19}$$

Inserting (B.18) and (B.19) in (B.3), merging the sums and concentrating the mean value operator on time dependent factors yields

$$R_x(\tau) \;= \tag{B.20}$$

$$\sum_{n=-\infty}^{\infty} \sum_{m=-\infty}^{\infty} \sum_{q=-\infty}^{\infty} \sum_{p=-\infty}^{\infty} \mathrm{E}\left\{\mathrm{e}^{j((n-m)\omega_0 + (q-p)\omega_T)t}\right\}\; \mathrm{e}^{j(n\omega_0 + q\omega_T)\tau}\; \overline{\hat{\hat{x}}_{\{m\}p}}\; \hat{\hat{x}}_{\{n\}q}$$

The mean value in (B.21) is different from zero only if

$$(n-m)\,\omega_0 + (q-p)\,\omega_T = 0 \tag{B.21}$$

Inserting (B.11) in (B.21) yields the similar condition

$$p = q + A\,(n-m) \tag{B.22}$$

In that case the mean value in (B.21) is 1, otherwise it is 0. Consequently, (B.21) can be reduced to

$$R_x(\tau) = \sum_{n=-\infty}^{\infty} \sum_{m=-\infty}^{\infty} \sum_{q=-\infty}^{\infty} e^{j(n\omega_0+q\omega_T)\tau}\, \overline{\hat{\hat{x}}_{\{m\}q+A(n-m)}}\, \hat{\hat{x}}_{\{n\}q} \tag{B.23}$$

The assumption that the amplitudes consist of only low frequencies is expressed as

$$|\,\Delta\omega\,| < \frac{\omega_0}{2} \tag{B.24}$$

Using the frequency representation expressed in (B.12), (B.24) yields

$$|\,\hat{\hat{x}}_{\{m\}p}\,| = 0 \quad \text{if} \quad |\,p\,| \geq \tfrac{A}{2} \tag{B.25}$$

$$|\,\hat{\hat{x}}_{\{n\}q}\,| = 0 \quad \text{if} \quad |\,q\,| \geq \tfrac{A}{2} \tag{B.26}$$

Using those conditions, (B.23) yields contributions only if $m = n$, and therefore reduces to

$$R_x(\tau) = \sum_{n=-\infty}^{\infty} e^{jn\omega_0\tau} \sum_{q=-\infty}^{\infty} e^{jq\omega_T\tau}\, \overline{\hat{\hat{x}}_{\{n\}q}}\, \hat{\hat{x}}_{\{n\}q} \tag{B.27}$$

Inserting (B.9) in (B.5) and using the same procedure as with $R_x(\tau)$ to determine the mean value yields the auto covariances of the amplitudes of harmonics

$$R_{\hat{x}_{\{n\}}}(\tau) = \sum_{q=-\infty}^{\infty} e^{jq\omega_T\tau}\, \overline{\hat{\hat{x}}_{\{n\}q}}\, \hat{\hat{x}}_{\{n\}q} \tag{B.28}$$

Inserting this in (B.27) yields the auto covariance of $x(t)$

$$R_x(\tau) = \sum_{n=-\infty}^{\infty} e^{jn\omega_0\tau}\, R_{\hat{x}_{\{n\}}}(\tau) \tag{B.29}$$

and consequently the power spectrum of the real variable $x(t)$ can be determined as the sum of n convolutions between $\delta\,(n\omega_0)$'s corresponding to the Fourier transforms of $e^{jn\omega_0\tau}$ in (B.29) and the Fourier transforms of the other factors in (B.29), i.e. the power spectra (B.6) of the amplitudes of harmonics.

Doing that, the power spectrum of the real variable $x(t)$ becomes (B.2) which is the sum of the power spectra of the amplitudes of the harmoncs, displaced according to their order. Consequently, each harmonic order contributes to $S_x(\omega)$ with power that is placed on the frequency axis according to the order of the harmonic.

Note that (B.15) and (B.5) yields

$$R_{\hat{x}_{\{n\}}}(-\tau) = \overline{R_{\hat{x}_{\{n\}}}(\tau)} \tag{B.30}$$

which ensures that $S_{\hat{x}_{\{n\}}}(\omega)$ is real according to the Fourier transformation (B.6), and consequently $S_x(\omega)$ is real according to (B.2).

C Cross power spectra between azimuth expansion coefficients of turbulence

The scope of this appendix is to determine the cross power spectra between azimuth expansion coefficients of the turbulence wind speed parallel with the main shaft in respective radii.

The considered component of the turbulent wind speed is denoted $\underline{v}(t,r,\theta)$ at a point (r,θ) in the rotor plane. The cross covariance $R_d(\tau,d)$ between $\underline{v}(t,r_1,\theta_1)$, and $\underline{v}(t,r_2,\theta_2)$ is presumed to depend uniquely on the distance

$$d = \sqrt{{r_1}^2 + {r_2}^2 - 2\, r_1\, r_2\, \cos(\theta_2 - \theta_1)} \tag{C.1}$$

which makes it possible to define the cross covariance as

$$R_d\left(\tau, \sqrt{{r_1}^2 + {r_2}^2 - 2r_1r_2\cos(\theta_2-\theta_1)}\right) = E\left\{\underline{v}(t,r_1,\theta_1)\ \underline{v}(t+\tau,r_2,\theta_2)\right\} \tag{C.2}$$

and the cross power spectrum as

$$S_d(\omega,d) = \frac{1}{2\pi}\int_{-\infty}^{\infty} R_d(\tau,d)\mathrm{e}^{-j\omega\tau}d\tau \tag{C.3}$$

At any time t and any radius r, $\underline{v}(t,r,\theta)$ is expanded in the azimuth angle

$$\underline{v}(t,r,\theta) = \sum_{n=-\infty}^{\infty} \tilde{v}_{\{n\}}(t,r)\mathrm{e}^{jn\theta} \tag{C.4}$$

where the complex expansion coefficients

$$\tilde{v}_{\{n\}}(t,r) = \frac{1}{2\pi}\int_0^{2\pi} \underline{v}(t,r,\theta)\mathrm{e}^{-jn\theta}d\theta \tag{C.5}$$

In accordance with the power spectrum definition (B.6), the *cross* power spectrum between the expansion coefficients $\tilde{v}_{\{m\}}(t,r_1)$ and $\tilde{v}_{\{n\}}(t,r_2)$ is defined as

$$S_{\tilde{v}_{\{m\}}(r_1),\tilde{v}_{\{n\}}(r_2)}(\omega) = \frac{1}{2\pi}\int_{-\infty}^{\infty} R_{\tilde{v}_{\{m\}}(r_1),\tilde{v}_{\{n\}}(r_2)}(\tau)\mathrm{e}^{-j\omega\tau}d\tau \tag{C.6}$$

where the *cross* covariance between the complex expansion coefficients is defined as

$$R_{\tilde{v}_{\{m\}}(r_1),\tilde{v}_{\{n\}}(r_2)}(\tau) = E\left\{\overline{\tilde{v}_{\{m\}}(t,r_1)}\ \tilde{v}_{\{n\}}(t+\tau,r_2)\right\} \tag{C.7}$$

in accordance with the definition of *auto* covariance (B.5) concerning complex variables.

Inserting (C.5) in (C.7) yields

$$R_{\tilde{v}_{\{m\}}(r_1),\tilde{v}_{\{n\}}(r_2)}(\tau) = \tag{C.8}$$
$$E\left\{\frac{1}{2\pi}\int_0^{2\pi} \underline{v}(t,r_1,\theta)e^{jm\theta}d\theta \; \frac{1}{2\pi}\int_0^{2\pi} \underline{v}(t+\tau,r_2,\theta)e^{-jn\theta}d\theta\right\}$$

Merging the integrals and concentrating the mean value operator on the time dependent factor

$$R_{\tilde{v}_{\{m\}}(r_1),\tilde{v}_{\{n\}}(r_2)}(\tau) = \tag{C.9}$$
$$\frac{1}{(2\pi)^2}\int_0^{2\pi}\int_0^{2\pi} E\left\{\underline{v}(t,r_1,\theta_1)\;\underline{v}(t+\tau,r_2,\theta_2)\right\} e^{-j(n\theta_2-m\theta_1)}d\theta_2 d\theta_1$$

Inserting (C.2) in (C.9)

$$R_{\tilde{v}_{\{m\}}(r_1),\tilde{v}_{\{n\}}(r_2)}(\tau) = \tag{C.10}$$
$$\frac{1}{(2\pi)^2}\int_0^{2\pi}\int_0^{2\pi} R_d\left(\tau,\sqrt{r_1{}^2+r_2{}^2-2r_1r_2\cos(\theta_2-\theta_1)}\right) e^{-jn(\theta_2-\theta_1)}e^{j(m-n)\theta_1}d\theta_2 d\theta_1$$

Substituting $\theta = \theta_2 - \theta_1$ yields

$$R_{\tilde{v}_{\{m\}}(r_1),\tilde{v}_{\{n\}}(r_2)}(\tau) = \tag{C.11}$$
$$\frac{1}{(2\pi)^2}\int_0^{2\pi} R_d\left(\tau,\sqrt{r_1{}^2+r_2{}^2-2r_1r_2\cos\theta}\right) e^{-jn\theta}\int_0^{2\pi} e^{j(m-n)\theta_1}d\theta_1 d\theta$$

If $m = n$ then the θ_1 integral in (C.11) is equal to 2π, otherwise 0. Thus, the cross covariance becomes

$$R_{\tilde{v}_{\{m\}}(r_1),\tilde{v}_{\{n\}}(r_2)}(\tau) = \tag{C.12}$$
$$\begin{cases} \dfrac{1}{(2\pi)}\displaystyle\int_0^{2\pi} R_d\left(\tau,\sqrt{r_1{}^2+r_2{}^2-2r_1r_2\cos\theta}\right) e^{-jn\theta}d\theta & \text{if } m=n \\ 0 & \text{otherwise} \end{cases}$$

Using that $R_d\left(\tau,\sqrt{r_1{}^2+r_2{}^2-2r_1r_2\cos\theta}\right)$ is even and periodic in θ, the valid cross covariances in (C.12) can be rewritten

$$R_{\tilde{v}_{\{n\}}(r_1),\tilde{v}_{\{n\}}(r_2)}(\tau) = \frac{1}{2\pi}\int_0^{\pi} R_d\left(\tau,\sqrt{r_1{}^2+r_2{}^2-2r_1r_2\cos\theta}\right)\left(e^{-jn\theta}+e^{jn\theta}\right)d\theta$$

$$= \frac{1}{2\pi}\int_0^{\pi} R_d\left(\tau, \sqrt{r_1{}^2 + r_2{}^2 - 2r_1r_2\cos\theta}\right) 2\cos n\theta d\theta$$

$$= \frac{1}{2\pi}\int_0^{2\pi} R_d\left(\tau, \sqrt{r_1{}^2 + r_2{}^2 - 2r_1r_2\cos\theta}\right) \cos n\theta d\theta \quad \text{(C.13)}$$

according to Eulers formulas.

Note that since $R_d(\tau, d)$ is real and even in τ, also $R_{\tilde{v}_{\{n\}}(r_1),\tilde{v}_{\{n\}}(r_2)}(\tau)$ must be real and even in τ. Inserting (C.13) in (C.6) yields

$$S_{\tilde{v}_{\{n\}}(r_1),\tilde{v}_{\{n\}}(r_2)}(\omega) = \quad \text{(C.14)}$$

$$\frac{1}{2\pi}\int_{-\infty}^{\infty}\frac{1}{2\pi}\int_0^{2\pi} R_d\left(\tau, \sqrt{r_1{}^2 + r_2{}^2 - 2r_1r_2\cos\theta}\right)\cos n\theta d\theta e^{-j\omega\tau} d\tau$$

Reversing the order of the integration and using (C.3) to substitute the τ-integral, (C.14) becomes

$$S_{\tilde{v}_{\{n\}}(r_1),\tilde{v}_{\{n\}}(r_2)}(\omega) = \frac{1}{2\pi}\int_0^{2\pi} S_d\left(\omega, \sqrt{r_1{}^2 + r_2{}^2 - 2r_1r_2\cos\theta}\right)\cos n\theta d\theta \quad \text{(C.15)}$$

Now it is assumed that $S_d(\omega, d)$ can be factorized as

$$S_d(\omega, d) = \chi(\omega, d)\, S_u(\omega) \quad \text{(C.16)}$$

where $S_u(\omega)$ is the power spectrum of the turbulence in any *fixed* point in the rotor plane, and $\chi(\omega, d)$ is the coherence between the turbulence in two points located with a distance d.

Inserting (C.16) in (C.15), and considering all m's and n's according to (C.12) yields the conclusion

$$S_{\tilde{v}_{\{m\}}(r_1),\tilde{v}_{\{n\}}(r_2)}(\omega) = F_{\tilde{v}_{\{m\}}(r_1),\tilde{v}_{\{n\}}(r_2)}(\omega)\, S_u(\omega) \quad \text{(C.17)}$$

where the admittance function of the azimuth expansion coefficients of turbulence in the two radii r_1 and r_2

$$F_{\tilde{v}_{\{m\}}(r_1),\tilde{v}_{\{n\}}(r_2)}(\omega) =$$

$$\begin{cases} \frac{1}{2\pi}\int_0^{2\pi} \chi\left(\omega, \sqrt{r_1{}^2 + r_2{}^2 - 2r_1r_2\cos\theta}\right)\cos n\theta d\theta & \text{if } m = n \\ 0 & \text{otherwise} \end{cases} \quad \text{(C.18)}$$

D Numeric method for determination of the admittance function

According to (6.1.9), the admittance function between the generalized external turbulence loads $x(t)$ and $y(t)$ of the same order n is defined as

$$F_{\tilde{x}_{\{n\}},\tilde{y}_{\{n\}}}(\omega) = \frac{\int_{r_{x0}}^{R}\int_{r_{y0}}^{R} \Psi_x(r_x)\,\Psi_y(r_y)\,\frac{1}{2\pi}\int_0^{2\pi} \chi\left(\omega, \sqrt{r_x{}^2 + r_y{}^2 - 2r_x r_y \cos\theta}\right)\cos n\theta\; d\theta\; dr_x\; dr_y}{\int_{r_{x0}}^{R}\Psi_x(r)dr \int_{r_{y0}}^{R}\Psi_y(r)dr} \tag{D.1}$$

where $\chi^2(\omega, d)$ is the coherence function of the turbulence perpendicular to the rotor plane between points in the rotor plane with the distanced d and at the frequency ω. Since $\chi(\omega, d)$, $\Psi_x(r)$, and $\Psi_y(r)$ change with the mean wind speed U_0, (D.1) should be calculated with the parameters n, ω, and with U_0 which is related to each load case. Moreover, this should be done for each combination of external loads $x(t)$, $y(t)$, i.e. in a matrix with rows and columns corresponding to generalized blade loads, blade root loads, and blade section loads.

Even a single calculation of the triple integral

$$I_{\tilde{x}_{\{n\}},\tilde{y}_{\{n\}}}(\omega) = \int_{r_{x0}}^{R}\int_{r_{y0}}^{R} \Psi_x(r_x)\,\Psi_y(r_y)\,\frac{1}{2\pi}\int_0^{2\pi} \chi\left(\omega, \sqrt{r_x{}^2 + r_y{}^2 - 2r_x r_y \cos\theta}\right)\cos n\theta\; d\theta\; dr_x\; dr_y \tag{D.2}$$

is rather time consuming if a minimum of exactness should be obtained with a standard trapezoidal integral method. Therefore, another numeric method is needed in order to table the triple integral. Such a method will be described in this appendix, using two different coherence functions and presuming that the weighted influence coefficients $\Psi_x(r)$ and $\Psi_y(r)$ in (D.1) are polynomiums of identical orders M

$$\Psi_x(r) = \sum_{m=0}^{M} a_x(m)\; r^m \tag{D.3}$$

$$\Psi_y(r) = \sum_{m=0}^{M} a_y(m)\; r^m \tag{D.4}$$

Inserting (D.3) and (D.4) in (D.2) yields

$$I_{\tilde{x}_{\{n\}},\tilde{y}_{\{n\}}}(\omega) = \sum_{m_x=0}^{M}\sum_{m_y=0}^{M} a_x(m_x)\; a_y(m_y)\; K_{\{n\}}(\omega, m_x, m_y) \tag{D.5}$$

in which

$$K_{\{n\}}(\omega, h, k) = \int_{r_{x0}}^{R} \int_{r_{y0}}^{R} {r_x}^h \, {r_y}^k \, \frac{1}{2\pi} \int_0^{2\pi} \chi\left(\omega, \sqrt{{r_x}^2 + {r_y}^2 - 2 r_x r_y \cos\theta}\right) \cos n\theta \; d\theta \; dr_x \; dr_y \tag{D.6}$$

Two coherence functions are considered. The simple Davenport model [3] and the more detailed Madsen model [4]. These models are selected because they easily allow for dimensionless frequencies, which is used to normalize the integrals.

The Davenport model is

$${\chi_D}^2(\mu_D) = \mathrm{e}^{-A_D \mu_D} \tag{D.7}$$

Here, A_D is a decay constant dependent on meteorological circumstances and the dimensionless frequency

$$\mu_D = \frac{\omega d}{U_0} \tag{D.8}$$

Davenport coherence is prescribed by the Danish code of practice [13]. Madsens model is

$${\chi_M}^2(\mu_M) = \mathrm{e}^{-\frac{A_M \mu_M^2}{B_M + \mu_M}} \tag{D.9}$$

with the two parameters A_M and B_M and the dimensionless frequency

$$\mu_M = \sqrt{\left(\frac{\omega d}{U_0}\right)^2 + \left(\frac{d}{L}\right)^2} \tag{D.10}$$

where $2\pi L$ denotes the turbulent length scale of.

Note that both μ_D and μ_M are proportional to d. That makes it possible to substitute the integrators in (D.6) according to

$$\nu = \frac{\mu}{d} r_x = \frac{r_x}{l} \tag{D.11}$$

$$\varrho = \frac{r_y}{r_x} = \frac{r_y}{l\nu} \tag{D.12}$$

where the length coefficient l is independent of r_x, r_y, and θ, but depends on which coherence formula is used. Inserting (D.8) and (D.10) in (D.11) yields the respective length coefficients

$$l_D = \frac{d}{\mu_D} = \frac{U_0}{\omega} \tag{D.13}$$

and

$$l_M = \frac{1}{\sqrt{\left(\frac{\omega}{U_0}\right)^2 + \left(\frac{1}{L}\right)^2}} \tag{D.14}$$

In (D.6), the distance

$$d = \sqrt{r_x{}^2 + r_y{}^2 - 2r_x r_y \cos\theta} \tag{D.15}$$

is used. Inserting this in (D.11) along with (D.12) yields

$$\mu = \frac{d}{r_x}\,\nu = \sqrt{1 + \varrho^2 - 2\varrho\cos\theta}\;\nu \tag{D.16}$$

According to (D.11) and (D.12), the reverse substitution is

$$r_x = l\nu \tag{D.17}$$

$$r_y = l\nu\varrho \tag{D.18}$$

which gives the Jacobi determinant of the substitution

$$J(\nu,\varrho) = \begin{vmatrix} l & 0 \\ l\varrho & l\nu \end{vmatrix} = l^2\nu \tag{D.19}$$

Now the double integral in (D.6) can be replaced by

$$K_{\{n\}}(\omega_\chi, h, k) = \tag{D.20}$$
$$\int_{\alpha_{x0}\nu_0}^{\nu_0} \int_{\alpha_{y0}\frac{\nu_0}{\nu}}^{\frac{\nu_0}{\nu}} l^2\nu(l\nu)^h(l\nu\varrho)^k \frac{1}{2\pi}\int_0^{2\pi} \chi_\mu\left(\sqrt{1+\varrho^2-2\varrho\cos\theta}\;\nu\right)\cos n\theta\; d\theta\; d\varrho\; d\nu$$

in which χ_μ denotes either χ_D or χ_M. The integration limiting parameters are

$$\nu_0 = \frac{R}{l} \tag{D.21}$$

$$\alpha_{x0} = \frac{r_{x0}}{R} \tag{D.22}$$

$$\alpha_{y0} = \frac{r_{y0}}{R} \tag{D.23}$$

and the frequency ω_χ is determined by either (D.13) or (D.14) as

$$\omega_\chi = \begin{cases} \frac{U_0}{R}\nu_0 & \text{if } \chi_\mu = \chi_D \\ \sqrt{\left(\frac{\nu_0}{R}\right)^2 - \left(\frac{1}{L}\right)^2} U_0 & \text{if } \chi_\mu = \chi_M \end{cases} \tag{D.24}$$

using (D.21) to substitute the l-parameter in (D.22) - (D.24). Doing the same in (D.20) yields

$$K_{\{n\}}(\omega_\chi, h, k) = R^{h+k+2}\, Q_{\chi\{n\}}(\nu_0, h, k, \alpha_{x0}, \alpha_{y0}) \tag{D.25}$$

in which

$$Q_{\chi\{n\}}(\nu_0, h, k, \alpha_{x0}, \alpha_{y0}) = \tag{D.26}$$
$$\frac{1}{\nu_0^{h+k+2}} \int_{\alpha_{x0}\nu_0}^{\nu_0} \nu^{h+k+1} \int_{\alpha_{y0}\frac{\nu_0}{\nu}}^{\frac{\nu_0}{\nu}} \varrho^k \frac{1}{2\pi} \int_0^{2\pi} \chi_\mu \left(\sqrt{1+\varrho^2 - 2\varrho\cos\theta}\ \nu\right) \cos n\theta \; d\theta \; d\varrho \; d\nu$$

can be tabled on hard disk with the parameters n, ν_0, h, k, α_{x0}, and α_{y0} for each of the coherence functions χ_D and χ_M. Combining (D.1), (D.2), (D.5), (D.6) and (D.25) we reach

$$F_{\tilde{x}_{\{n\}},\tilde{y}_{\{n\}}}(\omega_\chi) = \frac{\sum_{k=0}^{M}\sum_{k=0}^{M} a_x(h) a_y(k) R^{h+k+2} Q_{\chi\{n\}}\left(\nu_0, h, k, \frac{r_{x0}}{R}, \frac{r_{y0}}{R}\right)}{\int_{r_{x0}}^{R}\int_{r_{y0}}^{R} \Psi_x(r_x)\Psi_y(r_y)\, dr_y\, dr_x} \tag{D.27}$$

Still it is rather troublesome to determine $Q_{\chi\{n\}}$ numerically. The problems are

1. For high frequencies the coherence drops quickly from 1 to 0 when the distance increases, i.e. when the azimuth difference θ moves from 0 or 2π, or when the radius ratio ϱ moves from 1. Because of that the interval length for the numeric integration must vary to obtain a sensible relation between the amount of calculations and the exactness of the result.
2. The $\cos\theta$ factor fluctuates which increases the required number of θ-intervals.

For these reasons, the standard trapezoidal integral method and other more advanced standard integral methods are not practicable. In stead, the implementation of the integral is based on new method developed to take advantage of the monotony properties in the integrals. The idea is then to separate the integrals into intervals where the factors in the integrand are known to be monotonous.

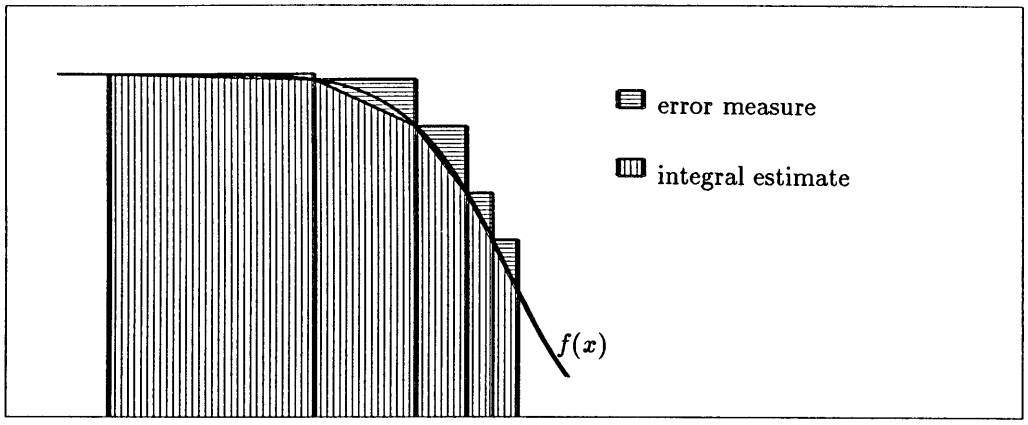

Figure D.1. Illustration of a simple error measure method used for numeric integration of a monotonous function $f(x)$.

A simple error measure method is illustrated in figure D.1 The method can be extended to comprise any integral

$$I = \int_a^b x^m f(x)dx \tag{D.28}$$

where $m \geq 0, b > a$, and $f(x)$ is monotonous in $[a, b]$.

Figure D.2 shows the definitions for a worst case analysis of (D.28) in a single interval. Sub division of intervals continues until the sum of error measures is below a certain percentage of the sum of integral estimates. The interval which should be divided is selected as the interval which has the highest error measure.

Inspecting figure D.2 , the estimate of the integral in a link of sub intervals i is defined as the sum of sub interval contributions

$$I_e = \sum^i \int_{x_i-\Delta x_i}^{x_i} x^m (f_{ei}(0) + \alpha_i x)dx \tag{D.29}$$

and the corresponding worst case error

$$E_w = \sum^i \int_{x_i-\Delta x_i}^{x_i} x^m (e_{wi}(0) + \alpha_i x)dx \tag{D.30}$$

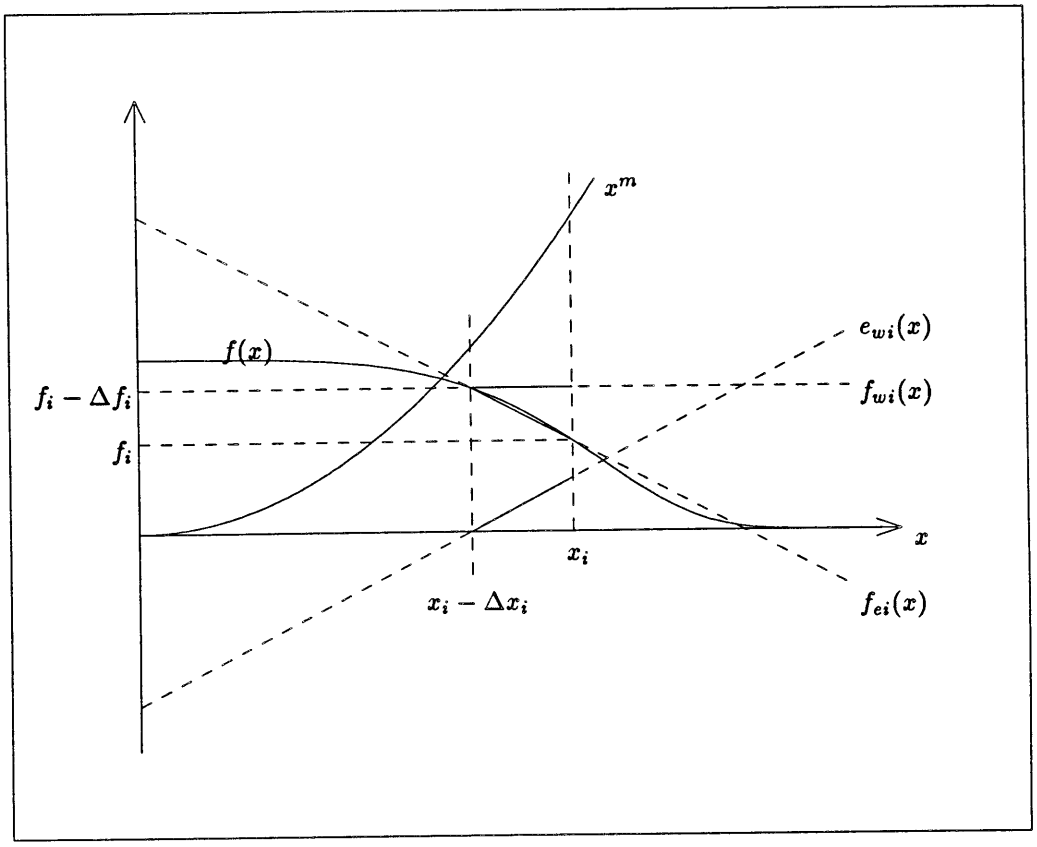

Figure D.2. Definition of the worst case analysis. The actual values of $f(x)$ are known in the terminal points of the interval i. They define the estimate of f in i which is denoted $f_{ei}(x)$. The worst case of $f(x)$ is $f_{wi}(x) = f_i - \Delta f_i$ (worse than $f(x) = f_i$ because of the factor x^m), which leads to the worst case error $e_{wi}(x) = f_{wi}(x) - f_{ei}(x)$.

in which

$$\alpha_i = \frac{\Delta f_i}{\Delta x_i} \tag{D.31}$$

$$f_{ei}(0) = f_i - \alpha_i x_i \tag{D.32}$$

$$e_{wi}(0) = \alpha_i(x_i - \Delta x_i) \tag{D.33}$$

Now, the polynomium integral parameters

$$c_i(k) = \frac{x_i^{k+1}}{k+1} \tag{D.34}$$

and their interval increment

$$\Delta c_i(k) = c_i(k) - c_{i-1}(k) \tag{D.35}$$

are defined. The integrals in (D.29) and (D.30) can then be found analytical as

$$I_e = \sum^{i} [\Delta c_i(m) f_{ei}(0) + \Delta c_i(m+1)\ \alpha_i] \tag{D.36}$$

$$E_w = \sum^{i} [\Delta c_i(m) e_{wi}(0) - \Delta c_i(m+1)\ \alpha_i] \tag{D.37}$$

Finally, the convergence can be tested by

$$\left|\frac{E_w}{I_e}\right| < \varepsilon \tag{D.38}$$

Note that this algorithm is very powerfull if the determination of (D.28) is combined for all m's considered. Note also that (D.34) is put in before (D.35) because it saves calculations when i is divided into two new sub intervals.

Unfortunately, it is not possible to foretell all monotony intervals in (D.26). However, the coherence is behaving so properly that it is possible to suggest a solution that has been tested intensively and found reliable.

Starting with the inner θ-intergal

$$I_{\theta\{n\}}(\nu, \varrho) = \frac{1}{2\pi} \int_0^{2\pi} \chi_\mu \left(\sqrt{1 + \varrho^2 - 2\varrho \cos\theta}\nu\right) \cos n\theta d\theta \tag{D.39}$$

it can be reduced to

$$I_{\theta\{n\}}(\nu, \varrho) = \frac{1}{\pi} \int_0^{\pi} \chi_\mu \left(\sqrt{1 + \varrho^2 - 2\varrho \cos\theta}\nu\right) \cos n\theta d\theta \tag{D.40}$$

It is straight forward to prove that both $\chi_D(\mu)$ in (D.7) and $\chi_M(\mu)$ in (D.9) are decreasing for $\mu \geq 0$, which is not supprising because μ is proportional to the distance.

Since the current μ parameter in (D.40) increases when θ runs from 0 to π, χ_μ is decreasing in that θ interval.

Unfortunately, $\cos n\theta$ fluctuates in the θ interval, and consequently it will increase in sub intervals where χ_μ decreases. This has lead to the idea of assembling the quater periods of $\cos n\theta$. That is done by rewriting (D.40) to

$$I_{\theta\{n\}}(\nu, \varrho) = \frac{1}{\pi} \int_0^{\frac{\pi}{2n}} \sigma_{\{n\}}(\nu, \varrho, \theta) \cos n\theta d\theta \tag{D.41}$$

in which the summed coherence

$$\sigma_{\{n\}}(\nu, \varrho, \theta) = \sum_{i=0}^{n-1} \left[(-1)^i \left(\chi_{\nu\varrho\theta}\left(\nu, \varrho, \frac{i}{n}\pi + \theta\right) - \chi_{\nu\varrho\theta}\left(\nu, \varrho, \frac{i+1}{n}\pi - \theta\right)\right)\right] \tag{D.42}$$

where the coherence is expressed by

$$\chi_{\nu\varrho\theta}(\nu,\varrho,\theta) \;=\; \chi_{\mu}\left(\sqrt{1+\varrho^2-2\varrho\cos\theta}\nu\right) \tag{D.43}$$

It is obvious that $\cos n\theta$ is decreasing in the θ interval $[0;\frac{\pi}{2n}]$. The summed coherence in (D.42) is more complicated, but tests has shown that it is decreasing. Consequently, the integrand in (D.41) can be assumed decreasing, and the algorithm for integration of monotonous functions can be applied.

Then (D.26) reduces to

$$Q_{\chi\{n\}}(\nu_0,h,k,\alpha_{x0},\alpha_{y0}) \;=\; \frac{1}{\nu_0^{h+k+2}}\int_{\alpha_{x0}\nu_0}^{\nu_0}\nu^{h+k+1}\int_{\alpha_{y0}\frac{\nu_0}{\nu}}^{\frac{\nu_0}{\nu}}\varrho^k I_{n\theta}(\nu,\varrho)d\varrho d\nu \tag{D.44}$$

Concerning the ϱ-integral in (D.44), tests has shown that $I_{\theta\{n\}}(\nu,\varrho)$ is increasing in the interval $[\alpha_{y0}\frac{\nu_0}{\nu};1]$ and decreasing in the interval $[1;\frac{\nu_0}{\nu}]$. To verify that monotony, think of ϱ as the ratio between the radii, and think of $I_{\theta\{n\}}(\nu,\varrho)$ as the admittance filter of the cross power between the turbulent wind speeds seen from the two radii. If the radiuses are identical, which they are if $\varrho=1$, then we should expect the admittance to be high, and moving away from $\varrho=1$ we would expect the admittance to drop simply because the wind speeds are less correlated when one of the radii are moved away from the other. Consequently, the interval should be devided at $\varrho = 1$ and the algorithm for (D.28) used on each of these sub intervals seperately.

Now we lack to foretell the monotony of only the ν integrand factor ($f(x)$ in (D.28)), which is the ϱ integral in (D.44)

$$f_{\chi\{n\}}(\nu,\nu_0,k,\alpha_{yo}) \;=\; \int_{\alpha_{y0}\frac{\nu_0}{\nu}}^{\frac{\nu_0}{\nu}}\varrho^k I_{\theta\{n\}}(\nu,\varrho)d\varrho \tag{D.45}$$

Test calculations have shown that this monotony is not systematic, but also that the integrand is very proper. Moreover, the wish to truncate the integrals at the blade section radii stations r_{x0} and r_{y0} has shown to meet the non monotony problem in a sufficient way.

The program unit, which has been used to calculate $Q_{\chi\{n\}}(\nu_0,h,k,\alpha_{x0},\alpha_{yo})$ has been implemented so that it returns a 4 dimensional data structure with the index parameters h,k, and sampled values of α_{x0} and α_{y0}.

This structure makes it possible to combine the calculations for all h's and k's considered as mentioned in the description of the algorithm for determination of (D.28), but it also makes it possible to combine the calculations for all samples of α_{x0} and α_{y0}, simply by starting to determine the integrals at the blade tip where α_{x0} and α_{y0} are nearly 1 and then reuse the integrals as α_{x0} and α_{y0} decrease stepwise towards 0.

Consequently, the ν integral in (D.44) is initially divided into sub intervals defined by the sampling of α_{x0}. If this sampling is selected reasonably close (decrements in α of the size 0.1 - 0.2 like ε in (D.38)), then the effect of the lack of monotony has shown to vanish.

To verify the integrations the asymptotes have been determined analytical. It has been shown that

$$Q_{\chi_D\{n\}}(\nu_0, h, k, \alpha_{x0}, \alpha_{y0}) \rightarrow \frac{K(h+k, max(\alpha_{x0}, \alpha_{yo}))}{\left(\frac{A_D}{2}\right)^2} \frac{1}{\nu_0^2} \tag{D.46}$$

and

$$Q_{\chi_M\{n\}}(\nu_0, h, k, \alpha_{x0}, \alpha_{y0}) \rightarrow \frac{\exp\left(\frac{\frac{A_M}{2} B_M}{(1+\frac{A_M}{2} B_M)^2}\right) K(h+k, max(\alpha_{x0}, \alpha_{y0}))}{\left(\frac{1+A_M B_M}{(1+\frac{A_M}{2} B_M)^2} \frac{A_M}{2}\right)^2} \frac{1}{\nu_0^2} \tag{D.47}$$

as

$$\nu_0 \rightarrow \infty \tag{D.48}$$

in which the function $K(h+k, \alpha)$ depends on only $h+k$ and the maximum value α of α_{x0} and α_{y0}. It is determined as

$$K(h+k, \alpha) = \begin{cases} \ln(\frac{1}{\alpha}) & \text{if } h+k = 0 \\ \\ \frac{1-\alpha^{h+k}}{h+k} & \text{otherwise (i.e. } h+k > 0) \end{cases} \tag{D.49}$$

Note that the asymptote depends on only the maximum value of α_{x0} and α_{y0}, simply because the coherence contributions only when the two points are close, i.e. when $r_x \simeq r_y$.

Note also that if $h+k = 0$ then the asymptotes are finite only if $\alpha > 0$. Still, the asymptotes have been verified when $\alpha > 0.05$, i.e. if one can avoid the aero forces from 0 to 5 % rotor disk radius, then the asymptotes are reliable.

Figure D.3 illustrates some level curves of $Q_{\chi\{n\}}(\nu_0, h, k, \alpha_{x0}, \alpha_{y0}.)$ in the α_{x0}, α_{y0} plane in a case where the frequency ν_0 is so high that $Q_{\chi\{n\}}(\nu_0, h, k, \alpha_{x0}, \alpha_{y0})$ can be assumed asymptotic. The figure also shows how a simple interpolation of $Q_{\chi\{n\}}(\nu_0, h, k, \alpha_{x0}, \alpha_{y0})$ between the nearest sample points of α_{x0} and α_{y0} can be unneccesarily defective.

According to the level curves in figure D.3, the value in ① should be determined as an interpolation between Ⓑ and Ⓒ. However, using standard interpolation between the nearest points, one would first interpolate between Ⓒ and Ⓓ (which is a quite good measure for the level in ① in this case) and between Ⓐ and Ⓑ (which gives a level that is too small). Then one should interpolate between those two sub interpolations. Consequently, the result is a level that is too low.

Therefore, the interpolation strategy illustrated in figure D.4 is suggested, presuming that

$$\alpha_{x0} \geq \alpha_{y0} \tag{D.50}$$

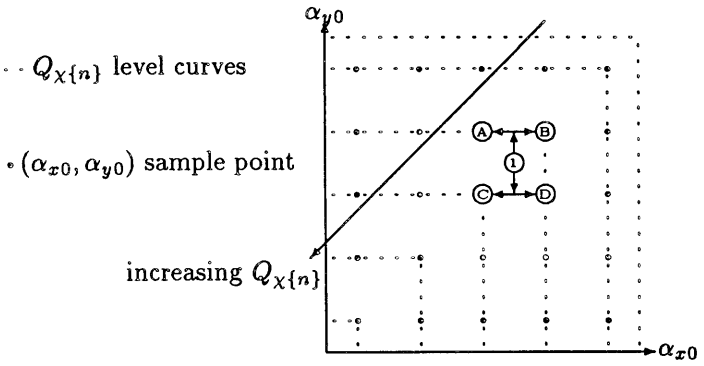

Figure D.3. The $(\alpha_{x0}, \alpha_{y0})$ plane illustrating the defect in interpolation to the value in point ⊙ using simple interpolation between the neares sample points ⊗, ⊖, ○, and ◎.

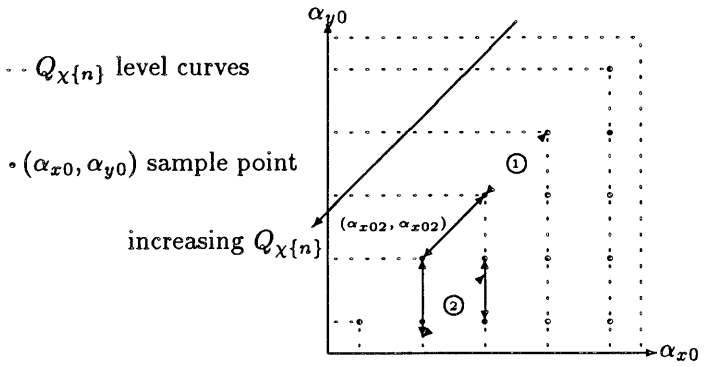

Figure D.4. The $(\alpha_{x0}, \alpha_{y0})$ plane illustrating the suggested strategy for interpolation to the values in the points ⊙ and ◎.

First we interpolate $Q_{\chi\{n\}}(\nu_0, h, k, \alpha_{x0}, \alpha_{x0})$ using only the sampled diagonal points where $\alpha_{y0} = \alpha_{x0}$, which is illustrated for point ① and ② in figure D.4. If $\alpha_{x0} \neq \alpha_{y0}$, which is the case for point ②, than we will also determine the increment $\Delta Q_{\chi\{n\}}(\nu_0, h, k, \alpha_{x0}, \Delta\alpha_0)$ due to the difference

$$\Delta\alpha_0 = \alpha_{x0} - \alpha_{y0} \tag{D.51}$$

and finally determine

$$Q_{\chi\{n\}}(\nu_0, h, k, \alpha_{x0}, \alpha_{y0}) \simeq Q_{\chi\{n\}}(\nu_0, h, k, \alpha_{x0}, \alpha_{x0}) + \Delta Q_{\chi\{n\}}(\nu_0, h, k, \alpha_{x0}, \Delta\alpha_0) \tag{D.52}$$

$\Delta Q_{\chi\{n\}}(\nu_0, h, k, \alpha_{x0}, \Delta\alpha_0)$ can be determined as a main interpolation (through the requested points ② as illustrated in figure) between two sub interpolations or extrapolations (the vertical double arrows in figure D.4).

This ends the description of a algorithm that determines the numerator in the admittance function (D.1) for any dimensionless frequency ν_0. The denominator

should not be determined. It is there simply to ensure that $F^0_{xy}(0) = 1$, and it vanishes when the admittance function is used in (3.1).

Still a strategy is needed to select ν_0 points. Tests have shown that $Q_{\chi\{n\}}(\nu_0, h, k, \alpha_{x0}, \alpha_{y0})$ is curved downwards in a double logarithmic graphic image, i.e. the double logarithmic slope in the interval $[\nu_{01}, \nu_{02}]$

$$\beta(\nu_{01}, \nu_{02}) = \frac{\ln Q(\nu_{02}, h, k, \alpha_{x0}, \alpha_{y0}) - \ln Q(\nu_{01}, h, k, \alpha_{x0}, \alpha_{y0})}{\ln \nu_{02} - \ln \nu_{01}} \tag{D.53}$$

is decreasing in ν_0

Figure D.5 shows a test of an algorithm in which the ν_0 points have been selected according to the convergence criteria. This criteria ensures that we get most calculations where $Q_{\chi\{n\}}(\nu_0, h, k, \alpha_{x0}, \alpha_{y0})$ is must curved. That improves the accuracy of the interpolation which is obviously done double logarithmic, and it also has the pleasant effect that only a few points are selected with high values of ν_0. That is plesant because the calculation time increases with ν_0 due to the increasing sharpness of the coherence.

Still some calculations must be performed at high frequencies. In order to save calculation time in those cases, an attempt has been done to include the asymptotic values (D.46) and (D.47) in the algorithm.

However, the step from numeric integration causes a discontinuity, which has shown to be hard to handle along with the slope criteria

$$\beta(\nu_{01}, \nu_{02}) - \beta(\nu_{02}, \nu_{03}) < \varepsilon \tag{D.54}$$

between all neighbouring ν_0 points

$$\nu_{01} < \nu_{02} < \nu_{03} \tag{D.55}$$

Besides, the asymptotes are sufficient only for very high ν_0 values, i.e. high R and $\omega_,$, and low U_0 values according to (D.24). Moreover, the limit ν_0 between numeric integration and asymptotic determination should be moved ahead when the order n increases.

All together, the use of asymptotes seems to be too troublesome, remembering that only a few calculations are required at high frequencies when the slope criteria is used.

Still the asymptotes are useful because the show that

$$\beta(\nu_0, \nu_0 + \Delta\nu_0) \to -2 \text{ as } \nu_0 \to \infty \tag{D.56}$$

which can be seen by inserting the assymtotic values from (D.46) and (D.47) in (D.53).

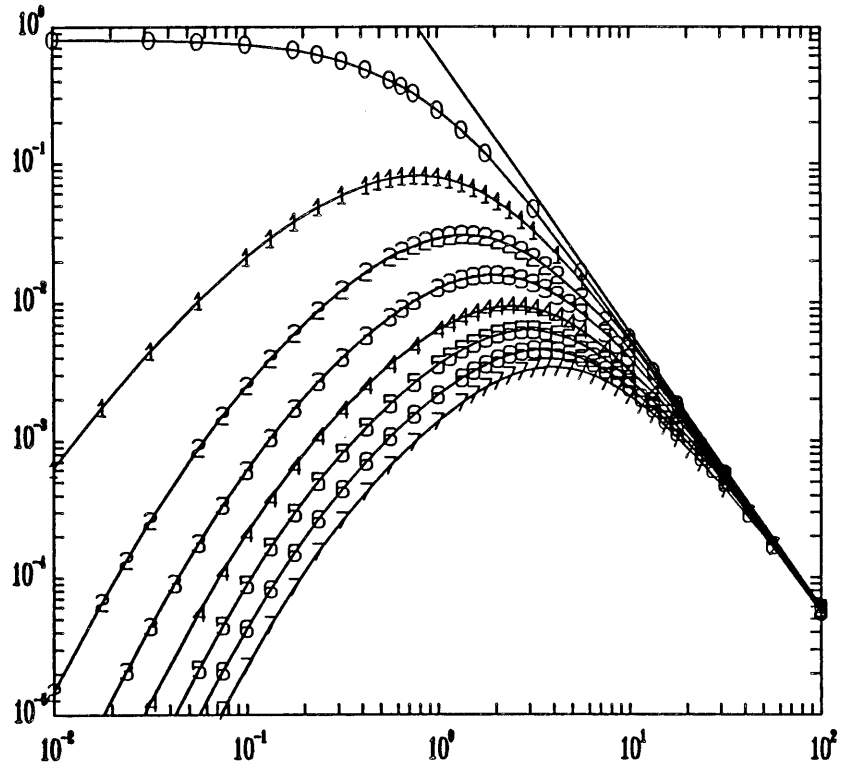

Figure D.5. The admittance term $Q_{\chi_M\{n\}}(\nu_0, 0, 0, 0.1, 0.1)$ plotted with the symbol of the order n in each calculation point. Besides, the asymptote is plotted without symbols. This asymptote is independent of the order n. The convergence fraction $\varepsilon = 0.25$ is used.

(D.56) can be build in the slope based algorithm to avoid the selection of new ν_0 points in an interval of high ν_0 values if the slope in that interval is approximately -2, i.e. if (D.54) is not satisfied but

$$\beta(\nu_{02}, \nu_{03}) + 2 < \varepsilon \tag{D.57}$$

then the new ν_0 points is always selected in the interval $[\nu_{01}, \nu_{02}]$. Otherwise the new ν_0 is selected in the widest of the intervals $[\nu_{01}, \nu_{02}]$ and $[\nu_{02}, \nu_{03}]$, using logarithmic width.

So far, we have used a maximum ratio ε in the convergence criterias (D.38) and (D.57). Tests has shown that the error is approximately one tenth of ε, and consequently a maximum ratio

$$\varepsilon \simeq 0.1 \tag{D.58}$$

yields an exactness at approximately 1% which is quite satisfactory. ε is also suggested to be used to determine the α_{x0} and α_{y0} samples. In order to make allowance for the ϱ substitution (D.12), it is required that

$$\alpha_{x0} > 0 \tag{D.59}$$

That limitation does not have a serious impact on the exactness, but it leads to the suggestion of the α_{x0} and α_{y0} sampling points

$$\alpha_0 = \left(\frac{1}{2} + p\right)\varepsilon \tag{D.60}$$

in which p has all the values of integes in the interval

$$0 \leq p < \frac{1}{\varepsilon} - \frac{1}{2} \tag{D.61}$$

Bibliographic Data Sheet **Risø–R–749(EN)**

Title and author(s)

Frequency domain modelling of wind turbine structures

Poul Sørensen

ISBN	ISSN
87–550–1978–1	0106–2840

Dept. or group	Date
Test Station for Wind Turbines Dept. of Meteorology and Wind Energy	April 1994

Groups own reg. number(s)	Project/contract No.
	ENS-1364/92-0005

Pages	Tables	Illustrations	References
87	1	17	14

Abstract (Max. 2000 char.)

The report offers a detailed description of the development of a frequency domain model of the structure of an operating horizontal axis wind turbine. The frequency domain model is implemented along with an analogous time domain model in the Risø PC code Design Basis 2.

The structure of an operating wind turbine displays essential non-linearities between structural variables on blades and tower respectively. These non-linearities are due to the rotation of the blades causing the transformations between the blade coordinate systems and the tower coordinate system to depend on the instantaneous azimuth positions of the blades.

Conventional frequency domain methods do not allow non-linearities. It is shown, however, that decomposing the structural variables into sums of harmonics in the (constant) angular frequency of the rotor, the non-linear relations are transformed into linear relations between the amplitudes of the harmonics. These linear relations between the amplitudes of the harmonics of the structural variables are readily transformed into the frequency domain and solved there.

Thus, the derivation of the amplitudes of harmonics of the loads is based on conventional frequency domain methods applied to the relations between the amplitudes of harmonics. Finally, the loads themselves are determined uniquely by their respective amplitudes of harmonics.

Design Basis 2 is used to verify the frequency domain model comparing loads on the structure calculated with the frequency domain model both to loads calculated with the time domain model and to measured loads. Examples show that frequency and time domain calculations of typical PSD's of loads are in good agreement. Design Basis 2 has also shown that the frequency domain model results in an extremely fast and easy-to-use calculation method.

Descriptors INIS/EDB

AERODYNAMICS; AZIMUTH; COMPARATIVE EVALUATIONS; COMPUTERIZED SIMULATION; D CODES; DYNAMIC LOADS; ENERGY SPECTRA; EXPERIMENTAL DATA; FREQUENCY ANALYSIS; HORIZONTAL AXIS TURBINES; ROTORS; STRUCTURAL MODELS; TURBINE BLADES; TURBULENCE; WIND LOADS

Available on request from:
Risø Library, Risø National Laboratory (Risø Bibliotek, Forskningscenter Risø)
P.O. Box 49, DK-4000 Roskilde, Denmark
Phone (+45) 46 77 46 77, ext. 4004/4005 · Telex 43 116 · Telefax (+45) 46 75 56 27